UCRL-3452
cy 2

UNIVERSITY OF CALIFORNIA

Ernest O. Lawrence Radiation Laboratory

TWO-WEEK LOAN COPY

This is a Library Circulating Copy which may be borrowed for two weeks. For a personal retention copy, call Tech. Info. Division, Ext. 5545

BERKELEY, CALIFORNIA

DISCLAIMER

This document was prepared as an account of work sponsored by the United States Government. While this document is believed to contain correct information, neither the United States Government nor any agency thereof, nor the Regents of the University of California, nor any of their employees, makes any warranty, express or implied, or assumes any legal responsibility for the accuracy, completeness, or usefulness of any information, apparatus, product, or process disclosed, or represents that its use would not infringe privately owned rights. Reference herein to any specific commercial product, process, or service by its trade name, trademark, manufacturer, or otherwise, does not necessarily constitute or imply its endorsement, recommendation, or favoring by the United States Government or any agency thereof, or the Regents of the University of California. The views and opinions of authors expressed herein do not necessarily state or reflect those of the United States Government or any agency thereof or the Regents of the University of California.

UCRL-3452

UNIVERSITY OF CALIFORNIA
Radiation Laboratory
Berkeley, California

Contract No. W-7405-eng-48

THE ENERGY LEVELS OF NEUTRON-DEFICIENT LEAD ISOTOPES

Arnold Rudolph Fritsch

(Thesis)

June 27, 1956

Printed for the U. S. Atomic Energy Commission

THE ENERGY LEVELS OF NEUTRON-DEFICIENT LEAD ISOTOPES

Contents

Abstract 5
I. Introduction 6
II. Experimental Procedures
A. Bombardment Techniques 9
B. Chemistry 10
C. Fission Competition 10
III. Half-Life Measurements
A. Bismuth-205 12
B. Bismuth-204 12
C. Bismuth-203 13
IV. Scintillation Spectra 14
A. Bismuth-205 14
B. Bismuth-204 16
C. Bismuth-203 21
V. Conversion-Electron Spectra 23
A. Magnetic-Lens Electron Spectrometer 23
1. Bismuth-204 25
2. Bismuth-203 27
B. Permanent-Magnet Electron Spectrographs . . . 28
1. Transition Assignments 34
2. Intensity Measurements 47
3. Auger Lines 52
4. Calibration of Spectrographs 55
VI. Numerical Correlations
A. Results with Lead-203, Lead-204, and Lead-205 . . 58
B. A Statistical Treatment of Transition Sums . . . 63
VII. Coincidence Studies
A. Bismuth-203 67
B. Bismuth-204 67
C. Bismuth-205 72
D. Positron Decay
1. Bismuth-204 74
2. Bismuth-205 75

VIII. Studies on Isomeric States

A. Lead-203m 76

B. Lead-204m 80

C. Lead-205m 89

IX. Decay Process

A. Decay Energy 94

B. Log ft Values 95

C. Lead-205 Decay 98

X. Conclusions

A. General Discussion 104

B. Lead-205 108

C. Lead-204 115

D. Lead-203 Energy Levels 124

E. Thallium-203 128

Acknowledgments 131

Appendix - Tables

1. Bismuth-203 and Bismuth-204 conversion lines from permanent-magnet electron spectrographs 132

2. Bismuth-205 conversion lines from permanent-magnet electron spectrographs 151

3. Assignment of transitions observed in permanent-magnet electron spectrographs 156

4. Conversion lines intensities in photographic plates 177

5. Lead-203, Lead-204, Lead-205, Lead-206, and Thallium conversion-line intensities 191

List of Tables 202
List of Illustrations 203
Bibliography 204

THE ENERGY LEVELS OF NEUTRON-DEFICIENT LEAD ISOTOPES

Arnold Rudolph Fritsch

Radiation Laboratory
University of California
Berkeley, California

June 27, 1956

ABSTRACT

An attempt has been made to establish the energy levels of Pb^{203}, Pb^{204}, and Pb^{205}. The transitions associated with the decay of Bi^{203}, Bi^{204}, and Bi^{205} have been studied with a scintillation spectrometer and various beta spectrometers. The spectra of these isotopes have been found to be very complex, with 17 transitions found for Bi^{203}, 66 for Bi^{204}, and 35 for Bi^{205}. Coincidence studies have been attempted upon these isotopes. The isomeric levels associated with the various lead nuclides have also been examined and data found giving additional information about the energy levels concerned in the isomeric decays.

Numerical correlations of the transitions found have been undertaken. An explanation for the long half life of Pb^{205} has been suggested. Positron decay of Bi^{205} has been found and a limit has been set upon the positron decay of Bi^{204}.

Tentative partial energy-level diagrams have been suggested in all cases. These have been based partly upon theoretical work available and partly upon consideration of the analagous neighboring nuclides.

I. INTRODUCTION

The six years that have elapsed since the introduction of the single-particle nuclear shell model by Haxel, Jensen, and Suess[1] and by Mayer[2,3] have witnessed many qualitative successes of the model in predicting and correlating static nuclear properties such as ground-state and isomeric spins, especially in regions near the closed shells. However, the complexity of the interactions among the many configurations involved in making up nuclear states has, in general, precluded the possibility of making detailed predictions of spins and energies of excited states. Pryce,[4] in 1952, pointed out that in the special case of nuclei that differ by one nucleon from the double closed shell of 82 protons and 126 neutrons, the lowest level should correspond almost exactly to that of a single particle moving in the equivalent potential of the core; further, he showed that a very simple treatment can qualitatively account for levels of nuclei that differ from the double-closed shell by two nucleons. A definite energy state is ascribed to each extra nucleon and in zero approximation all states of this configuration have the same energy; the degeneracy is removed by taking into account the interaction between the two nucleons.

Subsequently, a very detailed and careful experimental study of the levels of Pb^{206}, populated by electron capture of Bi^{206}, was made by Pryce and Alburger,[5,6] and remarkable success was achieved in correlating the observed level energies and spins with the theoretical predictions based upon the known levels of Pb^{207} and the particle-interaction theory of Pryce. The rather simple Pb^{207} level scheme is attributed to the levels of one hole in the 126-neutron shell which is quantum-mechanically equivalent to one particle outside the shell; the levels of Pb^{206} then arise from excitation of a pair of neutrons (holes). Experimentally, the level scheme of Pb^{206} was found to be complex, with 12 levels and 26 transitions between these levels. The success of Pryce and Alburger in elucidating this scheme was in part due to the high degree of accuracy of their energy measurements and in part due to a theoretical understanding of the problem which provided clues as to the probable locations and properties of the levels.

It is expected that the complexity of levels in Pb^{205} and Pb^{204} should be even greater than in Pb^{206} because of the compounding of interactions and configurations for three or four particles. Because the level schemes of these nuclides are of great interest in furthering our understanding of the workings of the shell model near the double-closed shell, the objective of this research was to gather as much and as detailed experimental data as possible concerning the energies and properties of these levels. At the start of this work there was available no theoretical treatment of the 3- and 4-particle problem, and it was not expected that a definite solution could be obtained by experimental means alone; this has proven to be the case, for the complexity of the Pb^{204} level scheme has been found to be extreme, perhaps more so than that of any other nucleus yet investigated by radioactive decay. It was fortunate that while this research was in progress, approximate theoretical calculations of the Pb^{204} energy levels were completed by W. W. True.[7] These have been of much help in the interpretation of the experimental data.

The excited states of Pb^{205}, Pb^{204}, and Pb^{203} are populated by the electron-capture decay of Bi^{205}, Bi^{204}, and Bi^{203} respectively; hence the experimental study here reported was concerned mostly with the latter three isotopes, although any discussion of the results must of necessity include the neighboring isotopes.

The well-known Pb^{207} decay scheme shows the levels of the odd-neutron states clearly and has an $\underline{M}$ 4 isomeric transition which is characteristic of the even-odd lead isotopes.[8] On the other hand, in the even-even isotopes the excited and ground states can be interpreted as combinations of single-particle states plus configurational interaction perturbations. The isomeric transitions found are the 145-μsec E3 in Pb^{206m},[5] the 68-min E5 transition in Pb^{204m},[9] and the 3.5-hr E5 transition in Pb^{202m}.[10] The existence of an even-even E5 isomeric transition is in itself of great interest, since no others are known experimentally.

The existing experimental data on Pb^{203}, Pb^{204}, and Pb^{205} are by no means complete, and leave many questions unanswered. In the even-odd cases, a 5.6-sec isomer was originally assigned to Pb^{202} by Hopkins,[11] but reassigned as Pb^{203m} with a half life of

6.6 sec by Fischer.[12] The energy of this isomeric transition has been variously reported as 800 to 900 kev. No isomeric state has been reported for Pb^{205}, but a number of transitions with a 14-day half life were observed in the course of the Bi^{206} work by Pryce and Alburger and assigned to Bi^{205}.[6] (These are listed in Table VI b.)

The work to date on Pb^{204} has been concerned mainly with the isomeric state, Pb^{204m}. Many workers have helped to show the decay scheme of Pb^{204m} to be a 912-kev E5 followed by 375-kev and 899-kev E2 transitions.[13, 14, 15, 16] The likeliest choice of spins would be 0+, 2+, 4+, and 9-. In attempting to establish this particular sequence of spins by means of angular correlation experiments, Krohn and Raboy[14] found it necessary to assume 1% M6 mixing in the 912-kev E5 and 1/2% M3 mixing in the 375-kev E2. In addition, the 4+ state depopulated by the 375-kev E2 has been shown by Sunyar et al.[17] to have a half life of 3×10^{-7} sec.

In considering these lead isotopes one should include the known work on levels of the neighboring Pb^{202}, Pb^{206}, and Pb^{207} isotopes. Both Pb^{206} and Pb^{207} have been thoroughly investigated. Pb^{207} has been studied by a number of workers; the most complete study was done recently by D. Alburger and A. Sunyar.[8] The level scheme obtained is clearly indicative of the expected single-particle states: the $p_{1/2}$ ground state and $f_{5/2}$, $p_{3/2}$, $i_{13/2}$, and $f_{7/2}$ excited states have been found together with five transitions occurring in their decay (569.7 ± 1,[18] 894 ± 7, 1063.9, 1430 ± 10, 1771 ± 5 kev).[8]

Previous work on the Pb^{202} decay scheme has been concerned wholly with the 3.5-hr isomer, Pb^{202m}. This isomer is analogous to Pb^{204m} except that the isomeric state decays not only by a high-energy E5 transition but also by low-energy E4 transition.[15]

In the sense that the research on Pb^{206} and Pb^{207} may serve as guides, it would seem that a still larger degree of complexity is to be expected in the studies of Pb^{203}, Pb^{204}, and Pb^{205}. This promise points out the necessity for obtaining energy measurements of high accuracy and using instruments of high resolution. Although all available means of approach were utilized in the course of the experimental work, the most fruitful work was done with the Permanent-Magnet Electron Spectographs, as is discussed in the following sections.

II. EXPERIMENTAL PROCEDURES

A. Bombardment Techniques

The activities were produced by means of alpha-particle bombardments with the 60-inch cyclotron upon enriched Tl^{203} samples obtained from Oak Ridge National Laboratory. These contained approximately 80% Tl^{203} and 20% Tl^{205}, in contrast to natural thallium, whose abundances are 30% Tl^{203} and 70% Tl^{205}. The target material used was in the form of Tl_2O_3 powder. This was placed in a small 5-mil platinum hat, together with a 1/2-mil platinum cover, and was firmly sealed in a water-cooled target holder and subjected to bombardment.

Based on work by E. L. Kelley,[19] the energies of the alpha particles were chosen in such a manner that a clear distinction could be made between the nuclides on a basis other than half life, since Bi^{203} and Bi^{204} have nearly identical half lives (about 11 hr).[20] Bi^{204} was produced through a series of bombardments at 38 Mev just below the (α, 4n) threshold. The main contaminant was 6-day Bi^{206}, produced by the (α, n) on Tl^{203} and (α, 3n) on Tl^{205}, with traces of 15-day Bi^{205} and 8.0-yr Bi^{207}.[20,21] Bi^{203} was obtained by full-energy alpha bombardments at 48 Mev. Approximately equal amounts of Bi^{203} and Bi^{204} were formed, together with Bi^{206}, and there was only a slight increase in Bi^{205} activity.

To obtain the 14-day Bi^{205}, bombardments were carried out just below the (α, 3n) threshold at 28 Mev. In this manner the full (α, 2n) cross section on Tl^{203} to produce Bi^{205} was utilized, while the production of Bi^{206} occurred only by the (α, n) reaction on Tl^{203}, and of Bi^{207} by the (α, 2n) reaction on Tl^{205}. By this means the major contaminant Bi^{206} was held to a minimum.

B. Chemistry

After bombardment the target material was dissolved in a minimum volume of concentrated hydrochloric acid, with gentle heating to speed the process. Upon cooling, the thallium in solution was recovered by three 10-ml extractions of diethyl ether, saturated with concentrated hydrochloric acid.[22] The aqueous phase of concentrated hydrochloric acid was then further heated to remove any traces of ether, and evaporated down to a volume of 1/2 ml.

The solution containing the activity was then placed on a Dowex-1 column.[23] The resin was 50- to 100-mesh, and the resin bed was 3 cm long and approximately 1 cm in diameter. The lead fraction was separated by elution with up to 50 ml of 0.1 N HCl. This was a convenient separation, as the bismuth fraction could not be stripped off the column with any concentration of hydrochloric acid, while the lead came off quite readily in 0.1 N HCl. The bismuth activity was removed from the column with 1 N H_2SO_4.

The H_2SO_4 solution containing the carrier-free bismuth fraction was first evaporated to dryness, and then dissolved in dilute hydrochloric acid. The bismuth activity was electroplated from this solution upon platinum or copper (depending upon the source required and the instrument used).

The lead fraction, in 0.1 N HCl solution, was also evaporated almost to dryness and then diluted with water to 10-ml volume prior to its being electroplated in the same manner as the bismuth.

C. Fission Competition

It is always necessary to consider the question of other activities' being present in a sample, in addition to the ones sought. In this case the fission products produced by thallium fission with alpha particles could possibly lead to nuclides that could in some way be carried through the simple chemistry involved in separating the bismuth fraction from the lead and thallium and finally be plated out with the bismuth activity.

Both W. F. Biller[50] and R. H. Goeckermann[51] have studied the fission of bismuth with high-energy particles. Goeckermann has extended this to the fission of lead and thallium. As one would expect, he finds that the symmetrical fission peak is broader at the higher energies and narrower at the lower. He also states that the Mo^{99} that lies at the peak of the fission curve accounts for about 5% of the total fission cross section at the higher energies, and therefore one can conclude that this figure gets larger as the energy decreases.

The most interesting of Goeckermann's results is the cross section of Mo^{99}, obtained by a 40-Mev deuteron bombardment on an enriched sample of lead containing 27% Pb^{204}. The reported cross section is about $10^{-29} cm^2$. This would approximately correspond, then, to a total fission cross section of 2×10^{-28} cm^2 or 0.2 mb. It is possible, therefore, to arrive at an order of magnitude of a few tenths of a millibarn for the Tl^{203} fission cross section with alpha particles.

Since the (α, n) cross sections in this region are on the order of 1 barn,[19] it is clear that the presence of any single fission-product activity in the target activity would be negligible even before chemistry.

III. HALF-LIFE MEASUREMENTS

A. Bismuth-205

A sample of Bi^{205} was followed for more than seven half lives with a Geiger-Müller counter to obtain a value for the Bi^{205} half life of 15.3 ± 0.7 days. Approximately 80% of the initial counting rate of the sample was Bi^{205}, the other 20% Bi^{206} and a very small amount of Bi^{207}. Since the half life of Bi^{206} is 6.4 days,[6] one can readily see that every half life of Bi^{205} decay was accompanied by an approximately twofold increase in its purity. The Bi^{207} did not contribute to any noticeable extent, since its half life is 8.0 years; also, it was produced in lower yield than Bi^{205} owing to the target enrichment in Tl^{203}.

The earlier work on Bi^{205} carried out by Karraker and Templeton[24] assigned a 14.5-day half life to Bi^{205}, which is just within the limits of the error in the present measurement. It should be noted that a most likely error in the Bi^{205} half-life measurement arises from the presence of the shorter-lived Bi^{206}, which is usually obtained in high yield in cyclotron production of Bi^{205}. This would mean that unless caution is taken to correct for all of the Bi^{206} present, the measured half life would be low.

B. Bismuth-204

A sample of Bi^{204} was followed carefully for a period of a week on a Geiger-Müller counter. The main contaminant present was 6.4-day Bi^{206} to the extent of 10% of the initial counting rate; the bombardment had been made below the (α, 4n) threshold to avoid the production of Bi^{203}. The absence of Bi^{203} was shown by a beta-spectrograph experiment on another part of the sample. The half life obtained in this work was 11.0 ± 0.5 hr which is in agreement with the 12 hr half life found by Perlman, et al.[25] However, a half life of 13.5 hr has been reported for Bi^{204} decay by Bergstrom et al.,[26] and this is in poor agreement with the present figure.

Another value recently reported by Wertheim and Pound for the half life seems to be in good agreement with the measured one of 11.0 ± 0.5 hr. Their value was 11.6 ± 0.2 hr.[27] Analysis of the

possible errors present leads one to note that the major error probably arises in the subtraction of long-lived constituents; if these are not fully accounted for one would then expect a longer apparent half life for Bi^{204}.

C. Bismuth-203

As earlier work by Neumann has shown the half life of Bi^{203} to be 12 hr,[28] and therefore almost identical with that of Bi^{204}; it was necessary to follow the decay of specific transitions in Bi^{203} on the double-focusing beta spectrometer,[29] whose resolution is about 0.3%. In this particular case the energy ranges investigated were swept through manually for greater accuracy.

The most prominent Bi^{203} line that one sees in a mixture of Bi^{203} and Bi^{204} is the K line of the 825-kev transition. The decay of this peak was followed extensively, as were the decays of the 825-kev L line, the 899-kev K line, and 912-kev K line of Bi^{204}. These were followed for more than seven half lives, with these results:

Bi^{203}, 11.5 ± 1.0 hours;
Bi^{204}, 11.5 ± 1.0 hours.

The Bi^{204} result agrees, within the limits of error, with the value obtained on the Geiger-Müller counter determinations. The larger limits of error in this case are due to the inherent problems involved in taking the area of peaks obtained, together with the problem of mechanical and electronic stability over a period of days in as complex an instrument as the double-focusing spectrometer when compared with the Geiger-Müller counters. Within the limits of error the half lives of Bi^{203} and Bi^{204} are the same. This has the effect of nullifying the possibility of assignment of electron lines by means of half life.

IV. SCINTILLATION SPECTRA

In most of the gamma-ray work the sources were simply prepared by evaporating a portion of the dilute hydrochloric acid solution containing the activity upon a platinum plate. They were then studied in the 50-channel gamma-ray scintillation spectrometer with a sodium iodide crystal detector. In some of the Bi^{204} work it was necessary to carry out a rapid separation of Bi^{204} from the 1-hr Pb^{204m} in equilibrium with it. This was accomplished by using a small amount of Dowex-1 resin containing the Bi^{204} activity and washing the resin with about 10 ml of 0.1 N HCl in a centrifuge cone. The resin was then washed once with 10 ml of water. A small portion of the resin was then immediately fixed upon a platinum plate and placed in the scintillation spectrometer.

A. Bismuth-205

The Bi^{205} source used in this work was rather pure, with essentially no Bi^{206} and less than 1% of Bi^{207}. The gamma-ray spectrum, upon careful analysis, shows distinct peaks at 180 to 280, 570, 700, 1000, and 1770 kev. The scintillation spectrum from 0 to 1200 kev is shown in Fig. 1. The 1000-kev peak is broad and would indicate some unresolved gamma rays. The large 180-to-280-kev peak is the result of the backscatter. Again a greater complexity is suggested in the decay of Bi^{205} by comparison with Bi^{207} scintillation spectrum, which is also shown in Fig. 1. The Bi^{207} gamma spectrum only has the 570- and 1064-kev peaks. Also, the Bi^{205} has an underlying continuum in the scintillation spectrum, evident in comparison with Bi^{207}.

An analysis of the gamma rays of Pb^{205} from the scintillation spectrum alone is somewhat difficult, since the complexity does not permit the required background correction to be made readily. This is especially so in the 570-kev peak, and somewhat less so in the 700-kev peak. However, the approximate results obtained for the gamma transition intensity, corrected for the sodium iodide crystal efficiency,[30] are as follows:

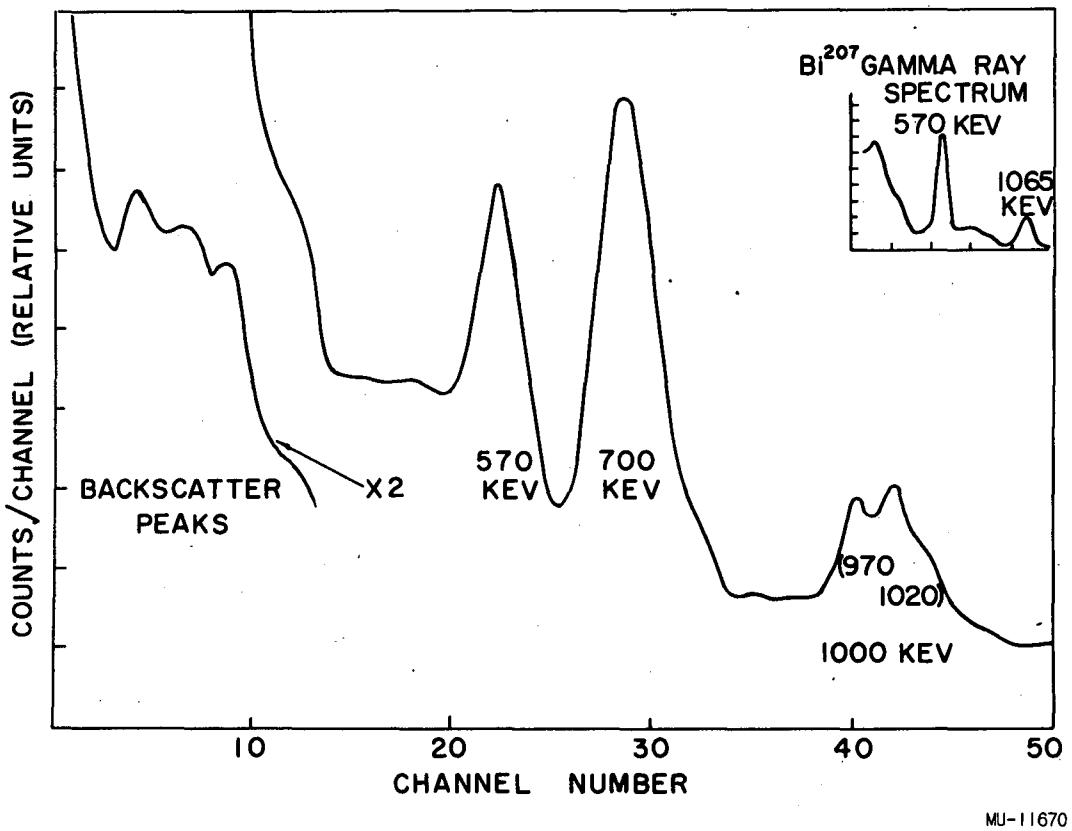

Fig. 1. Bi^{205} gamma-ray spectrum (+ Bi^{207} spectrum).

Energy	Intensity
570	0.35
700	1.00
1000	0.62
1770	2.0

It seems unlikely from the scintillation spectrum that other gamma rays of equally high transition intensity exist, and since it follows that the most intense transitions lie lowest in the decay scheme, one is able to conclude from this work that these transitions must either go directly to ground or populate one another in some manner. Simply on a basis of intensity, it is likely, then, that the 1770-kev transition goes directly to ground. Further interpretation cannot be made solely on the basis of the gamma spectrum.

B. Bismuth-204

The sources used were such that Bi^{204} accounted for approximately 90% of the gross counting rate, with Bi^{206} contributing the remainder. However, because of the great complexity of Bi^{204} decay, the Bi^{206} gamma rays were not readily seen in the spectrum.

The gross spectrum as shown in Fig. 2 is compared with the spectrum obtained for the 68-min Pb^{204m} isomer, which has known transitions at 375 kev, 899 kev, and 912 kev. It is clear that there are many other transitions taking place in Bi^{204} to account for the underlying continuum. The peaks one can distinctly see are at 375 kev, 670 kev, and 900 kev. The low-energy spectrum contains lead K x-rays together with a backscatter peak of about 180 kev and the Compton shoulder of the 375-kev gamma ray.

Since the Bi^{204} decay populates the isomer Pb^{204m}, an attempt was made to measure the extent of this population by a comparison of the 375-kev peak with the 900-kev peak, with and without the isomer present. The difficulties that arise in such a measurement are due to the small differences involved between the two cases. The solution becomes almost unobtainable if one realizes that a fair amount of Bi^{206} is also present. However, the experiment was carried out, and it illustrates the difficulties encountered with the complex decay of not only Bi^{204}, but also Bi^{203} and Bi^{205}.

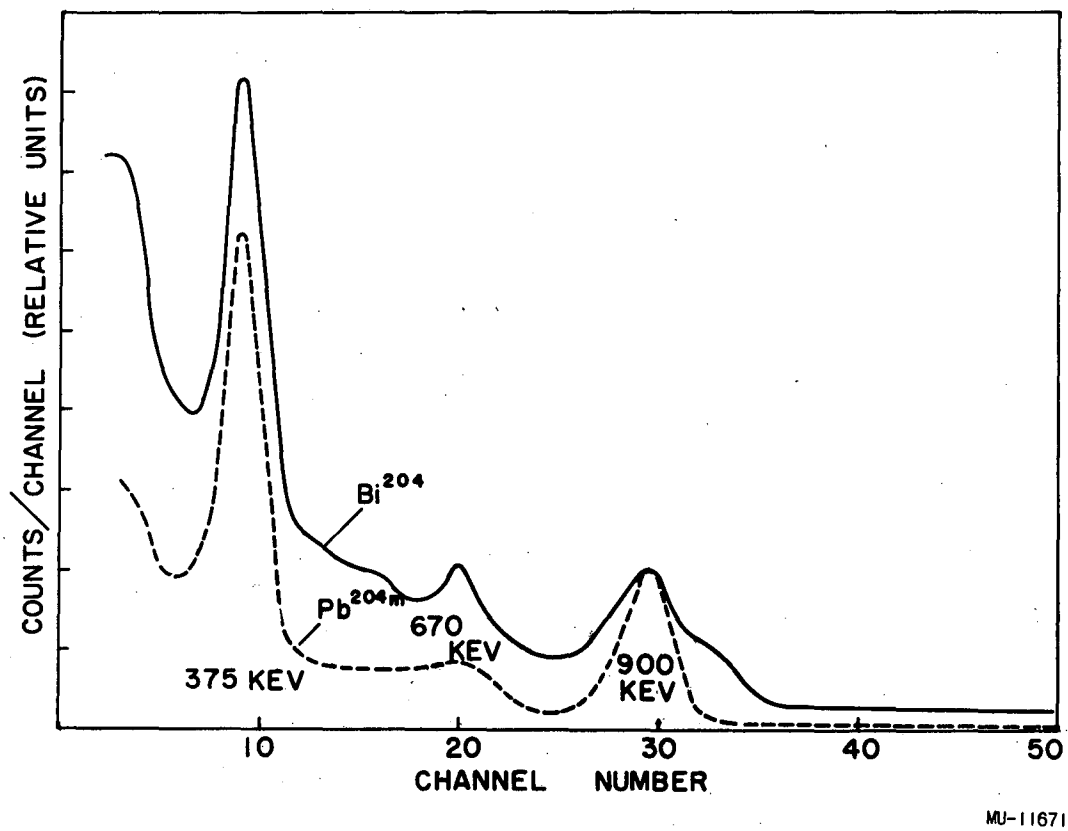

Fig. 2. Bi^{204} and Pb^{204m} gamma-ray spectrum .

A series of bismuth samples were chemically separated from the isomer and immediately counted on the scintillation spectrometer. The samples were counted again after a period of about one Bi^{204} half life, at which time the Pb^{204m} daughter had come into equilibrium with the Bi^{204} parent. If there is an appreciable population of the isomeric state in decay, then an increase in the uncorrected scintillation spectrum should be found in the ratio of the 375-kev peak to the 900-kev peak after the Pb^{204m} had come to equilibrium with the Bi^{204} parent.

In order to eliminate the graphical error involved in summing the peaks, the isomer Pb^{204m} with its known decay scheme was used as a standard. The ratio for the sodium iodide detector's efficiency as given by Kalkstein and Hollander[30] is

$$\frac{375}{900} = 3.7_2.$$

Two Pb^{204m} sources were counted, and the resulting 375- and 900-kev peaks were summed. Since, in summing a peak, a certain amount of arbitrariness is involved in deciding how much background to subtract out, the Pb^{204m} peaks were summed in such a manner as to obtain the best agreement with the reported efficiency ratio and yet to use the identical procedures in correcting for the background in each case.

Because of the complexity of the Bi^{204}, it was felt that these procedures applied to the Bi^{204} samples would eliminate--at least to some extent--the errors involved in background corrections. The results of this Pb^{204m} work, when corrected for the fact that there are two 900-kev transitions to one 375-kev transition in the decay, were

$$\frac{375}{900} = 3.8_6,\ 3.6_2;\ \text{Av.} = 3.7_4.$$

By this method a series of five bismuth samples were analyzed on the gamma-ray spectrometer immediately after a separation from Pb^{204m}, and then again after the Pb^{204m} had come to equilibrium with its parent. The results of these experiments were as follows:

Ratios of transitions at 375 kev to those at 900 kev		
	Bi^{204}	$Bi^{204} + Pb^{204m}$
1.	1.5_4	1.4_2
2.	1.4_9	1.0_3
3.	1.4_1	1.3_5
4.	1.6_8	1.0_9
5.	1.3_6	1.1_0
Av 1.5_0; Av dev. 0.064; Av = 1.1_7; Av dev. 0.095		
Difference = 0.3		

These results can be analyzed only in the light of the 6-day Bi^{206} present along with the Bi^{204}, since the difference to be expected from the population of the isomeric state by Bi^{204} would have been in the direction of increasing the ratio of the 375-kev peak to the 900-kev peak. This discrepancy can be explained when one realizes that the 803-, 880-, and 895-kev transitions in Pb^{206} would be counted in the 900-kev peak.[3,6] These transitions, since they are among the most intense present in Pb^{206}, would be expected to contribute, on the basis of the reported decay scheme, 1.8 counts to the 900-kev peak for each count from Bi^{206}. Compared to this, Bi^{206} contribution to the 375-kev peak is negligible. Since approximately 10 hr or one half life of Bi^{204} was allowed to elapse before recounting the samples, the Bi^{206} would be expected to produce such a result--providing, of course, that the population of the isomeric state were not large. Because of the errors in the work, apparent in the resulting ratios, it is difficult to give any accurate figure for the amount of Bi^{206} present. However, a value somewhere between 10 and 20% of the initial counting rate in the 900-kev peak could be attributed to Bi^{206} from these results. The only conclusion one can draw as to the isomeric population in the decay is that the population is small and probably no greater than 25%.

Neglecting the 10% or so of Bi^{206} contamination present, one can obtain a rough picture of the decay of Bi^{204} in terms of the first two excited states. The value for the ratio of 375-kev peak to the 900-kev peak immediately after separation is 1.5. Correcting the value for the sodium iodide crystal efficiencies, one gets 0.40 as the transition ratio. We are, of course, neglecting conversion effects, which in this case are less than 5%. The interpretation of this would be that 40% of the decay to excited states goes through the second excited state, while 100% goes through the first excited state.

In order to get some rough values of the direct population to ground in the decay of Bi^{204}, the x-ray peak was examined. The results, corrected for crystal efficiency, were as follows:

Peak	Transitions	Relative intensities
x-ray	54,000	0.97
375	20,400	0.38
900	56,000	1.0

It should be pointed out that these values were obtained from samples of Bi^{204} some 15 hr after bombardment. This would lead to error in the 900-kev peak and correspondingly in the x-ray peak, as already discussed.

However, since no value is known for the number of x-rays per decay in Bi^{204}, the results become even more approximate in that it is necessary to assume a value. If one assumes that all decays go through the first two excited states, a value of about 1.05 is called for. Since there is no way of predicting the amount of population to higher states that de-excite through the 375- and 900-kev gamma rays, the value of 1.05 was used as a limiting value.

On this basis the value expected for the x-ray peak if all the decays were to go through excited states would be 1.05. If there were any considerable direct population to ground the value of the x-ray peak would be larger. It would then appear from the results that the direct population to ground is at best very small.

The gamma-spectrum work would then lead one to the conclusion that most if not all of the Bi^{204} decays go through the 900-kev level and that about 40% of them go through the 1275-kev level. There is

a small population of the isomeric state and little or no direct population of the ground state. It is, of course, impossible to tell from this whether the 900-kev and 1275-kev levels themselves are being directly populated by electron capture, and to what extent this population occurs.

C. Bismuth-203

The gross gamma spectrum obtained for Bi^{203} was of little use, since Bi^{204} was also present in almost equal quantity. Because the Bi^{204} spectrum is far from simple itself, the addition of Bi^{203} resulted only in more of a "continuum" in which only the stronger peaks were observable, as shown in Fig. 3.

Analysis of the scintillation spectrum shows a smooth tail from about 1 Mev out to approximately 2.0 Mev. The broad peak at 880 kev can be assigned to the 899-kev and 912-kev transition in Pb^{204} and the 825-kev isomeric transition in Pb^{203}. The other peak present besides the K x-ray and the backscatter peak at about 260 kev is the one at 375 kev, which corresponds to the known 375-kev transition of Pb^{204}.

It is quite apparent, then, that any transitions that might have been seen in pure sources of Bi^{203} are here obscured by the presence of Bi^{204}.

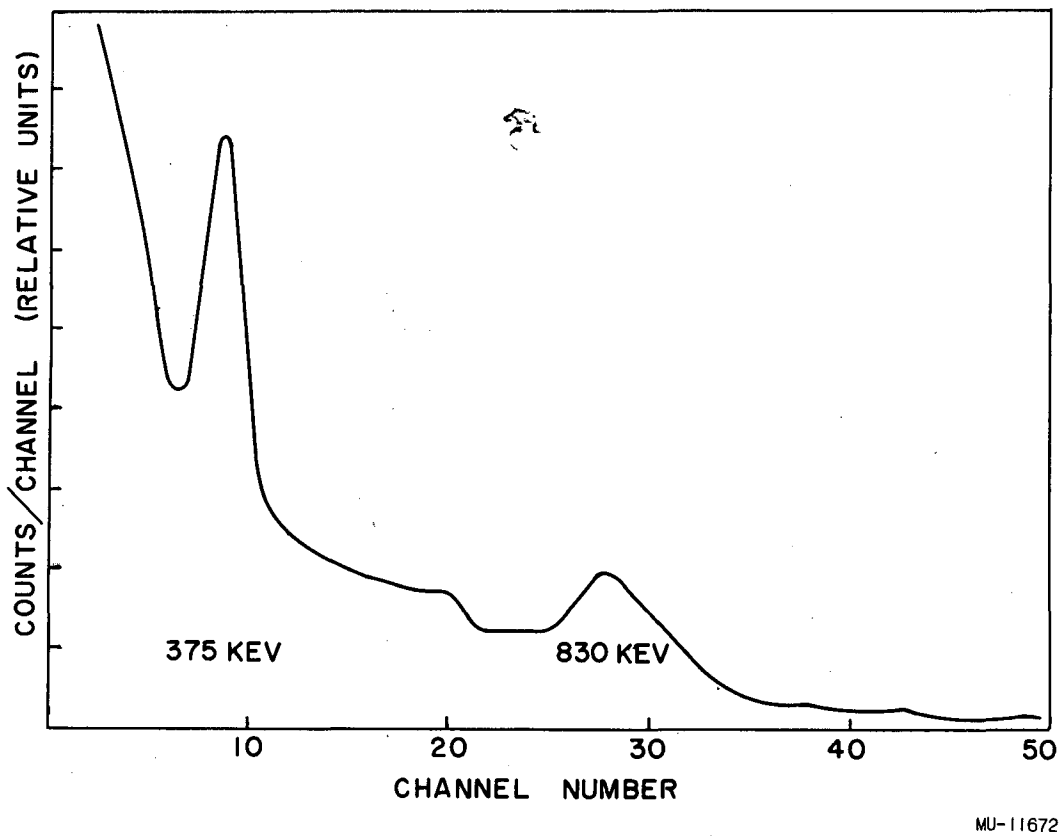

Fig. 3. Bi^{203} gamma-ray spectrum.

V. CONVERSION-ELECTRON SPECTRA

From the indications, in the scintillation gamma spectra, of the complexity in Pb^{203}, Pb^{204}, and Pb^{205}, the next step in this investigation was to use instruments with higher resolution. Experiments were then performed on the conversion electron spectra resulting from the transitions involved in de-excitation. The first instrument tried was the magnetic-lens electron spectrometer, which has a resolution of approximately 2%.[31] Samples of Bi^{203} and Bi^{204} were run on this instrument, but the electron spectrum still left a great deal to be desired in resolution of the complex groups.

The highest-resolution instruments available were the permanent-magnet electron spectrographs,[32] which were then used with great success in examining the electron lines associated with the decay of Bi^{203}, Bi^{204}, and Bi^{205}. In all of this work the inherent complexity of the decay processes involved has been the most striking feature.

A. Magnetic-Lens Electron Spectrometer

The sources of Bi^{203} and Bi^{204} studied on the magnetic-lens electron spectrometer were electroplated on a 1-mil copper foil. The foil was previously masked off with tape in such a manner as to expose only an area of 5 mm^2, in order to produce as nearly as possible a point source for which the instrument was designed. The foil was then mounted on a lucite ring that was fitted to the source probe prior to the actual study of the sample in the instrument.

Samples of Bi^{203} and Bi^{204} with an initial activity of 10^7 to 10^8 electrons/min were easily obtainable, and as the transmission of the magnetic-lens electron spectrometer is about 1% there was more than a sufficient amount of activity. The magnetic lens uses as a detector an anthracene crystal which, because of the electronics involved, has an inherent amount of "noise," especially in the very high-energy regions where internal conversion is low. In order to minimize the noise the photomultiplier tube voltage was adjusted in such a manner as to give the best count-to-noise ratio possible. This resulted in an effective electron-energy threshold of about 100 kev and influenced the electron-line intensity measurements up to about 250 kev.

The energies obtained are good in most cases to 2 to 3%. However, because of the complexity, no attempt was made to secure greater accuracy with this instrument. The only problem in assignment of the electron lines to the various nuclides involved was in differentiating the long-lived lines of Bi^{206} from the shorter-lived lines of Bi^{204} and Bi^{203}, but this is easily done.[6] Of course, samples of Bi^{204} and Bi^{206} were run initially and then samples of Bi^{203}, Bi^{204}, and Bi^{206} were run to distinguish the Bi^{203} from the Bi^{204}.

A series of Bi^{204} peaks were followed over several half lives in order to check the assignment of lines to this isotope. The average of the various results was

$$\text{Average } T_{1/2} = 11 \text{ hr}$$

This is in good agreement with other half-life work.

The results of these energy measurements are shown in Table I.

Table I

Transitions obtained on the magnetic-lens spectrometer

	Electron energy (kev)	Possible assignment	Previously observed transitions
Pb^{203}	621	709K	--
	734	822K	--
	1432	1520K	--
Pb^{204}	130	218K	--
	138	226K	--
	207	295K	--
	290	378K	(375)
	365	380L	(375)
	583	671K	--
	658	673L	--
	813	901K	(899, 912)
	893	908L	(899, 912)
	962	1050K	--
	1037	1052L, 1125K	--

Table I continued

	Electron energy (kev)	Possible assignment	Previously observed transitions
Pb^{204} (cont)	1114	1202K	--
	1178	1622K	--
	1188	1203L, 1276K	--
	1244	1259L	--
	1260	1348K	--
	1357	1445K	--
	1373	1461K	--
	1423	1438L	--
	1438	1526K	--
	1617	1705K	--
	1800	1888K	--
	1837	1925K	--
Pb^{206}	164	180L	(184)
	172	260K	(262)
	184	188M	(184)
	260	348K	(343)
	405	493K	(497)
	424	512K	(516)
	446	534K	(537)
	508	523L	(516)
	527	542L	(537)
	614	629L	(620, 632)
	725	813K	(803)
	1637	1725K	(1720)
	1735	1750L	(1720)

1. Bismuth-204

The assignments given to the 375-, 899-, and 912-kev transitions are in agreement with previous work on Pb^{204m} by Bergstrom and Wapstra.[33] However, it is clear from the results that only the most intense transitions can be recognized, because of the over-all

complexity. The higher-energy region above 1 Mev has a more doubtful status, since the transitions observed are very weak. In many cases the lines reported were not always resolved and the energy measurements were poorer.

All possible electron lines have been listed in this high-energy region, although the apparent complexity made a clear assignment impractical except for the most intense lines. The ratio of the 375-kev to the unresolved 900-kev K line was

$$375K/900K_{av} \approx 1.3.$$

On the basis of a 40% population of the 375-kev transition and approximately 100% population of the 899-kev transition, as shown in the gamma spectrum work, a conversion coefficient was determined for the 900-kev gamma-ray doublet. The values reported for these transitions in Pb^{204m} are[16]

$$375 \text{ kev } \alpha_K = 0.044,$$
$$899 \text{ kev } \alpha_K = 0.0069,$$
$$912 \text{ kev } \alpha_K = 0.059.$$

Using the above value of 375 kev α_K, one finds the conversion coefficient of the 900-kev peak to be

$$\alpha_{K900} \approx 0.014.$$

The explanation of this result is that the isomeric level in Pb^{204} is being populated. The value obtained from this conversion coefficient for the population is about 12%. The population of the isomeric state evidences itself in still another manner. Since the K/L ratio of the 899-kev E2 is much larger than that of the 912-kev E5, one would expect the unresolved K peak to contain more 899-kev character than the L peak. This is seen in Table I, where the energy resulting from the K peak is 901 kev whereas that from the L peak is 908 kev.

A value for the population of the isomeric state can also be obtained from the measured K/L ratio of the unresolved 900-kev peak, which is 2.3. The K/L ratios reported for the resolved electron lines are[16]

$$899 \text{ K/L} = 5.6,$$
$$912 \text{ K/L} = 1.4.$$

Again taking into account the gamma-spectrum work as it concerns the population of the first two excited states, one finds that a value of 11% population of the isomeric state will explain the observed K/L ratio.

Both values obtained for the population of Pb^{204m} from the decay of Bi^{204}, 11% and 12%, are in agreement. They represent, in terms of conversion electrons, almost equal K-line intensity of the 899-kev E2 transition and the 912-kev E5 transition.

The K/L ratios were also measured for a number of the other intense transitions. The only previously reported K/L has been for the 375-kev transition. The results are

$$K/L \sim 2.1; \text{ reported}^{16}\ K/L = 2.3.$$

These would seem to agree well. Additional K/L ratios studied were

at 670 kev, K/L = 5.7;
1050 kev, K/L = 2;
1202 kev, K/L = 3.5.

The 670-kev K/L ratio is in agreement with the M1 assignment.[6,34] The K/L ratios for the 1050-kev and 1202-kev transitions seem far out of line from the values expected for any common transitions, and their probable explanation lies in the complexity of the L peaks. In other words, the L lines for these transitions probably occur beneath the K lines of some other transitions.

The K/L ratios resulting from some of the lower-energy transitions were also studied, but here again the complexity evidenced itself. The results were also affected to a large extent by the threshold of the anthracene crystal detector.

2. Bismuth-203

The fact that only three transitions were observed in the decay of Bi^{203} is clear evidence of the need for higher resolution in order to analyze the complex electron spectra. The line at 621 kev is only a very small peak, which is doubtful to the extent that longer-lived components were seen in it, mainly the K line of the 703-kev transition in Bi^{205}. The 734- and 1432-kev both were very strong, and there is no question as to their existence. The L line corresponding to the 734-kev K line has been obscured by more intense K lines of the 899- and 912-kev transitions in Bi^{204}.

Because of the complexity of the combined $Bi^{203,204}$ spectrum, no intensity measurements were attempted.

B. Permanent-Magnet Electron Spectrographs

Four permanent-magnet electron spectrographs are in operation at this laboratory, covering these energy ranges

PM I	0 to 80 kev,
PM II	0 to 275 kev,
PM III	0 to 890 kev,
PM IV	0 to 1650 kev.

These instruments have been discussed in detail elsewhere;[32] it should be sufficient to say that Alnico magnets are responsible for the magnetic field. Between these the "camera" is placed. The "camera" is an evacuated chamber with a means of holding the photographic plate and source in reproducible positions and defining the electron beam by a slit system. The resolution of these spectrographs is about 0.1 to 0.2%. In all high-resolution instruments, however, the transmission is low, on the order of 0.05%. They are in effect infinite-channel instruments, since the electrons are recorded photographically, and are therefore especially convenient for Bi^{203} and Bi^{204}, where the short half life might otherwise present a difficulty.

The sources for the permanent-magnet electron spectrographs were prepared by electroplating the bismuth or lead activity upon a 5-mil platinum wire from a dilute hydrochloric acid solution. The total length of the wire mounted in the source holder was perhaps 3 cm, with the activity confined to a length of about 1 cm in the center of the source holder.

The source so prepared and placed in the spectrograph then resulted in innumerable approximations to images of the wire in the photographic plate, corresponding to the various conversion lines. Examples of these plates are shown in Fig. 4. The first set of photographic plates shows the spectra obtained for a Bi^{204} sample in Spectrographs II, III, and IV respectively, while the second set of plates shows the same spectra for a Bi^{203} and Bi^{204} mixture. The stronger lines are noted in each case and their assignment is discussed in detail later. Naturally both sets of plates contain Bi^{205}

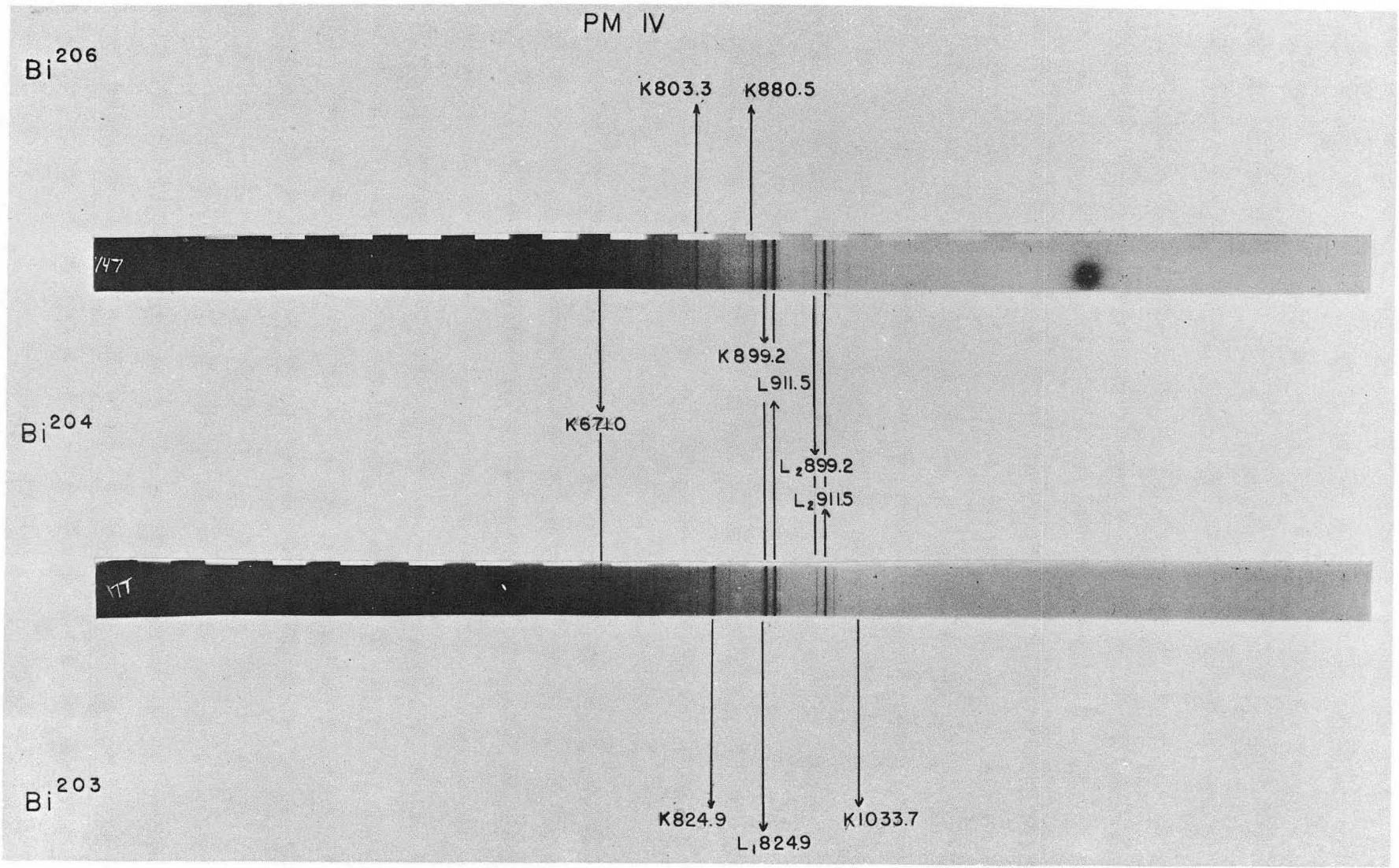

ZN-1521

Fig. 4a. Photographic-plates obtained in Bi^{203} and Bi^{204} work.

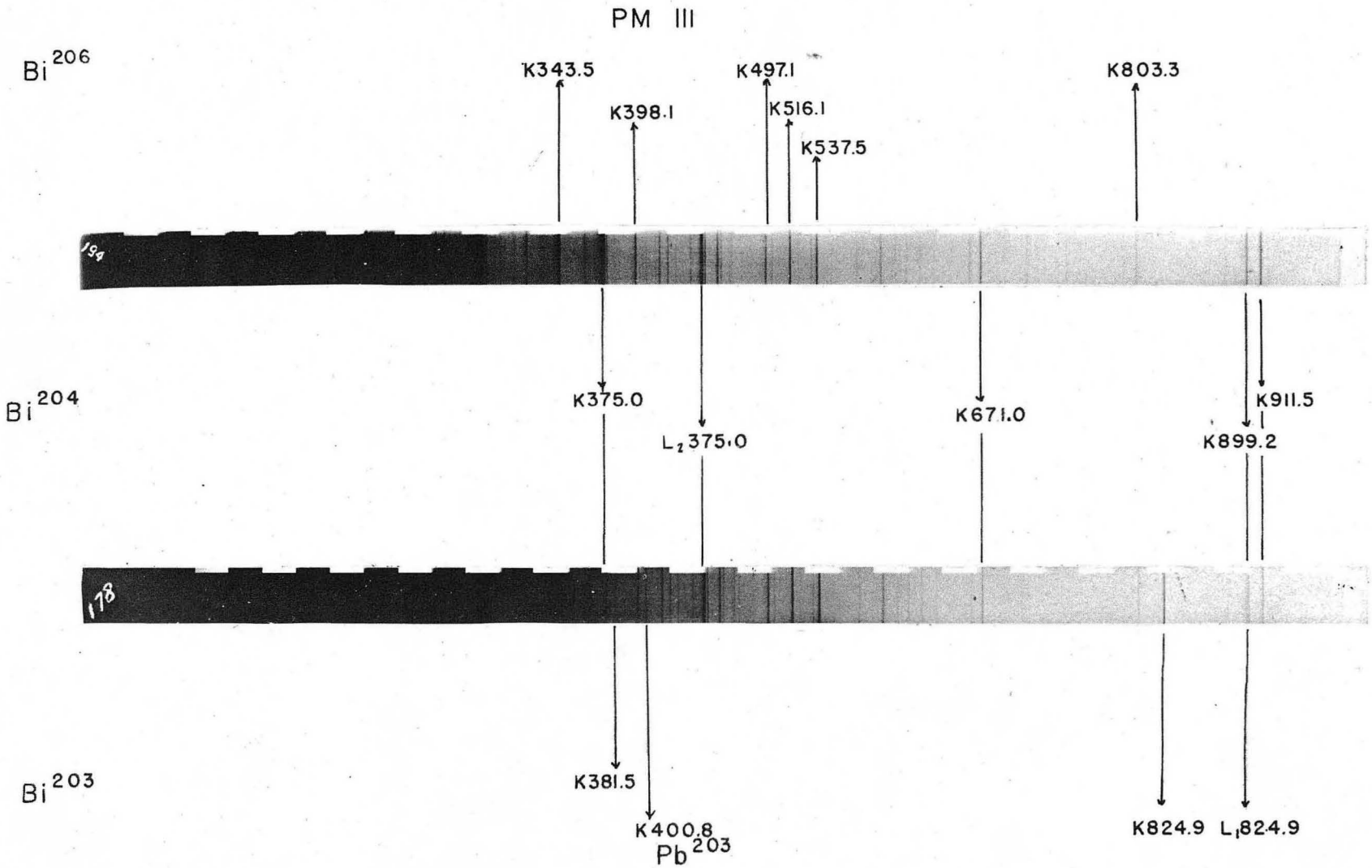

Fig. 4b.

ZN-1522

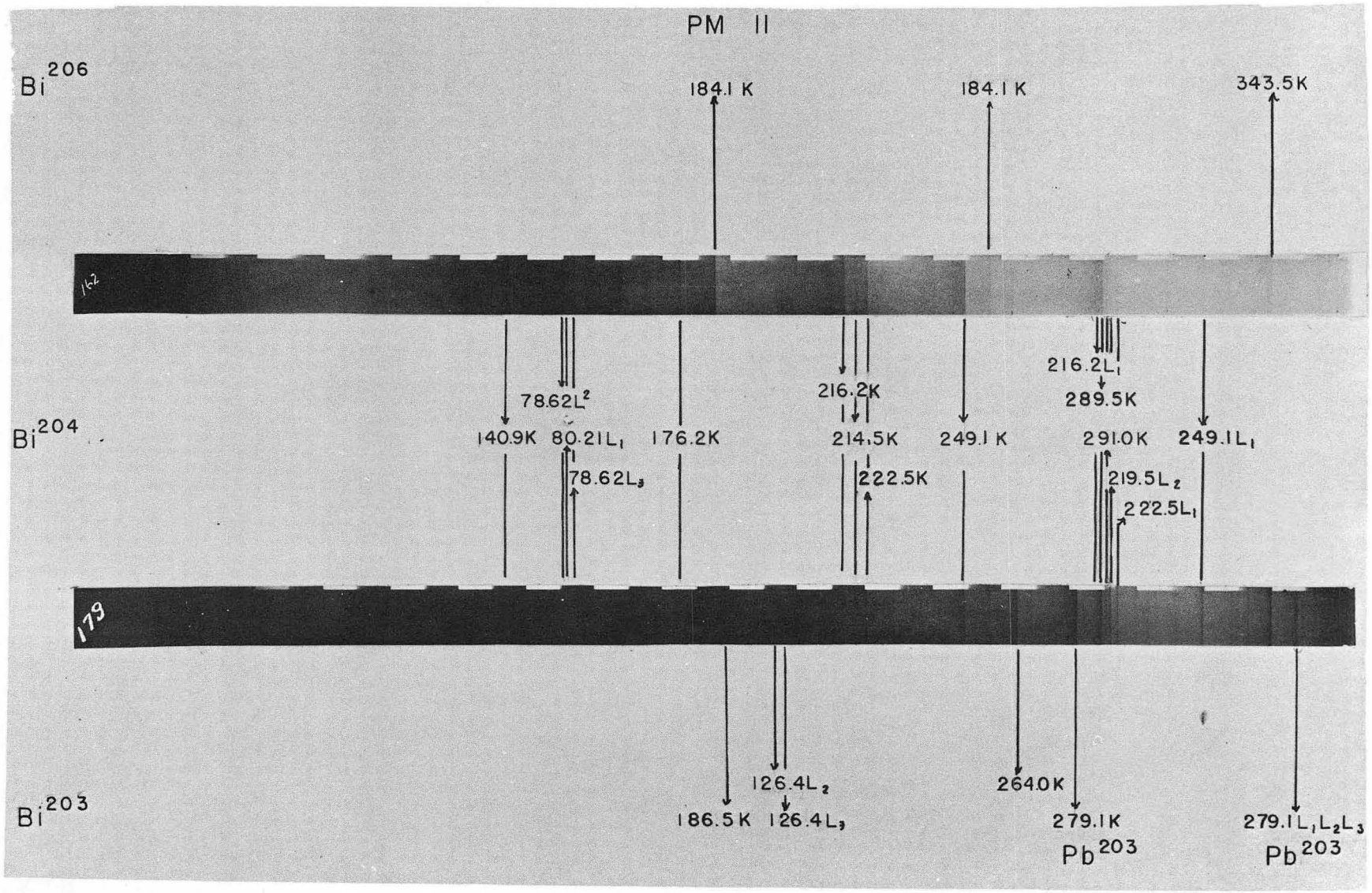

Fig. 4c.

ZN-1523

and Bi^{206} lines as well. The second series also includes the conversion lines seen in the decay of Pb^{203} to Tl^{203}.

The complexity one observes in these plates is quite striking. The ability of the permanent-magnet electron spectrographs to deal with this complex spectrum is neatly illustrated in Fig. 5 by the densitometer plot obtained from the region of 760 to 850 kev, in the course of the intensity work on Bi^{204} decay to be discussed later. The region includes the K lines of the 880.5-kev and 895.2-kev transitions and the L_1 line of the 803.4-kev transition in Pb^{206}, and the K lines of the 899.2-, 911.5- and 918.4-kev transitions in Pb^{204}, as noted. The resolution is on the order of 0.13%. Because of this resolution, these instruments proved to be well suited to the analysis of the various conversion lines.

In Tables AI and AII of the appendix are listed the conversion lines found with the spectrographs in studies of Pb^{203}, Pb^{204}, and Pb^{205} respectively. The lines listed are accompanied by a visual intensity, relative to the particular plate; but because of the inherent human error involved, these intensities are very roughly approximate. The human factor confronts the experimenter also in the observation of the conversion lines themselves. Since the eye is far more sensitive in distinguishing weak lines than any instrument such as a densitometer, the weaker lines are based solely on visual scrutiny. In extreme cases the existence of a given line is questionable, since some impurities or vertical nonuniformity in the emulsion can often be mistaken for a very weak line. To overcome this problem as much as possible, transition assignments had been made only to such lines as had been observed on three or more plates, or to lines seen on only two occasions providing that on one of these times, the line had an intensity of "very weak" or greater; the exception being the higher-energy region of PM IV, where no overlap is possible. In this case assignment required only visual intensity of "very weak" or greater. The visual intensities used are:

vs -- very strong,
s -- strong,
m -- moderate,
w -- weak,
vw -- very weak.

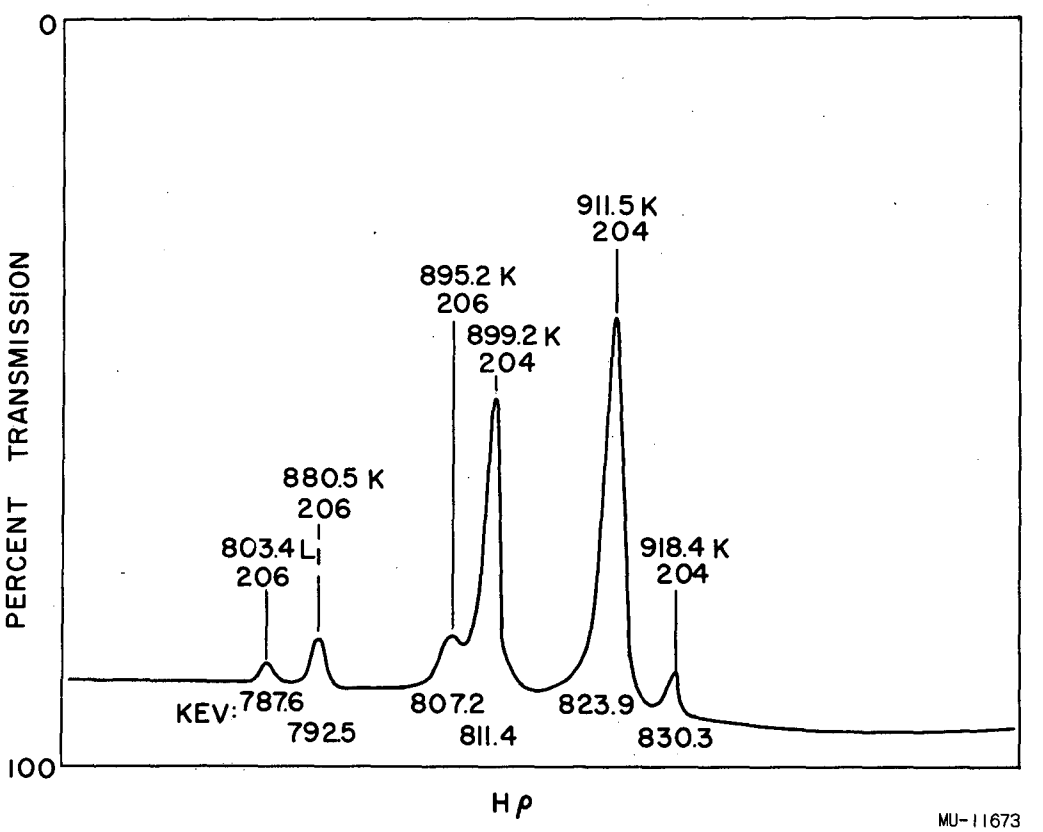

Fig. 5. Densitometer curve for Bi^{204}-Bi^{206}, 800-830 kev.

There are, in addition to these, lines that are stronger and weaker than this spectrum of intensities would allow. However, because of the nature of the photographic process as shown in the density-versus-exposure curve, the linearity is limited, and any direct interpretation is therefore also limited. The intensities are roughly graded in factors of two; that is, a moderate line is about twice as intense as a weak one and a strong line is about twice as intense as a moderate line. No correction has been made for film efficiency or geometry.

The conversion lines in Tables AI and AII have also been listed by photographic plate number, distinguishing them as to the spectrograph used and the isotope studied. Plates 147, 148, 162, and 194 contain Bi^{204}, Bi^{205}, Bi^{206}, and Bi^{207} lines, while Plates 177, 178, 179, 180, and 215 contain also Bi^{203} and consequently conversion lines from the decay of Pb^{203}.

1. Transition Assignments

Included in the list of conversion lines is the assignment made to the lines. There are a fair number of lines left unassigned, but because of the visual methods used, these represent lines of little or no confidence. In Table AIII of the Appendix, the assignment of each transition has been given in terms of the conversion lines, and in some cases a probable multipole order has been noted on the basis of K/L ratio or L-subshell ratio. Each conversion line is followed by a relative visual intensity and an actual photographic one in those cases where densitometry was possible. The assignments of conversion lines used the lead and thallium binding energies given by Church et al.,[35] and these are listed in Table II.

The assignments of conversion lines as compiled in Table AIII are dependent upon the judgment of the experimenter and therefore are subject to error. For the more intense transitions, or those known beforehand, there is little or no difficulty in the assignment of conversion lines. The problem arises, of course, in the weaker transitions.

Table II

Lead and thallium binding energies (in kev)		
	Pb	Tl
K	88.00	85.52
L_I	15.86	15.34
L_{II}	15.20	14.70
L_{III}	13.03	12.65
M_I	3.85	3.70
M_{II}	3.56	3.41
M_{III}	3.07	2.95
M_{IV}	2.58	2.48
M_V	2.48	2.38
N_I	0.89	0.84
N_{II}	0.76	0.72
N_{III}	0.64	0.61
N's	0.1	0.1
O's	0.1	0.1

No practical solution exists to this problem since its roots lie partly in the visual reading of the photographic plate. The approach used in this work has been to make a distinction in transition assignment as to the number and "quality" of conversion lines included in each transition. This is not the same criterion used in deciding the actuality of a line, as mentioned previously. The transitions have been broken into three confidence groups. The first of these groups corresponds to those transitions for which two or more conversion lines have been assigned. The second group again contains transitions that have two or more conversion lines assigned, but because of the weakness of some of the lines or possible ambiguity in assignment these are of a more doubtful sort. The third confidence group contains all transitions that have been assigned on the basis of one line alone. In all cases this has been the K line, although L-line assignments were attempted; however, they proved to be less satisfactory in every instance.

It should be emphasized that these groupings are not clearly definitive of the actual confidence one may have in a line, but just a somewhat quantitative means of making a broad distinction, and a large overlap is inherent. The third group contains perhaps the broadest spread of actual confidence in a line. It is a characteristic of such transitions as E1 and M1 in this region of atomic number that the K-to-L ratio remains practically constant, from about 5 to 7.[6, 34] Therefore, if the K line of a weak transition were seen, it would not be unexpected that the L line lie beyond the limits of detection. In the higher-energy spectrum M2, M3, and E2 transitions also attain large K/L ratios, so that it would be the rule rather than the exception in this region to see a weak K line corresponding to a weak transition and not observe the L line. In a sense, then, a broad graduation exists in this third confidence group, with the highest confidence within the group occurring in the higher-energy regions.

The transitions found in the decay of Bi^{203}, Bi^{204}, and Bi^{205} are listed in Table III. The transitions are reported in confidence groups as just discussed. The energies given are within ± 0.1%. Listed beside the energies are the conversion lines observed for each particular transition. For these transitions in the third confidence group, the number of times the K-conversion line was seen as well as the maximum intensity at which it was observed are also presented.

A list of some of the stronger transitions observed in Bi^{203} and Bi^{204} decay has recently been published by the Swedish group of Bergstrom et al.[26] They were unable to differentiate most of the new transitions because of the similar half lives of Bi^{203} and Bi^{204}. The transitions observed in the work presented here have been compared with the reported values, and assignments made wherever possible, as listed in Table IV.

Three uncorrelated transitions remain at 477, 498, and 757 kev. The K line corresponding to a transition at 477 kev has been observed in the Pb^{204} electron spectrum, but it has been assigned as the L_1 line of the 405.5-kev transition, since no L line corresponding to its assignment as a K line of the 477-kev transition is in evidence. The reported transition at 498 kev is a difficult case to analyze since an intense Pb^{206} transition exists at 497.2 kev. In one plate a vvw line was read at 410 kev, a slightly higher energy than the K line of the 497.2-kev gamma ray, but this is an extremely doubtful line. It is possible that in the Swedish work the decay of the K-line peak from the 497.2-kev transition was followed and components of 12 hr and 6 days were observed, thus giving rise to the reported assignment of a 498-kev transition. The reported transition at 757 kev is not explainable. The only line observed in this work in the K-line region of this transition was the N_1 line of the 671.0-kev gamma ray. However, despite the three differences discussed, the agreement in terms of transition assignment is quite satisfactory between the two works. Whether this sort of agreement will carry over into the weaker transition assignments is still uncertain.

Table III

Transitions found in Bi^{203}, Bi^{204}, and Bi^{205} decay

	Energy (kev)	Conversion lines observed
Bi^{203}		
First Confidence Group		
	126.4	$L_2L_3M_2M_3N$
	186.5	KL_1M_1
	264.0	KL_1M_1
	819.7	KL_1
	824.9	KL_1M_1
	1033.7	KL_1
Second Confidence Group		
	60.08	L_1N_1
	117.7	$KL_1M_1N_1$
Third Confidence Group		
	381.5	K ms2
	465.4	K vvw2
	606.1	K vw2
	625.0	K vw2
	708.4	K s2
	722.1	K w2
	1536.4	K vw

Table III continued

	Energy (kev)	Conversion lines observed
Bi^{204}		
First Confidence Group		
	78.62	$L_2L_3M_2M_3N_2$(M1)
	80.21	$L_1L_2M_1N_1$
	100.4	$L_1L_2M_1$
	119.8	KL_1
	140.9	KL_1M_1
	144.5	$KL_1M_1N_1$
	170.0	KL_1M_1
	176.2	KL_1M_1
	212.7	KL_1
	216.2	KL_1M_1
	219.5	$KL_2L_3M_2M_3N_1$
	222.5	$KL_1M_1N_1$
	227.1	KL_1
	240.7	KL_1M_1
	249.1	$KL_1M_1N_1$
	289.5	KL_1
	291.0	KL_1
	330.9	KL_1
	375.0	$KL_1L_2L_3M_1N_1$
	405.5	KL_1
	412.4	KL_1
	421.8	KL_1
	438.8	KL_1
	501.8	KL_1
	522.2	$KL_2L_3M_2$
	532.6	KL_1
	661.5	KL_1
	663.4	KL_1L_2
	671.0	$KL_1L_3M_1N_1$

Table III continued

	Energy (kev)	Conversion lines observed	
Bi^{204} continued			
	710.4	KL_1	
	725.3	KL_1	
	791.9	KL_1	
	899.2	$KL_1L_3N_1$	
	911.5	$KL_2L_3M_2N_2$	
	918.4	KL_1M_1	
Second Confidence Group			
	105.5	L_1	
	109.1	$L_1L_2M_2$	
	164.9	KL_1	
	184.9	L_1L_2	
	213.5	KL_2	
	252.4	KL_1	
	440.2	KL_1	
Third Confidence Group			
	168.8	K	w4
	209.1	K	vw2
	332.1	K	w2
	340.6	K	vw3
	376.8	K	wm4
	468.3	K	w4
	542.2	K	vw3
	545.7	K	vw3
	548.8	K	w3
	585.4	K	w4
	615.2	K	vw2
	646.4	K	vvw3
	684.3	K	vvw4

Table III continued

	Energy (kev)	Conversion lines observed	
Bi^{204} (cont)			
Third Confidence Group			
	718.5	K	w4
	745.2	K	w3
	748.5	K	vvw2
	765.4	K	vw3
	832.3	K	vw3
	834.3	K	vw3
	844.1	K	w-m4
	933.6	K	vw-vvw2
	1056.7	K	vw-w2
	1139.8	K	vw-vvw2
	1203.9	K	vw2
	1211.5	K	vw1
Bi^{205}			
First Confidence Group			
	112.2	L_2L_3	
	260.5	KL_1	
	282.4	KL_1	
	284.0	KL_1M_1	
	349.3	KL_2	
	570.7	KL_1M_1	
	579.7	KL_1M_1	
	703.3	$KL_2L_3M_2$	
	987.5	KL_1	
	1043.5	KL_1	

Table III continued

	Energy (kev)	Conversion lines observed	
Bi^{205} continued			
Second Confidence Group			
	31.1	L_1M_1	
	32.8	L_1M_1	
	131.2	$L_1L_2L_3$	
	148.6	KL_2	
	526.0	KL_1	
	758.6	KL_1	
Third Confidence Group			
	192.6	K	vvw1
	383.3	K	vv2
	493.5	K	vw3
	511.7	K	w3
	531.1	K	vvw1
	550.3	K	vw2
	573.7	K	vvw2
	626.2	K	vw1
	744.6	K	vvw2
	910.7	K	vw3
	1014.0	K	vvw2
	1073.3	K	vvw1
	1190.1	K	vw2
	~ 1346	K	vvw1
	~ 1617	K	vvw1

Table IV

Comparison of Bi^{203} and Bi^{204} transitions with reported results (energies in kev)

Bergstrom et al.	This Work	Isotope
219	219.5	204
240	240.7	204
249	249.1	204
264	264.0	203
289	289.5	204
374.7	375.0	204
421	421.8	204
467	468.3	204
477	---	204
498	---	---
502	501.8	204
532	532.6	204
661	661.5	204
662	663.4	204
671	671.0	204
	708.4	204
709		
	710.4	203
718	718.5	204
722	722.1	203
757	---	---
825.2	824.9	203
899.3	899.2	204
911.7	911.5	204
918	918.4	204

The final transition energies quoted in Tables III and AIII are felt to have an error of 0.1% or less. This limit is probably best illustrated by a comparison of the results of our energy measurements with other reported results besides the Bi^{206} work of Pryce and Alburger, which was used to standardize PM III and PM IV. This has been done for Pb^{203} decay and for Bi^{205} and Bi^{207} decay, and is shown in Table V. The Pb^{203} work is quite satisfactory. The Bi^{207} value and its subsequent agreement is unusual since it is based upon only two measurements of a very weak K-conversion line. The stronger 569.7-kev transition was not observed, since the 570.7-kev transition associated with Bi^{205} decay effectively cover it up.

Although the Bi^{205} agreement looks quite phenomenal, it is somewhat doubtful. Bergstrom et al.[26] make no mention as to what energy standards were used in arriving at the reported energies. It is quite likely that they proceeded in the same manner as this work did, using the intense lines of Bi^{206} decay to calibrate their instrument. If this is so, then the small differences shown are only reading errors occurring in the analysis of the conversion spectra. The intensities reported by Bergstrom et al., are also listed along with the energies in Table V. The Pryce and Alburger results on Bi^{205} are only reported to be within limits of ± 0.2 of a percent.[6] All the differences then are well within the limits of error.

Considering the agreement of the previous results it does not seem unlikely that the energies reported in this work are within the limits of ± 0.1 of a percent. On a relative basis, within the set of reported transitions the error could be considerably less, although no clear means is available to prove this. However, as will be discussed, it is hoped that this relative agreement might make numerical correlations of the transitions successful in their application.

Table V

Comparison of Pb^{203}, Bi^{205}, and Bi^{207} transition energies (in kev) with results reported elsewhere

Pb^{203}

J. Prescott[36]	Wapstra et al.[37]	Thulin and Nybo[38]	Wapstra[39]	This Work
280	279	279	279.17±.05	279.1
400	400			400.6

Bi^{207}

Yavin and Schmidt[40]	Alburger and Sunyar[8]	This work
1063.43	1063.9	1063.5

Bi^{205}

This work	Bergstrom et al.	Pryce and Alburger
112.2		
260.5	260.0 (1100)	
282.4	282.0 (400)	
284.0	283.9 (1500)	284.4
349.3	349.4 (280)	
383.3	383.2 (60)	
493.5	493.6 (110)	
511.7	511.7 (220)	
526.0		
531.1	531.7 (28)	
550.3	550.0 (63)	
570.7	571.0 (740)	
573.7		
579.7	580.0 (240)	
626.2	625.2 (67)	
703.3	703.3 (1000)	703.7
744.6	745.0 (21)	
758.6	758.3, 761.0 } (51)	
910.7	910.8 (98)	911.6

Table V continued

Bi^{205}		
This Work	Bergstrom et al.	Pryce and Alburger
987.5	987.8 (275)	988.6
	1002.7 (21)	
1014.0	1014.2 (49)	
1043.5	1043.7 (325)	1044.6
1073.3		1074.1
1190.1	1190.3 (76)	1189.8
	1337 (3)	
~ 1346	1351.5 (11)	
	1502.5 (4)	
	1552.0 (8)	
~ 1617	1614.6 (31)	1615.4
	1766.4 (436)	1766.3
	1777.4 (52)	1778.8
	1863.3 (20)	1864.2
	1906.5 (6)	

Numbers in parentheses refer to reported K-line electron intensity measurement.

2. Intensity Measurements

There are a number of factors involved in the translation of the photographic blackening of a given line into an intensity measurement for the conversion line. These factors include: the photographic development process, the efficiency of the photographic plate for recording various energy electrons, and the geometry of the instruments used. It is hoped that each of these factors can be simply treated and be easily corrected for in each measurement.

However, before these factors can be applied, it is necessary to have a value for the photographic density for a conversion line. These were obtained by measuring a given photographic plate with an A. R. L. - Dietert Recording Densitometer. As a result a continuous conversion-line spectrum is obtained for each plate. (An example of this was shown in Fig. 5.) The relative intensities of the peaks are measured by the method of Slätis.[41] These relative photographic intensities are then converted into conversion-line intensities.

The photographic development factor is a rather straightforward one, since it is merely an expression of the photographic density of a line in terms of the length of exposure: the D log E curve. In order to facilitate the process, this correction is made in the initial step of measurement and the relative photographic intensities I_p when corrected for the photographic development process involved, are expressed in minutes of exposure of a Sr^{90} standard source. The D log E curve was then measured for each batch of film by merely exposing portions of the plate to the Sr^{90} source for different lengths of time and, after analyzing these in the densitometer, plotting the results in such a manner as to allow a direct translation of maximum peak height to photographic intensity I_p, as suggested by Slätis.

The efficiency of the response of the photographic film, η to electrons of various energies is not easily found. Since the photographic film was Kodak No Screen X-ray Film, which was manufactured on glass backing especially for these spectrographs, no experimentally measured curve was available. Previous measurements of No Screen X-ray Film had been carried out on celluloid-backed film.[42,43] It was therefore found necessary to carry out a series of

measurements of the efficiency. This is being done in this laboratory by Frederick L. Canavan. The results of his measurements indicate a somewhat thicker photographic emulsion than in previous work and a small increase in film efficiency at higher energies (because of the glass backing). The experimental results then gave η, the efficiency, as a function of energy, which is indirectly proportional to the intensity. Account of this factor is taken by dividing the photographic intensity by the efficiency: I_p/η.

The third major factor one needs to consider is the geometry of the instruments used. It was fortunate that the theoretical calculations of the geometry had been carried out by Wooster[44] for just such an arrangement as presented by the permanent-magnet spectrographs. The results of these calculations in the simplest approximation is that the intensity of a line is inversely proportional to ρ, the radius of curvature for a particular line. A first-order correction upon this simple result would seem to be that this is valid only in the region where the geometrical broadening of a line is equal to or less than the natural width of the line. After this point it would seem that the geometrical line-broadening effectively cancels the simple geometry correction. However, owing largely to the lack of good experimental data, this region of geometrical line-broadening, which is the region of low ρ, is disregarded, because the various permanent magnets overlap sufficiently to obviate any necessity of using a correction.

The photographic intensity can then be converted to conversion-line intensity by

$$I = I_p \times \rho \times 1/\eta .$$

The procedure satisfies the requirement of being simple and easily corrected for in each measurement. It was carried out for each photographic plate. The results of this analysis are listed by plate number in Table AIV of the Appendix; so that one may check the intensities against the visual intensities given in Tables AII and AIII, the conversion lines. Table AIV has been arranged stepwise from I_p, the photographic intensity, through the geometrical

correction and η, the film efficiency, to the final value for the intensity I. This enables one to interpret the resulting intensities I more clearly in the light of the photographic intensities, which represents the actual state of affairs. In most cases large deviations in I can be explained by small initial values of I_p, which (because they were small) were extremely sensitive to errors.

Since the values of I obtained would be relative only to a given photographic plate, it was necessary to normalize all the intensities for a given isotope to some particular conversion line set at 1000. The normalized intensities are denoted by I_s in Table AIV. The electron lines chosen for the normalization were as follows:

Isotope	Conversion line
203	824.9-kev K line
204	899.2-kev K line
205	703.3-kev K line
206	537.5-kev K line

Unfortunately, in none of these cases did the chosen line appear on all the photographic plates of a given isotope. It was therefore necessary to use a second and sometimes a third electron line that could in some manner be related back to the initial choice. In most cases a second line was selected on the basis of a reasonable agreement of normalized values between different plates with respect to the primary conversion line. An average of these values was found and this average value was used as a secondary normalization on those plates in which the primary line was absent. The lines chosen for the normalization are indicated in Table AIV.

The results of the normalization, I_s, are tabulated by isotope in Table AV of the Appendix. For Pb^{204} and, in selected instances, for Pb^{206}, the various values of intensity I_s obtained for a given conversion line are averaged and the average value of the intensity I_{avg} is listed. Since the accuracy of these intensity results is difficult to predict except by comparison with known data, the conversion lines in Pb^{206} and Pb^{205} were used to provide such a comparison. Pryce and Alburger report their Pb^{206} intensity with an error of 15% above 250 kev and 30% below 250 kev. The

intensity values of Pb^{205} given by Bergstrom et al. in a preliminary investigation of the isotope[26] do not include the limits of error. However, the values for both Pb^{205} and Pb^{206} have been compared with the results obtained in this work, as also shown in Table AV.

The over-all picture one obtains from this comparison is that most of the intensities are in agreement to within 25%. A notable failure of the intensities obtained from the photographic plates is in the low-energy region. This is clearly shown in both the Pb^{205} and Pb^{206} comparisons. The region below 300 kev or so seems to become progressively worse in comparison with the known values as the energy of the conversion line decreases. In Pb^{206} the value of the 184.1-kev K-line intensity is lower by a factor of 3 or so than that reported by Pryce and Alburger.[6] It would seem, then, that the intensity measurements obtained on the basis of the photographic plates are good to within 25% except in the low-energy region, where the values represent only a little better than order-of-magnitude reliability.

No specific explanation of this discrepancy in the low-energy regions of the electron spectra is possible. At first thought one might be tempted to explain this all in terms of a geometrical discrepancy. In other words, the discrepancy would be some function of ρ. But there are many values for a conversion line listed in Table AV that agree with one another, although they result from two different permanent-magnet spectrographs and therefore different values of ρ. This would seem to indicate that geometrical considerations are not the primary causes of the difference. On the basis of these similar results from different spectrographs, the discrepancy would then appear to be mainly a function of energy. This energy factor might evidence itself in the shapes of the conversion lines, somewhat in the manner indicated by the results of Wooster's work,[44] mentioned previously. The difficulty with this particular argument is that in many cases, during the calculation of the intensities of the conversion lines, the half width was also considered. It was found that the half width of a line, obtained by the method of Slätis,[41] was close to being identical throughout the electron spectrum. There

were, of course, a few exceptions, resulting mainly from unresolved lines. Because the half widths were the same within the limits of the measurements, they were not considered in the calculation of the photographic intensity, as they would only introduce an additional uncertainty associated with their measured values.

Since this energy effect, which could possibly be responsible for the intensity differences observed in the low-energy region, did not appear in the half widths of the line, it must be present elsewhere. It is possible that the major portion of the electrons corresponding to a given low-energy conversion line does not appear in the peak at all, but in the tail. In this case the half widths would not necessarily indicate any differences. In this sense, then, a sharp peak for the line sits upon a broad unresolved peak composed of a large part of the conversion electrons, and since the broad peak would just be part of the background for the low-energy lines, one would measure only the fraction of the electrons in the sharper peak. A situation such as this could possibly be caused by scattering, the angular effect of which is quite dependent upon energy. It should be understood, however, that this is highly speculative. No quantitative corrections are available. This means that comparisons of intensities of low-energy electrons with those of high-energy electrons are very uncertain and give only very rough approximations to the correct values.

The intensity values I_s within the limits just established have been utilized in the assignments of conversion lines (Table AIII) to make multipole order assignments where possible. The resulting values for the K/L ratios and L-subshell ratios have been compared with the theoretical values of Rose[34] for a given transition. The K/L ratios obtained from the theoretical work are in good agreement with those reported by Pryce and Alburger for Pb^{206}. On the basis of K/L and L-subshell ratios and lifetime considerations, a tentative multipole order assignment has been made wherever possible, as indicated in Table AIII. Often, however, especially for high-energy transitions, no assignment can be made readily since either there is only a K line seen for the transition, or the L conversion is in the L_1 subshell and the L_1 line is weak. In the latter case E1 and M1 and sometimes E2 transitions are indistinguishable.

The assignments based upon the L-subshell ratios seem the most certain, since the lines compared lie so close to one another. Also it would seem the intensity discrepancies might be smaller when one compares intensities of K, L, and M lines of a particular transition, rather than making comparisons of intensities at large energy differences. In order to study this, the intensities of the Pb^{206} lines were used. K/L ratios for the various transitions were obtained. These were compared with the K/L reported by Pryce and Alburger and with their transition multipole order assignment, as shown in Table AIII. The results of this comparison seem to indicate that although the discrepancy encountered is somewhat less, there is still a large difference (although it would seem clear from some of the disagreement in the higher-energy K/L ratios that this difference might be due largely to the errors involved in measuring the intensities of some of the weak L lines).

The one clear thing that emerges from these considerations is the need for further intensity work upon photographic recording instruments (such as the permanent-magnet electron spectrographs), in order not only that good measurements may result, but also that the factors involved in intensity measurements of this sort may be understood.

3. Auger Lines

The Auger lines resulting from the conversion process in lead nuclides were observed in the course of the work. It was of interest to examine these Auger lines, since there was evidence for the existence of conversion lines of interest in the region of the Auger group.

In previous work Bergstrom and Hill had made precision measurements of Auger electron energies from decay of electron-capture thallium isotopes.[49] They found that the energy of any $KL_xL'_y$ Auger line is given to an accuracy on the order of parts per 1000 by

$$E_{KL_xL'_y} = (E_K - E_{L_x})_Z - (E_{L_y})_Z + \Delta Z.$$

Here $\Delta Z = 0.6$ when L_x is L_1, L_2, or L_3 and L'_y is L_1 or L_2, and $\Delta Z' = 0.8$ when L_x is L_1, L_2, or L_3 and L'_y is L_3.

The results obtained upon analysis of the KLL Auger group are expressed in terms of an experimental ΔZ, and are tabulated in Table VI. The accuracy of the measurements is such that an error of plus or minus one-tenth in ΔZ is to be expected. Our values, $\Delta Z = 0.5$ and $\Delta Z' = 0.7$, are in agreement with those of Bergstrom and Hill. However, the $\Delta Z'$ is based on only the KL_3L_3 value. The intensity of the observed KLL Auger lines also seems to agree with previous work. The KLM and KLN Auger groups have also been considered; the results are in Table VI. Here, because of the small effect of ΔZ upon the M and N binding energies, no value for ΔZ has been obtained. On the whole the agreement within the group seems to be good.

Table VI

KLL Auger lines
computed values for ΔZ (energies in kev)

E_{av}	KL_1	KL_2	KL_3	L'_1	L'_2	L'_3	ΔZ
56.04	72.14			16.10			0.46
	72.14				15.46		0.45
56.68							
		72.80		16.12			0.49
57.35			72.80		15.45		0.49
	72.14					13.21	0.51
58.93							
			74.97	16.04			0.34
		72.80				13.20	0.44
59.60							
			74.97		15.37		0.33
61.68			74.97			13.29	0.67
			L'y	16.11	15.46	13.21	
		Av	ΔZ	0.47	0.45	0.51	
					ΔZ_{av}	= 0.48	

KLM Auger lines

E_{av}	KL_1	KL_2	KL_3	M'_1	M'_2	M'_3	M'_4	M'_5
68.14	72.14			3.96				
68.56	72.14				3.58			
69.04	72.14					3.10		
69.60	72.14							2.54
71.11			74.97	3.86				
71.29			74.97		3.68			
71.91			74.97			3.08		
72.22			74.97				2.75	
	Pb Binding Energies			3.85	3.56	3.07	2.58	2.48

4. Calibration of Spectrographs

In the course of the work, two new electron spectrographs were set up in addition to PM I and PM II (of 52 gauss, and 99 gauss, respectively) were already in operation. The new instruments had effective magnet fields of about 220 and 350 gauss, and are designated PM III and PM IV.

As it turned out, the calibration of these instruments was quite conveniently done in conjunction with the work on the decay of Bi^{203}, Bi^{204}, and Bi^{205}, since the method of production provides one with a large amount of Bi^{206} activity along with the other nuclides. The Pb^{206} level had been studied intensively by Pryce and Alburger and others, and as a consequence the energies of the Pb^{206} transitions were known to quite high accuracy. Pryce and Alburger report the K-line energies for 19 of the transitions associated with the decay of Bi^{206} to ± 0.05 %. The accuracy of their measurements, together with the abundance of Pb^{206} lines (especially in the higher-energy regions), provided us with an excellent standard.

The Pb^{206} lines chosen as primary standards were the more intense K lines. The L and M lines associated with these were sometimes used, but since there is always some doubt as to the assignment of multipolarity to a transition and the multipole mixing involved, it was felt that this uncertainty, manifested in the L and M subshells, required the L and M lines to be considered as secondary standards. The lines used are in Table VII, and there the distinction has been made as to the spectrograph that was involved.

The actual processes involved in measuring the true dimensions of the cameras in both instruments, as well as the mechanics of the calibration have been discussed fully.[32] However, one new aspect has been introduced into the calibration. Up to this date the actual physical measurements had been used unaltered. These include the distance a, from the center of the slit to the first reference notch of the photographic plate holder; h, the distance from the source to the slit, and of course the $\Delta\ell_I$'s, the distances from the first reference notch to the various other reference notches. Initial calibrations based on the actual physical measurements resulted in

Table VII

Conversion lines -- standards

	PM III		PM IV	
	Energy (kev)	Transition	Energy (kev)	Transition
Primary Standard				
	184.1	K	398.1	K
	262.8	K	497.1	K
	343.4	K	516.1	K
	398.1	K	537.5	K
	497.1	K	620.6	K
	516.1	K	632.2	K
	537.5	K	803.3	K
	620.6	K	880.5	K
	803.3	K	895.1	K
	880.5	K	1018.8	K
Secondary Standard				
	184.1	L_1		
	184.1	M_1	398.1	L_2
	343.4	L_1	343.4	L_1
	343.4	M_1	497.1	L_1
	398.1	L_2	516.1	L_2
	497.1	L_1	803.3	L_1
	516.1	L_2	890.5	L_2
	516.1	M_2	895.1	L_1
	537.5	L_1		
Iodine-131				
	80.16	K	284.3	K
	80.16	L_1	284.3	L_1
	80.16	M_1	364.5	K
	284.3	K	364.5	L_1
	364.5	K		
	364.5	L_1		

a roughly parabolic curve for the magnetic field. In PM III this deviation in the magnetic field for ρ, the radius of curvature of the electron path, going from 2.5 cm to 15 cm, amounted to 1%. Naturally this is not a convenient result when one wishes to determine energies of 0.1% or less. It was found empirically that the addition of 0.18 cm to a, the distance from the center of the slit to the first reference notch, reduced this 1% deviation to less than 0.1% over the same range. It should be noted that the correction made to a is far outside any physical error made in measurement. An analogous correction was made with PM IV in order to hold the deviation of the magnetic field to within 0.1% or so.

The basis for making this empirical correction is that the instruments are relative in their energy measurements and not absolute. The correction then merely becomes a constant of the instrument. The result of this correction is that the magnetic field is practically a constant and thus one is able to notice smaller deviations in the calibration and also--as a result-- to obtain a more accurate calibration than if the magnetic field varied widely.

The Pb^{206} calibration was checked and the instruments further calibrated with I^{131}. The transitions used were those measured by Dumond and co-workers and reported[45] as

80.164 kev,

284.307 kev,

364.467 kev.

The conversion lines used in the calibration are listed in Table VI. No distinction has been made (as for Bi^{206}) between primary and secondary standards, since the L and M lines used agree quite well with the over-all results. The I^{131} calibration agreed well within the limits of 0.1% with the Pb^{206} work.

VI. NUMERICAL CORRELATIONS

A. Results with Lead-203, Lead-204, and Lead-205

In an attempt to obtain a decay scheme, a program was initiated in which the transitions of Pb^{204} and Pb^{205} were studied numerically. Basically this meant that all possible sums of two transitions were taken and each sum of two compared with all single transitions and all other sums of two. All differences of two transitions were also considered, and these again were compared to all singles and all other differences. The reason for considering the sums in attempting to construct a decay scheme is quite evident. The differences were considered, although they gave the same results as the sums, because they bring out the cases where there are two levels so close together that the transition between them is too weak to be seen. A constant small difference in a number of transitions would point this out.

Since in the cases involved there were about 35 and 65 transitions each, the more usual procedure of doing the work manually was unsuitable. A program was therefore constructed for an IBM 650 digital computer, which in a short time gave the desired results. One slight variation was introduced; the Pb^{204} transitions were run in two groups representing essentially different degrees of confidence in the gamma rays.

The limits set upon the sums and differences were 0.1%, corresponding to the accuracy of any given single transition. On the basis of the probability studies it was felt that if a value of 0.2% were accepted for the sums and differences, as it might well be, the results would be too unmanageable. In fact, the 0.1% results proved to be unwieldy, since for Pb^{204} we obtained a list of 2650 sums, while for Pb^{205} there were 570 sums.

The results were listed in such a manner that they were repetitious, and all the sums involving any particular single transition were listed under that transition. This was also done separately for the differences. The working tables of sums are then 10,600 long for Pb^{204} and 2,280 for Pb^{205}. Because of the great number of sums

involved, only the sums of two with singles are listed in Table VIII for Pb^{204} and Pb^{205}.

The transitions in Pb^{203} were also considered. However, since the number of Pb^{203} transitions is so much smaller, the results were obtained manually. The results are listed in Table VIII. Because of the paucity of Pb^{203} transitions in comparison with Pb^{204} and Pb^{205}, both sums of two with singles and with other sums of two are given.

The analysis of these results is discussed in later sections dealing with the energy levels of the isotopes.

Table VIII

Numerical correlations, Pb^{204} and Pb^{205}
(energies of transitions given in kev)

Pb^{204}	Single	Sum 1 +	2	Single	Sum 1 +	2
	219.5	78.62	140.9	646.4	100.4	540.7
	249.1	80.21	168.8	646.4	144.5	501.0
	289.5	80.21	209.1	646.4	240.7	405.5
	330.9	78.62	252.4	661.5	119.8	542.2
	405.5	164.9	240.7	661.5	222.5	438.8
	412.4	80.21	332.1	661.5	249.1	412.4
	412.4	184.9	227.1	663.4	78.62	585.4
	421.8	209.1	212.7	663.4	140.9	522.2
	438.8	216.1	222.5	663.4	330.9	332.1
	440.2	109.1	330.9	671.0	168.8	501.8
	440.2	212.7	227.1	671.0	249.1	421.8
	440.2	213.5	227.1	671.0	330.9	340.6
	468.3	216.2	252.4	684.0	216.2	468.3
	468.3	219.5	249.1	710.4	164.9	545.7
	501.8	80.21	421.8	710.4	168.8	542.2
	501.8	170.0	332.1	710.4	209.1	501.8
	501.8	212.7	289.5	718.5	170.0	548.0
	501.8	249.1	252.4	718.5	176.2	542.2
	522.2	100.4	421.8	718.5	216.2	501.8
	532.6	119.8	412.4	725.3	78.62	646.4
	542.2	164.9	376.8	728.3	176.2	548.8
	542.2	252.4	289.5	745.2	212.7	532.6
	545.7	168.8	376.8	745.2	222.5	522.2
	545.7	213.5	332.1	745.2	332.1	412.4
	548.8	80.21	468.3	748.5	216.2	532.6
	548.8	109.1	440.2	765.4	216.2	548.8
	548.8	216.2	332.1	765.4	219.5	548.7
	585.4	209.1	376.8	765.4	222.5	542.2
	615.2	176.2	438.8	791.9	176.2	615.2
	615.2	209.1	405.5	791.9	249.1	542.2
	615.2	240.7	375.0	791.9	289.5	501.8

Table VIII continued

Pb^{204} Single	Sum 1	+ 2	Single	Sum 1	+ 2
832.3	168.8	663.1	1056.7	213.5	844.1
832.3	170.0	661.5	1056.7	222.5	834.3
832.3	289.5	548.2	1056.7	291.0	765.4
832.3	330.9	501.8	1056.7	330.9	728.3
834.3	412.4	421.8	1056.7	332.1	725.3
834.3	109.1	728.3	1056.7	144.5	911.5
834.3	219.5	615.2	1056.7	212.7	844.1
834.3	249.1	585.4	1139.8	222.5	918.4
834.3	332.1	501.8	1139.8	240.7	899.2
844.1	78.62	765.4	1139.8	375.0	765.4
844.1	375.0	468.3	1139.8	421.8	718.5
844.1	405.5	438.8	1139.8	460.3	671.0
899.2	252.4	646.4	1203.9	412.4	791.9
899.2	376.8	522.2	1203.9	438.8	765.4
911.5	78.62	832.3	1203.9	532.6	671.0
911.5	119.8	791.9	1203.9	542.2	661.5
911.5	240.7	671.0	1211.5	376.8	834.3
911.5	249.1	661.5	1211.5	501.8	710.4
911.5	684.0	227.1	1211.5	548.8	661.5
911.5	289.5	621.7	1211.5	548.8	663.4
918.4	170.0	748.5			
918.4	332.1	585.4			
918.4	326.8	542.2			
933.6	100.4	832.3			
933.6	140.9	791.9			
933.6	168.8	765.4			
933.6	184.9	748.5			
933.6	209.1	725.3			
933.6	222.5	710.4			

Table VIII continued

Single	Sum 1	+ 2	Single	Sum 1	+ 2
Pb^{205}					
526.0	32.8	493.5	1502.5	744.6	758.6
910.7	284.0	626.2	1552.0	580.3	1002.7
987.5	284.0	703.3	1614.6	703.3	910.7
1002.7	91.9	910.7	1614.6	626.2	987.5
1043.5	284.0	758.6	1614.6	570.7	1043.5
1043.5	493.5	550.3	1614.6	112.2	1502.5
1043.5	511.7	531.1	1777.4	703.3	1073.3
1073.3	493.5	579.7	1863.3	511.7	1351.5
1337.0	349.3	987.5	1863.3	526.0	1337.0
1337.0	579.7	758.6	1906.5	570.7	1337.0
1351.5	349.3	1002.7			

Pb^{203}

Sums of two				Singles	Δkev	Δ %
60.1	+	708.4	=	186.5	0.0	.00%
				186.5		
824.9	+	708.4	=	1533.3	3.1	.2%
				1536.4		
Sums of two				Sums of two		
186.5	+	819.8	=	1006.2	0.3	.03%
381.5	+	625.0	=	1006.5		
264.0	+	824.9	=	1088.9	1.0	.09%
381.5	+	708.4	=	1089.9		
606.1	+	824.9	=	1431.0	.5	.04%
708.4	+	722.1	=	1430.5		

B. A Statistical Treatment of Transition Sums

In any such work as this, in which a large number of transitions are found, the question always arises as to the validity of a decay scheme based upon arithmetical treatment of the transitions. It is common practice to compare all sums of two transitions with all single transitions and all other sums of two, and to note those that agree within certain set limits of error. A less common practice is to take all the differences of two transitions and compare these with all single transitions and all other differences. A study involving sums of three is rarely attempted with large numbers of transitions.

Applying much the same method as one would to chances involved in coincidence counting, one can obtain a rough value for the accidental agreement of such sums. This was done with the assistance of Prof. John Rasmussen. If one assumes a random distribution of transitions, ρ, expressed as gamma rays per kev, then one obtains an expectation for singles of

$$P_1(E) = \rho$$

in the energy interval one chooses to consider (see Fig. 6).

A similar expectation of sums of two transitions would extend over twice the interval over which the singles are spread. For convenience, consider the singles to extend over an energy interval from 0 to I; then the sums of two would go from 0 to 2I. The total number of sums for ρ gamma rays in an interval is $1/2\ (\rho\ I)^2$. Also, the area beneath the curve is $1/2\ (\sigma\ 2I)$, as shown in Fig. 6, where σ corresponds to the geometrical height of the triangle. Since both are equal one finds, upon equating,

$$\sigma = 1/2\ \rho^2 I.$$

The expectation function for the sums of two then becomes

$$P_2(E) = \frac{E\,\rho^2}{2} \quad (\text{for } E \leq I)$$

$$= (2I - E)\,\frac{\rho^2}{2} \quad (\text{for } I \leq E \leq 2I).$$

Now one needs to consider the limits of error involved. The percentage error can be expressed as $E\delta$, where δ is the percent error and E the energy as noted above. The combinations of these

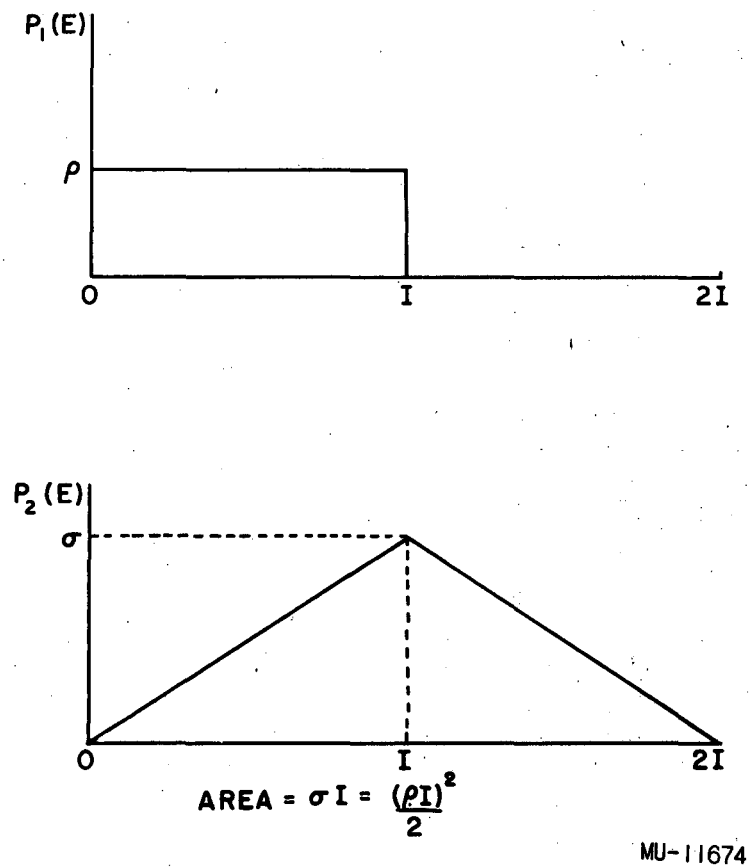

Fig. 6. Probability distribution of transitions.

expectation functions are as follows:

Singles-singles,

$$P_1(E) \cdot P_1(E) \cdot 2E\delta = 2\rho^2 E\delta;$$

Singles-sums of two,

$$P_1(E)\, P_2(E) \cdot 2E\delta = \rho^3 E^2 \delta;$$

Sums of two-sums of two,

$$P_2(E)\, P_2(E) \cdot 2E\delta = 1/2\, \rho^4 E^3 \delta.$$

In order to obtain total chance expectation it is necessary to integrate the combined expectation function over the energy interval. For the integration over the interval 0 to I, the results are:

Singles-singles,

Total chance expectations = $\rho^2 \delta I^2$;

Singles-sums of two,

Total chance expectations = $1/3\, \rho^3 \delta I^3$;

Sums of two-sums of two,

Total chance expectations = $1/8\, \rho^4 \delta I^4$;

These formulas may now be applied to actual cases, but for illustration a series of calculations based on the assumption of 10, 50, and 100 transitions in the region from 0 to 1000 kev are shown in Table IX. The percentage error assumed, δ, is 0.1%.

The last part of the illustrative calculation pertains to the question of a number of sums agreeing with one single transition. The expectation for n sums to be within the set limits of error of agreement with a particular single is, then, the chance expectation to the nth power.

The results seem discouraging for those cases in which there are many transitions. It would seem then that any decay-scheme construction is difficult when sums of two are used with sums of two as a basis. The use of singles with sums of two seems to afford the greatest prospect of success in establishing a decay scheme.

The main fault in these calculations is the initial assumption of a random distribution of transitions. No account has been taken of any order in distribution of energies; and if such order exists in these difficult cases, the chance coincidences may well be less.

Table IX

Total Chance Expectations of Transitions

Transitions	ρ		
	0.01	0.05	0.1
single-single	0.1	2.5	10
single-sums	0.33	41.3	333
sums-sums	1.25	782.0	12,500
$(\text{single-sum/kev})_{1\ \text{Mev}}$	0.001	0.125	1

VII. COINCIDENCE STUDIES

A. Bismuth-203

Because the Pb^{203} gamma spectrum is highly unresolved, (as previously discussed), and the work done on Pb^{204} showed few conclusive data, no coincidence work of any sort was attempted for Pb^{203} (Bi^{203}).

B. Bismuth-204

Coincidence studies were carried out in an attempt to ascertain the level scheme of Pb^{204}. The instruments used were two gamma-gamma coincidence systems, one with a resolving time of about 10^{-7} second[46] and the other 10^{-9} second.[47] An electron-electron coincidence arrangement was also utilized.

As already mentioned, the only three photopeaks discernible in the Pb^{204} gamma ray spectrum are the 375- and 671- kev peaks and that for 899-kev plus 912 kev. Initially, and without full realization of the complexity involved gamma-gamma coincidences were run with the prominent photopeaks, with the help of Frank S. Stephens.

The results of the gamma-gamma coincidence runs using K x-rays, 375-kev gamma-rays, and the 900-kev peak as gates, showed little difference from the singles spectrum except in the intensity of the peak gated upon. The similarity in results was caused naturally by the underlying continuum of gamma rays associated with Bi^{204} and Bi^{206} decay. This meant, considering the window width of the gate, that one always had a large mixture of gamma rays involved, so that the average result of all the coincidences was more or less the same.

The results one was able to obtain from this are only in terms of the K x-rays and the 375-kev and 900-kev peaks, since these are the only peaks capable of being resolved. The 375-kev gamma ray was 31% in coincidence with K x-rays, in contrast to 54% for the 900-kev peak. The difficulty here is that there is no convenient measure of the Bi^{206} present in the sample because of the inherent complexity, and therefore the assumption was made, in obtaining these results, that all the K x-rays could be attributed to the decay of Bi^{204}.

When coincidences were run with the 375-kev gamma ray as the gate the 900-kev peak was in approximately 100% coincidence, while the K x-rays were there in about 250% coincidence. The value for the 900-kev peak agrees with the known Pb^{204m} decay scheme. The value for the K x-rays is only roughly approximate, since a 500-milligram silver absorber was used in this work to diminish the K x-ray stack-up with the other peaks. The absorber reduced the K x-ray intensity by a factor of about eight. The results obtained with the 900-kev peak as the gate show about 40% coincidence with the 375-kev gamma ray and about 40% again with the K x-rays. The value for the K x-rays is again only approximate. The 40% figure for the 375-kev transition is in agreement with the previous gamma work.

The high-energy region, above 900 kev, was also studied. A continuum was observed with a few small variations. The tail of this continuum extended out to 2.3 Mev. In order to diminish any stack-up problems, the singles spectrum was run with a 4-gram lead absorber in front of the NaI detector, since a relatively strong sample was required. The integrated number of counts above 1100 kev was about 300, while the total number of counts in the 900-kev peak amounted to 4170. The values one obtains upon correcting these figures for absorption by the lead and for efficiency of the detector are approximately

Energy	Counts
900 kev	135,000
1100 kev	~ 120,000

If one considers the three small variations upon this high-energy continuum at 1300, 1400, and 1800 kev as peaks, one finds (after correcting for absorption and efficiency) that they correspond to 12% of the 900-kev peak. In all of this it should be remembered that the 900-kev peak is complex, composed of about 15% of the 912-kev and 85% of the 899-kev transitions.

Coincidences were run with the high-energy region by means of an integrated gate that accepted all gammas above 1100 kev. Once

more, to avoid stack-up with K x-rays, a 500 mg silver absorber was used. For 20,000 events recorded by the gate the 375-kev gamma ray was in 22% coincidence, while the 900-kev peak had 35% coincidence. The rough indication here is that a considerable amount of the depopulation of the high-energy transitions goes through to the second excited state. Undoubtedly stack-ups of the 375- and 900-kev peaks with other peaks in the continuum are included in these coincidences, but no correction is available for these.

The values for the percent coincidences are in all cases based on an approximate 1/3 geometry factor for the detector. This value is good to within about 10%; however, no account is taken of electronic efficiencies. It was interesting to observe in all cases a high-energy shoulder on the 900-kev peak, which was attributed to stack-up with K x-rays and low-energy gamma rays that were not entirely removed by the silver absorber.

It seems that no decay scheme could be ascertained from the above gamma-gamma coincidence work. The one avenue of approach still remaining was to take advantage of the known delay of 3×10^{-7} sec in the second excited state. For this purpose a fast-coincidence apparatus was utilized, with the aid and cooperation of Donald Strominger, the resolving time of which was on the order of 10^{-9} sec. With this circuit it was hoped that one could distinguish between the transitions going through the second excited state and those going directly to the first excited state.

In order to test the circuit experimentally, a Pb^{204m} sample was examined. The singles spectrum showed the broad complex 900-kev peak and the 375-kev peak. By running prompt coincidences with the 900-kev peak (in order to avoid the inherent underlying Compton continuum of the 375-kev peak), we were able to so drastically reduce the size of the 900-kev peak that the only photopeak present was the 375-kev one. This clearly showed that the circuit was able to differentiate between the 912-kev transition, which was delayed by 3×10^{-7} sec, and the prompt 899-kev gamma ray. Prompt coincidences were then run with a Pb^{204} sample, again gating on the 900-kev peak.

A large 375-kev peak was observed along with some indication of the 900-kev peak. No other peaks were observed in the spectrum. Inserting a delay of 1.6×10^{-7} sec into the coincidence circuit, one was able to observe the 900-kev peak prominently, while the 375-kev peak was almost completely gone. Again there were no other prominent gamma rays apparent. These fast-coincidence results seem to rule out any chance of gaining needed experimental knowledge of the decay scheme through the gamma rays involved, possibly because of the poor resolution associated with the gamm-ray detection.

It was hoped that use of electron-electron coincidence, with its increased resolution, would bring forth some results. With the cooperation of Jose Juliano this was tried with the back-to-back lens spectrometers. These are essentially two iron-free beta-ray spectrometers so arranged that 180° coincidences can be carried out. Each has a resolution of approximately 2% and a transmission of about 1%. The electron spectrum obtainable with this instrument was comparable with that obtained on the magnetic-lens spectrometer previously discussed. From earlier work on the instrument, the resolving time of the circuit was found to be 3×10^{-7} sec. One serious disadvantage of this instrument was found in the NaI detectors used in the lens spectrometers. Because of the long light pipes required, the background count was high, 3700 cpm on one side and 2700 cpm on the other. Four peaks were studied in the electron spectrum: the 375-kev K line; the 671-kev K line; the 900-kev K line, which was composed about 85% of the 899-K line, and the first discernible high-energy peak; and the 1044- and 1056-kev K lines. The 1044-kev K line was long-lived, and belonged to the decay of Bi^{205}.

The results of the coincidence experiments carried out are listed in Table X. These results seem to indicate that, in addition to the well-established coincidence between 899-, 375-kev K lines, the 671 may be in coincidence with the 899-kev and the 375-kev K lines, suggesting that it perhaps populates the second excited state.

It is more difficult to draw a conclusion concerning the 1050-kev K line. Unfortunately a chance counting rate was not obtained experimentally, and one is always a bit skeptical about assuming a resolving time that was measured at a previous date.

Table X

Electron-Electron Coincidence Results

Energy of K-line gate (kev)	Peak (cpm)	Energy of K line in coincidence (kev)	Peak (cpm)	Coincidence (cpm)	Calc. chance (cpm)
899	8300	375	9200	1.3	0.7
671	4400	375	6700	0.9	0.4
671	4300	899	7800	0.8	0.4
671	4100	1050	110	0.25	0.11
899	6200	1050	110	0.3	0.15
375	11,500	1050	110	0.35	0.22

However, the point brought out by this work is shown in the 1050-kev K-line coincidence study. The majority of the transitions occurring in Pb^{204} are of this nature, weak and unresolved in a crude electron spectrum. It is clear that as high a counting rate as the one used is not desirable with an instrument of such slow resolving time, in that it produces such a large chance rate. Ideally, a low counting rate and a long counting time are needed. Unfortunately, for a nuclide like Bi^{204} with an 11-hr half life, long counting times are difficult because the Bi^{206} activity grows in rapidly. In light of these results it would seem then that electron-electron coincidences with the present instrument are not satisfactory in determination of the decay scheme.

The experimental coincidence work done offers little hope of thoroughly examining Bi^{204} decay. Perhaps the best means of studying Bi^{204} would be afforded by electron-gamma coincidence, where one could obtain the advantage of a high-resolution gate but a high geometry factor could still be retained.

C. Bismuth-205

Before one can attempt to carry out coincidence studies of any sort, a sample of pure 15-day Bi^{205} is required, especially free of any large quantities of 6-day Bi^{206}, whose reported decay scheme is just slightly less complex than that of Bi^{205}. As previously stated, the Bi^{205} was prepared by bombarding a mixture of Tl^{203} and Tl^{205} with 28-Mev alpha particles (remaining below the (α, 3n) threshold). By this means the most favorable ratio of Bi^{205} to Bi^{206} activity is obtained. The resulting activity was then studied in the permanent-magnet spectrographs and no coincidence studies were attempted until the electron spectra showed the absence of all but the most intense Pb^{206} lines. A sample was also followed periodically in the 50-channel pulse-height analyzer to ascertain the amount of Bi^{206} present. After a period of about 2.5 months, or about five half-lives of Bi^{205}, the activity remaining had little Bi^{206}. It was with this source that the gamma-gamma coincidence work was done with the help of Donald Strominger.

Because of the convenience of the long half life, 15 days, it was possible to cover the gamma-ray spectrum quite thoroughly, the prominent peaks at 570, 703, 1000, and 1770 kev as gates, as well as attempting to gate with unresolved gamma rays known from the conversion electron work. As would be expected, only the prominent peaks were successfully investigated. The over-all continuum due to the Compton-scattered gamma rays and unresolved photopeaks was too large to permit study of other gamma rays in detail.

The results of the work showed that the photopeak at 1770 was partly in coincidence with the 703-kev transition. On the basis of an integral gate, which considered all pulses above 1750 kev, one finds that the 703-kev transition is in about 25% coincidence with a transition of more than 1750 kev energy. The only other conclusive result obtainable from the gamma-gamma coincidence work was that the 570-kev transition is in coincidence with the 1044-kev gamma. This distinction between the equally intense 988- and 1044-kev gamma rays was accomplished by using a very narrow window on

the gate, so that coincidences were found predominantly on the high-energy side of the broad 1000-kev photopeak. Considering the entire peak, the 570 was in approximately 20% coincidence. The percent coincidence quoted is only an approximate value, since not only geometry but also the electronic efficiency of the coincidence circuit had to be estimated.

A search was conducted for a short-lived isomeric state in Bi^{205} decay. By gating with the K x-rays and comparing the resulting coincidence spectrum with the singles spectrum, one was clearly able to discern that none of the more intense transitions was delayed, since both spectra were almost identical. By gating on the K x-rays and inserting appropriate delays into the coincidence circuit, one could set a limit of about 5×10^{-9} sec on the 703-kev E2 gamma ray. An approximately corresponding limit can be set upon the other transitions.

Electron-electron coincidences were attempted on a sample of Bi^{205}; however, it was too weak at the time to enable one to do a great deal with it. By examining in coincidence two of the more intense lines in the spectrum, the 284-kev K line and the 703-kev K line, one was able to conclude--on the basis of the negligible counting rate--that the 284-kev transition was an M1 and the 703-kev transition was an E2, if they were in coincidence. In terms of transition intensity, this would mean that the 703-kev level is being populated only to a very small extent by the 284-kev transition, and the particular conversion coefficients involved are the basis for almost equal intensity of the two lines in the conversion-electron spectrum.

As with Bi^{204} coincidence work, very little information can be obtained beyond establishing the most intense gamma rays in the decay scheme. As with Bi^{204}, it would perhaps be fruitful to examine a sample of Bi^{205} by means of electron-gamma coincidence. The convenient half life of Bi^{205} also suggests more intensive electron-electron coincidence work, since the long counts necessitated to establish a true coincidence are easily achieved.

D. Positron Decay

1. Bismuth-204

In order to determine the maximum number of positrons per disintegration, gamma-gamma coincidences were run with the 510-kev annihilation radiation energy, with the cooperation of Donald Strominger. The experimental procedure was to place the two NaI detectors 20 or 30 cm apart at an exact 180° angle, and then set the single channel used as the gate on the annihilation peak at 510 kev. The signal side was fed into the 50-channel pulse-height analyzer. Because of the nature of the annihilation process, conservation of momentum requires that the two 510-kev gamma rays be emitted at 180°. Therefore, if one detects a 510-kev gamma ray on the gate side of the coincidence arrangement, one can expect another 510-kev gamma ray at the signal side in about 100% geometry--providing, of course, that the two detectors are on an exact 180° angle to each other.

On the other hand, coincidences occurring between transitions present in the decay scheme are reduced by a factor equal to the geometry involved. This method then provides a means by which a small unresolved annihilation peak can become a prominent peak in the spectrum.

Experimentally the Bi^{204} source was compared to a Na^{22} standard which decays 100% by positron emission. This enabled one to obtain a value for the crystal efficiency and any electronic efficiencies involved. The results of the Bi^{204} work allow one to set a generous upper limit of 0.6% for positron emission. It is a limit because there was no discernible peak. The spectrum obtained in coincidence was quite analogous to almost every other coincidence spectrum taken of Pb^{204}. In order to set this limit, the region determined by the Na^{22} annihilation peak was assumed to be all due to positron emission (after a suitable background correction had been made).

This result is in agreement with the limit found in Bi^{206} decay by Pryce and Alburger[6] of 0.04%. The indications seem to be that the decay of odd-odd nuclei such as Bi^{204} and Bi^{206} proceed almost entirely by electron capture, with no measurable amount of positron emission.

2. Bismuth-205

The search for positrons in Bi^{205} was made in exactly the same manner as in Bi^{204}. The Bi^{205} source used was a rather weak one because of the desire to insure the absence of the other activities. A correspondingly weak Na^{22} standard was chosen.

The coincidence spectrum obtained was unlike any of the previous coincidence spectra of Bi^{205}. It was, however, quite similar to the Na^{22} spectrum. The value one could set upon positron emission was 3.3%. This is undoubtedly a fair measure of the actual positron emission present in Bi^{205}, since the resulting spectrum was indicative of positron emission and nothing else.

The result would indicate that 3.3% of the decay is occurring through positron emission and 96.7% by electron capture. As the odd-odd nuclei such as Bi^{204} and Bi^{206} do not have a measurable amount of positron decay, this value of 3.3% for the odd-even nucleus Bi^{205} must represent to some extent a characteristic of the neutron pairing found in Bi^{205}, but not in Bi^{204} or Bi^{206}.

VIII. STUDIES ON ISOMERIC STATES

A. Lead-203m

A 5.6-sec isomer of Pb^{203m} was first found by Hopkins[11] and assigned to Pb^{202m}. The later assignment to Pb^{203m} was made by Fischer.[12] The value obtained for the half life in this work was 6.6 sec. In both cases the isomeric transition decayed by a gamma ray of about 800 to 900 kev energy.

A series of experiments was therefore designed to clarify the energy and half life of the isomeric state in Pb^{203}. The half-life experiments were carried out with the use of a single-channel pulse-height analyzer connected to a Speedomax pen recorder. The chart travel time was adjusted to a maximum, the speed of which was 30 in./min, or 1 inch every 2 sec. By placing the Pb^{203m} activity in the counter and following its decay curve as traced by the pen upon the Speedomax, one could conveniently determine a half life. The minimum half life that can be measured by such means is dependent on the cross-chart travel time for the particular pen. On the recorder used this was 1 sec; therefore a generous lower limit on the half lives that could be measured would be about 2 sec.

The chemistry used was the procedure described previously, except that the parent Bi^{203} activity was allowed to remain upon the Dowex-1 column. The Pb^{203m} was milked off the column with a small volume of 0.1 N HCl, which was rapidly forced through the column and onto a platinum plate. The plate was immediately placed in the counter. The entire time required was only about 5 sec.

In actual practice the single channel was set on the x-ray peak and the window set at the fullest width, including most of the low-energy backscatter peaks within the range. It was thought to obtain in this way as large a counting rate as possible in order to obtain as smooth a curve from the pen as possible. To avoid wasting the time necessary for the recorder to respond to the initial activity, the pen previous to the introduction of the Pb^{203m} activity into the counter was kept near the anticipated initial activity of the sample by means of a long-lived radioactive source which was placed appropriately near the counter, but immediately removed upon introduction of the Pb^{203m} sample into the counter.

The results of a series of runs carried out over a period of 24 hr are given in Table XI. The three groups correspond to three different times during which the experiment was run; the half life obtained was 7.05 ± 0.5 sec. This result was somewhat higher than previously reported ones; however, agreement can be found with the limits of error.

It should be noted that in each case a long-lived tail due to 1-hr Pb^{204m} activity present along with the Pb^{203m} had to be subtracted out. Because of the great differences in half life this presented no problem. A possible reason that could be suggested for a somewhat higher result than the correct one would be the presence of the long-lived activity used to keep the pen in the optimum position. However, this is an improbable source of error, since the activity was removed very rapidly and the very earliest portions of the decay curves analyzed were discarded.

Table XI

Pb^{203m} half-life measurements

Half-life in seconds			
I	II		III
7.5	6.25		7.2
7.35	7.2		7.8
6.25	6.6		6.9
7.7	6.6		
7.2	7.05	Average half life =	7.05 sec
8.4	7.8		
7.5	7.35	Average div. =	0.48 sec
6.6	5.6		
5.6			
7.8			
6.9			

The long-lived component in the sample was shown to be Pb^{204m} by a pulse-height analysis on the 50-channel analyzer. The spectrum showed the presence of two photopeaks, at 375 kev and 900 kev. The activity was also seen to die out with a half life of

about 1 hr, with some indications of an even longer-lived component showing up in the gamma spectrum. A peak corresponding to the 279-kev transition in the decay of the 52-hr Pb^{203} was seen after most of the Pb^{204m} activity had died out.

In order to determine the energy of this isomeric transition more accurately and also to do coincidences upon it, the Pb^{203m} activity was studied on the 50-channel pulse-height analyzer with the help of Frank Stephens. The method employed in this case was to have the Pb^{203m} activity flow directly from the resin bed through the counter by means of a continuous flow of eluting solution through a tygon tubing system. The rate of flow was increased by making the whole system a closed affair with a reservoir providing about 5 to 10 ft of pressure head. After proper lead shielding of the NaI crystal used as the detector, ample activity was available for the coincidence studies.

The resulting singles spectrum of Pb^{203m} shown in Fig. 7 was first looked at thoroughly. The only photopeak seen had an energy of 826 ± 5 kev. This was accompanied by a lead x-ray peak and a backscatter peak. The spectrum of Pb^{203m} was further compared with that of a Mn^{54} standard, containing a single gamma ray of 840 kev. From the almost identical spectra of Mn^{54} and Pb^{203m} it was concluded that there were no other transitions associated with Pb^{203m} whose intensities were more than 2% of the 826-kev transition. A background correction was made by stopping the flow through the tubing and running a background count after a suitable length of time had elapsed for the Pb^{203m} to decay. The background spectrum naturally was that of Pb^{204m}; and by this means a completely pure spectrum of Pb^{203m} could be obtained.

To study the isomeric transition further, coincidences were run with the 826-kev gamma ray as the gate. The only peaks seen in the coincidence study were a backscatter peak of the 900-kev gamma ray and the 375-kev transition, both in Pb^{204m}. These were observed because of the overlap in the gate window width, which included part of the 900-kev gamma peak of Pb^{204m}. The results showed that for 105,000 counts of the gate there were 15 counts

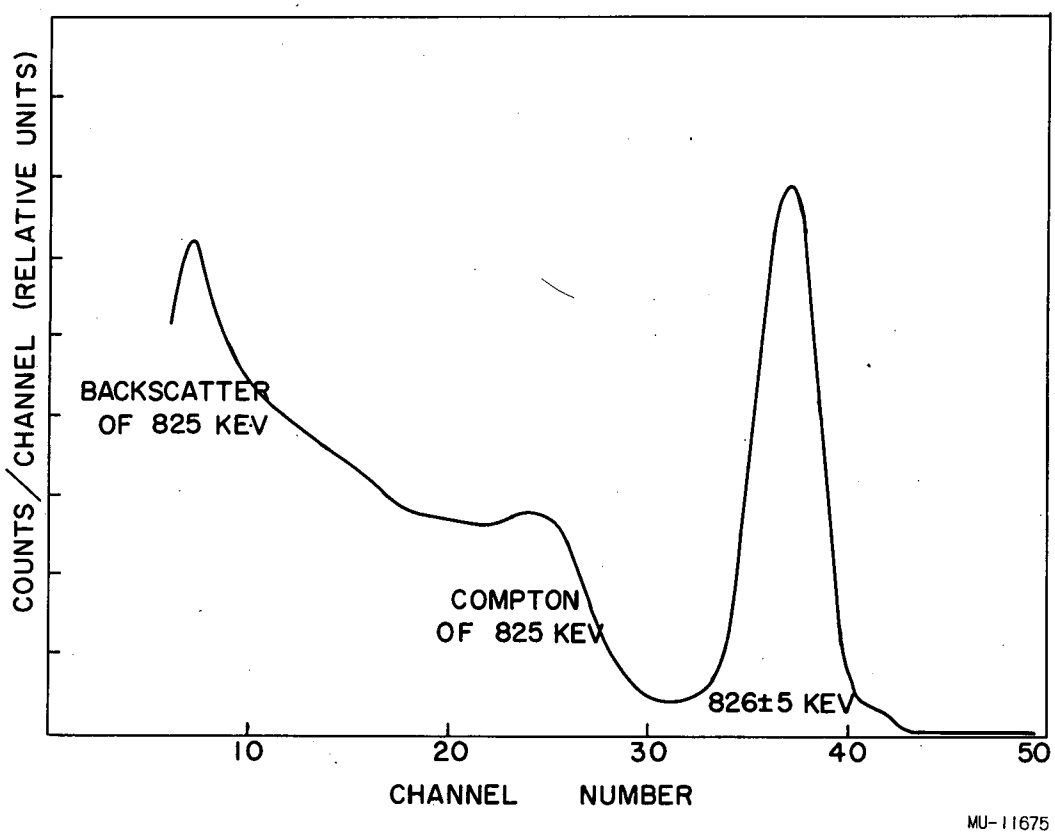

Fig. 7. Pb^{203m} gamma-ray spectrum.

in the 375-kev peak, the largest in the spectrum. This shows conclusively that the 826-kev gamma ray in Pb^{203m} decays directly to ground state and that the isomeric state is at 826 kev. However, one cannot completely rule out levels lower in energy than this, populated by the isomeric state, but can only say that the population--if any--is small and less than a few percent.

B. Lead-204m

Numerous studies have been carried out on the 68-min isomer Pb^{204m}. There are still many points in its decay open to question, however. Since Pb^{204m} is the framework upon which the decay scheme of Pb^{204} must be constructed, a reinvestigation of the isomer was carried out.

Perhaps the most puzzling features of the decay scheme were brought forth by Krohn's and Rabory's gamma-gamma angular correlation work.[14] In order to accept the spin sequence 0+, 2+, 4+, 9- -- which is expected from the multipolarity of the transitions E2, E2, E5--they were forced to conclude that the 375- and 912-kev transitions were of mixed multipolarity. They reported that a 1/2% E2-M3 mixture for the 375-kev gamma ray and a 1% E5-M6 mixture for the 912-kev gamma ray would explain their experimental results. However, they felt that these results could also be explained by the presence of weaker transitions not yet observed in the isomer. Nijgh has noted that the Swedish group in Stockholm has sought other transitions unsuccessfully.[6]

From the permanent-magnet spectrograph work carried out upon samples of Bi^{204} we had great interest in the existence of weaker transitions in the isomeric decay, because the transition data obtained indicated as many as six sums of two gamma rays that agreed within 0.1% with the 911.5-kev E5 isomer transition. It is difficult to explain this large number of sums on the basis of accident, as shown in the statistical arguments presented previously. We therefore carried out two experiments with the permanent-magnet spectrographs in which we attempted to find these weaker transitions in Pb^{204m}. These instruments were chosen because their infinite channel characteristics allowed the whole spectrum to be examined at once.

The Pb^{204m} was obtained in both cases from milkings of Bi^{204} which had been produced and chemically separated as previously described. The Bi^{204} was allowed to remain upon the column and the lead fraction was separated from it by washing with 0.1 N HCl. The Pb^{204m} activity was then electroplated from the solution onto a 5-mil platinum wire in preparation for use in the spectrographs.

In order to obtain the maximum activity available, necessary because of the spectrograph's low transmission, a multiple exposure method was used. In actual practice this consisted of using a series of wires and re-exposing the same photographic plate in the spectrograph in this way building up the intensity of the photographic images. Since the Pb^{204m} half life is about 1 hr, the timetable called for mounting a wire in the spectrograph and replacing it every 2 hr with a fresh source. (For the sake of convenience two different source holders were used for the wires instead of one. A short time before a decayed wire was removed from the spectrograph, a fresh source of Pb^{204m} was milked from the parent Bi^{204}, electroplated, and mounted in the other source holder.) In both experiments six separate wires were exposed. The reason for limiting the number of wires to six in a series was due to the low amount of activity available on the later wires. Initially, of course, some Pb^{204m} produced directly in the bombardment was available, so that the first few wires usually provided 75% of the total activity. The results one obtained were extremely gratifying so far as reproductivity and line shapes were concerned, since they were about as good as those obtained with exposures of a single wire.

In both experiments PM IV was employed, in order to afford as large a geometry as possible and to cover the entire energy spectrum. The lines observed on the stronger of the two plates are listed in Table XII. Transitions corresponding to the 375.0-, 899.2-, and 911.5-kev gamma rays in Pb^{204m} are assigned along with 279.1-kev transition occurring in Pb^{203} decay. The presence of Pb^{203} is explainable if one assumes that the alpha energy used was above the (α, 4n) threshold, thus producing Pb^{203}. The Pb^{203} assignment was further checked by rerunning a wire for a few days; the plate showed the presence of only the long-lived 279.1-kev transition. To clarify the position of the new and unassigned

conversion line at 201.7-kev, a second experiment was carried out, identical to the first except that the alpha energy was kept below the (α, 4n) threshold. The results of this plate were identical with the first except that the 279.1-kev Pb^{203} lines were absent. The 201.7-kev line was again seen in the same intensity.

Table XII

Conversion lines observed in Pb^{204m}

Energy conversion line (kev)	Visual intensity	Assignment Energy (kev)	Assignment Transition
193.7	w	279.1	K (Pb^{203})
201.7	vw	289.5	K
264.7	vvw	279.1	L_1L_2(Pb^{203})
266.9	vvw	279.1	L_3(Pb^{203})
287.7	vs	375.0	K
359.7	m	375.0	L_2
362.2	w-vw	375.0	L_3
371.6	w	375.0	M_2
374.1	vw	375.0	N_2
811.9	vw	899.2	K
824.0	s-m	911.5	K
896.3	m	911.5	L_2
899.8	vw-vvw	911.5	L_3
908.9	w	911.5	M_2
911.6	vw	911.5	N_2

The question then naturally arises as to the assignment of this line. It must first be noted that this same line occurs in the Bi^{204} decay, and is indeed one of the most intense lines seen in this spectrum. The best energy obtainable for this line is 201.5 kev on the basis of the Bi^{204} spectrum. Upon analysis of the Bi^{204} spectrum, the following choices are available in assigning this line as either a K line of a low-multipole-order transition where one would not expect to see the L line in the Pb^{204m} exposure, or as an L line of a high multipole transition where the K-to-L ratio would be such that the K line would not be observed in the Pb^{204m} plates.

If 201.5-kev line is K line

289.5

201.5	273.5 (M)
88.0 K	15.9 L_1
289.5	289.4

If 201.5-kev line is L line

216.6

128.6 (VW)	201.5(VVS)	203.0(MS)
88.0 K	15.2 L_2	13.0
216.6	216.7	216.0

The choice of assignments is straighforward at this point if one realizes that the energies are accurate to within 0.10%. The assignment of the 201.5-kev line would then be satisfied only by the 289.5-kev designation. The absence of the M_1 line, which should be seen, can be explained by the presence of the 375.0-kev K line at 287.0 kev, which would effectively cover up such an M_1 line. The alternate assignment of the 201.5-kev conversion line as an L_2 line of a 216.7-kev gamma ray is poor. The 203.0-kev line does not agree within the limits of error for the L_3 line of a 216.6-kev transition. Since the only possible K and L assignments require the 201.5-kev line to be an L_2 line, and since the K-to-L ratio would indicate a high multipole order, it would be necessary to see a strong L_3 line in conjunction with the 201.5-kev L_2 line. The 203.0-kev line can not cover up the expected L_3 for such a transition, since the L_3 line would be expected at a higher energy. Another factor in favor of the 289.5-kev assignment is that the 128.6-kev line can be assigned as an L line of a 144.5-kev transition, which includes K, L, M, and N conversion lines. The 203.0-kev line can be assigned to a 291.0-kev transition where K and L_1 lines are seen. On the other hand there is no other choice for the 273.5-kev line except to call it a K line by itself; but no L-line assignment is available to go with this K line. Accepting, then, the presence of a 289.5-kev transition, one is tempted to make an M1 assignment to it because of its apparent K/L ratio and L_1 subshell conversion.

The 289.5-kev transition is ruled out as a parallel gamma-ray for the 375-kev gamma ray, since the lower-energy transition, the electron lines of which would be expected to be more intense, is not observed. The 289.5-kev transition could still occupy a position in the decay scheme between the known 2+ and 4+ levels, but this would require only population of the state by a high-energy gamma ray from the isomeric state or a high-energy transition from this state to ground state.

In an attempt to clarify the position of this transition in the Pb^{204m} decay scheme a series of coincidence measurements was carried out with the cooperation of Frank Stephens. Gamma-gamma coincidences were run with an integrated gate that accepted all pulses of higher energy than 1 Mev. A 3-in. sodium iodide crystal was used on the gate side to increase the efficiency of detection for the high-energy gamma rays. This presented a problem as far as stack-up of the gamma rays was concerned. The problem was circumvented by use of a 5-gram lead absorber on the gate side, which effectively absorbed out all the low-energy gamma rays. The results obtained for this arrangement were compared with the ones obtained from gating on the 900-kev gamma-ray peak. In both cases a 375-kev photopeak was observed, with a broad peak corresponding to back-scatter peak.

If one normalized the 375-kev peak in both cases the rest of the spectrum obtained was in good agreement, indicating the absence of other transitions. The coincidences obtained when the high-energy gate was used are attributed to a stack-up of the two 900-kev transitions, which would not be affected greatly by the use of absorber.

The negative results obtained leave only one other choice available for the placement of the 289.5-kev transition. The placement of the 289.5-kev transition as directly depopulating the isomeric state is ruled out because of the K-to-L ratio, which infers a low multipole order and short lifetime. This means that the 289.5-kev transition can be placed only so that it populates the 4+ level. This is in any case the most likely choice when we make a comparison with the levels in the known decay scheme of Pb^{206}. The 289.5-kev transition

would then be quite analogous to the 343.5-kev M1 transition in Pb^{206}. Gamma-electron coincidences were run in order to examine this possibility, but were unsuccessful because of the backscatter peak of the 900-kev gamma rays, which obscured the presence of a weak 289.5-kev gamma ray. The conversion coefficients are such that the 289.5-kev transition is relatively much stronger in the electron spectrum than in the gamma spectrum. A thin anthracene crystal was used as the electron detector and coincidences were run with the 375-kev and 900-kev gamma rays; singles were also run. The resolution available was not sufficient for any conclusions; and although the 900-kev coincidence spectrum looked similar to the 375-kev, no limit could be set.

As the placement of the 289.5-kev transition was unattainable experimentally, the only alternative was to place it in the scheme by use of sums with other weak transitions seen in Bi^{204} decay. No sums were found that would place the 289.5-kev transition between the known Pb^{204} levels. One was therefore forced to choose the most likely placement of the level on semitheoretical grounds and to re-examine the photographic plates for such a transition.

The most likely position that the 289.5-kev transition would occupy is directly above the 4+ state. Therefore, a sum with the 911.5-kev E5 would be required.

A transition was then sought, the energy of which corresponded to 911.5 minus 289.5, or about 622.0 kev; also its multipolarity would probably be E5. The difficulty here is that a somewhat prominent Pb^{206} transition occurs at 620.4 kev. A re-examination of the PM IV plates showed in all cases a line that had been previously designated as broad. There seemed to be the indication of a weaker line of higher energy than the 620.4-kev K line. The PM III plates showed these lines resolved, and it was also probable that a line was read corresponding to the L line of a transition higher in energy than the 620.4 kev. This line, however, is in considerable doubt. These results were:

PM IV

532.7(W)	533.6(VW)
88.0 K-206	88.0 K
620.7	621.6

PM III

532.6(W)	533.9(VVW)	606.4(VVW)
88.0 K-206	88.0	15.2 L_2
620.6	621.9	621.6

Av. = 621.7 kev .

These lines were missed in the initial reading of the photographic plates because of their low intensities. It should be noted that the intensities of K and L lines of the 621.7-kev transitions are about the same, and these and the L_2 subshell all agree with an E5 or other high electric multipole order assignment, providing that the doubtful L line is real. The resulting sum is 621.7 plus 289.5, which gives 911.2 as compared with 911.5 kev, a discrepancy of only 0.03% and well within the limits of error.

The question of intensities still needs to be settled before this assignment can be accepted. The theoretical K-conversion coefficient for a 289.5-kev M1 is about 1, while that of a 621.7-kev E5 is about 0.2, though in this case the theoretical L-line conversion coefficient would also be 0.2. This would mean that in the Pb^{204m} electron spectrum, if the K-conversion coefficients are 50% and 17% respectively, the 621.7-kev K line should be about one-third as strong as the 289.5-kev K line, without consideration of geometrical corrections.

If one considers the geometry involved, the K line of a 621.7-kev transition would have a ρ equal to 17.3 cm, while the 289.5-kev K line would have a ρ of 9.4 cm. This would mean, for equal intensity at the source, that the 621.-kev line would be about half as strong as the 289.5-kev K line on the photographic plate. The expected photographic intensity of the 621.7-kev line on the Pb^{204m} plate would then be one-sixth that of the 289.5-kev K-line. The weakest line detectable in the Pb^{204m} spectrum is about the intensity of the 375.0-kev N_1 line. By visual estimate, a lower limit to detection based on the N line is about

a factor of 2 weaker, on the photographic plate. The 621.7-kev K line would then be about one-third this limit and not expected to be seen. The relative increase in intensity of the 289.5-kev as compared to the 621.7-kev transition in the Pb^{204} spectrum is explainable by assuming population of the 289.5-kev level from other levels in Pb^{204} besides the isomeric state, or by direct electron-capture population.

If this new level is then assigned tentatively as 4+, on the basis of the Pb^{206} comparison and the assumption that the 289.5-kev is an M1 transition, with the 621.7-kev transition assigned as an E5, it becomes possible to make a comparison between the relative abundances of the two E5's. From the Pb^{204m} spectrum, the ratio of the 289.5-kev K line to the 375-kev K line is 0.027. If one uses a conversion coefficient of 50% for the 289.5- and the experimental value of 4.4% for the 375-kev transition, one finds that the transition intensity ratio of the 289.5 to the 375.0 is 0.0024. This corresponds to about 2.4 decays of Pb^{204m} out of 1000 going through the 289.5-kev transition. Theoretically, assuming the usual $2\Delta I+1$ dependence, one finds that the 621.7-kev E5 transition should be about 1/75 as strong as the 911.5-kev. Comparison between the two results shows that the 621.7-kev E5 is slowed down by a factor of approximately 5.

When the approximations made in the foregoing argument are considered, the result seems to be in agreement with what one might expect. A problem arises if the 289.5-kev transition seen in the Pb^{204m} work is not populated by the 621.7-kev E5 transition alone, but the other transitions occur which compete with the 911.5-kev isomeric transition and also indirectly populate the 289.5-kev gamma-ray's level. The 621.7-kev E5 transition might then be slowed down by a much greater factor than five. However, this is usually explainable in terms of a two-particle change between the initial and final configurations involved.

The present experimental work on Pb^{204m} seems to give credence to the existence of another 4+ level in the Pb^{204m} decay scheme, as shown in Fig. 8, which would explain some of the angular correlation results. The 621.8-kev transition is shown by a dashed line in Fig. 8, since it was not observed directly in the isomeric studies.

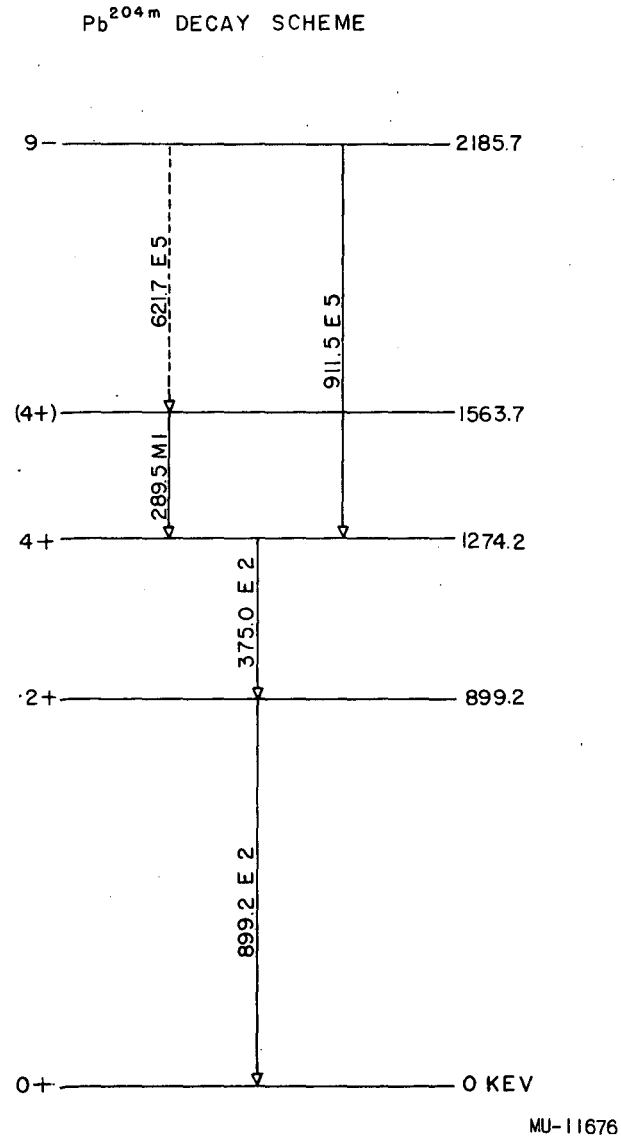

Fig. 8. Pb^{204m} decay scheme.

The six sums obtained from the Bi^{204} decay data that agree well with the 911.5-kev E5 transition energy are still not proved or disproved by this work. However, it is not supposedly possible to study these sums in terms of intensity considerations. Unfortunately, owing to the large errors involved in measuring intensities with the permanent-magnet spectrographs, little of a decisive nature can be done for every sum. The sums in question (listed in Table VII) must be considered rather qualitatively. It would seem likely that no sum involving two strong transitions could be real and still not be observed in the Pb^{204m} work. This would indicate that the sums would be more explainable with one or both of the transitions weak. Most of the sums listed fall into this second category. This problem of intensities will be discussed in greater detail in consideration of the possible decay schemes of Bi^{204}.

C. Lead-205m

Since isomers of Pb^{201}, Pb^{203}, and Pb^{207} are known, a search was made for the isomeric state associated with Pb^{205}. The even-odd isomers of Pb^{203} and Pb^{207} are directly populated to a considerable extent in the decay of Bi^{203} and Bi^{207} respectively,[8, 12] since the ground-state spins of both Bi^{203} and Bi^{207} are probably large. Therefore, it is not unexpected that an isomer in Pb^{205} with the high spin is populated. It was thought, then, that any isomeric state associated with Pb^{205} should be seen through the decay of the 15-day Bi^{205}.

From the known half lives of the 0.8-sec Pb^{207m} [48] and the 7-sec Pb^{203m} isomer[12] one is able to predict a half life of 1.5 to 2 sec for Pb^{205m},[26] assuming an M4 isomeric transition as in the others. Therefore, one could not use the procedure that was outlined in the Pb^{203m} determination, since this half life would be shorter than the cross-chart travel time for the recording pen. One could also say that the energy of the isomeric transition lay between 900 and 1000 kev on the basis of the known Pb^{203m} and Pb^{207m} energies of 825 and 1064 kev respectively. There are two reported Pb^{205} transitions in this region, at 910 and 988 kev.

Two experiments were carried out in the search for the isomer, the second a repetition of the first. In both cases Tl^{203} was bombarded with alpha particles well below the (α, 3n) threshold in order to produce as pure a sample of Bi^{205} as possible. The amount of Tl^{203} was five to six times the normal quantity of Tl^{203} used, in order to compensate somewhat for the Bi^{205} long life. The bismuth activity was subjected to the regular chemical procedure as previously described, but the activity was allowed to remain upon the ion-exchange column.

The column was then fitted into a high-pressure flow system similar to the one used for Pb^{203m}. A reservoir of 0.1 N HCl eluant was placed some 10 ft above the column, providing a considerable pressure. The eluant, upon leaving the column, was immediately led through a long length of 3-mm-bore glass tubing. The glass tubing passed directly beneath the sodium iodide crystal of a single-channel pulse-height analyzer. It was arranged in such a manner that the sodium iodide crystal could be moved along this length of glass tubing in order to determine a half life. The sodium iodide detector was in a lead housing and was further shielded from the bismuth activity on the column by additional lead bricks. The background rate at the minimum distance from the column was 850 counts/min with only the lead housing, but it was reduced to 60 counts/min with these additional lead bricks.

Since the expected energy of the isomer lay in the 900- to 1000-kev region, the single channel was set on 950 kev and the window opened wide. In this manner the expected region was well included.

It was also necessary to determine the flow rate along the glass tubing in terms of centimeters per second. This was done by measuring the time required to have 40 ml flow past a given point. On the basis of a series of measurements conducted at the full flow rate, this was 40 min per 20.5 sec, or the flow along the glass tubing was 27.6 cm/sec.

The results of a series of measurements based on this flow rate are shown in Table XIII. The distances listed in the table are measured from the start of the glass tubing with time zero arbitrarily set at 0 cm. The problem of statistics that had to be contended with is quite evident in the value for the difference at 60 cm.

Table XIII

Experimental search for Pb^{205m}

Distance (cm)	Time (sec)	Total counts/10 min	Background counts/10 min	Difference
0	0	505.3 ± 7.1	450.7 ± 6.7	54.4 ± 13.8
10	0.37	465.8 ± 6.8	427.2 ± 6.5	38.6 ± 13.3
20	0.73	454.5 ± 6.7	426.7 ± 6.5	27.8 ± 13.7
30	1.09	438.9 ± 6.6	422.1 ± 6.5	16.8 ± 13.1
40	1.45	421.8 ± 6.5	413.7 ± 6.4	8.1 ± 12.9
60	2.17	403.3 ± 6.5	429.2 ± 6.5	1.9 ± 13.0

The values in Table XIII when plotted, give a half life of the isomeric state of 0.7 sec, as shown in Fig. 9. The values from 0 to 30 cm lie on the line, but the last two values lie below it. This discrepancy again is within the statistics. This measured isomeric half life is in agreement with the reported 0.799-sec[48] half life of the isomeric state in Pb^{207m}. The Pb^{207m} was observed experimentally because of the wide window chosen in the single-channel pulse-height analyzer, which included the 1064-kev M4 transition of Pb^{207m} in the window range. The limits one can set on any longer-lived state corresponding to Pb^{205m} are that its intensity in the experiment has to be less thab 1/4 that of the Pb^{207m} in order not to be detected. Another less likely alternative would be that the Pb^{205m} has a half life less than 0.3 sec and could not be observed in this experiment.

In order to prove the assignment of this activity to Pb^{207m}, the 570-kev E2 transition associated with Pb^{207m} was looked for with the single-channel analyzer. Because of the crystal efficiency, the 570- could be expected to be more prominent than the 1064-kev transition, but in order to insure an even higher counting rate a somewhat different arrangement was used. A coiled length of small-bore tygon tubing replaced the glass tubing, with the coils of the tubing directly beneath the sodium iodide crystal; the whole was assembled with adequate lead shielding. In this assembly approximately 2 sec was required for the eluant to reach the detector from the resin bed.

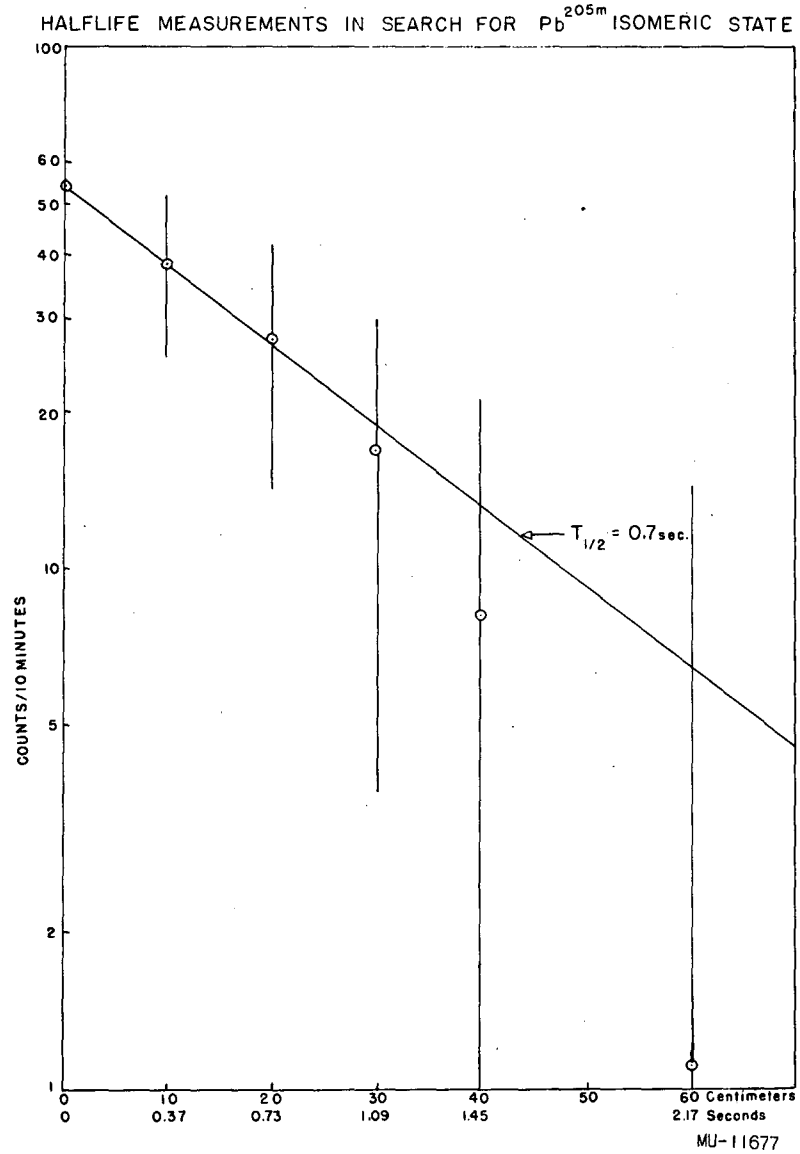

Fig. 9. Half-life measurements in search for Pb^{205m} isomeric state.

The results of this experiment proved the existence of a peak around 570 kev, with a maximum difference between counting rates of 225 counts per min. That this was due to an isomeric state was shown by reducing the flow rate. This was accomplished by removing the reservoir that supplied the pressure. At the reduced flow rate the previous peak-height counting difference was reduced to 10 cpm. The experiment substantiated the assignment of the 0.7-sec isomeric state to Pb^{207m}, and not Pb^{205m}.

It is possible, on the basis of this work, to set a lower limit in the population of the isomeric state in Pb^{205m} by Bi^{205}. Using the facts that the isomeric state in Pb^{207m} is populated 90% by Bi^{207} decay and that the relative cross sections for an (α, 2n) reaction are approximately the same for Bi^{205} as for Bi^{207}, one can determine this limit. Since the target material was isotopically enriched in Tl^{203} to a factor of four to one, the atom yield of Bi^{205} and Bi^{207} should be in a similar ratio. Assuming half lives of 15.3 days for Bi^{205} and 8 yr for Bi^{207},[21] one finds as a result that the population of an isomeric state in Pb^{205m} by decay of Bi^{205} is less than 0.03%.

It should be pointed out that this limit applies to population of an isomeric state in Pb^{205m} similar to the states seen in Pb^{203m} and Pb^{207m}. This would require the isomeric state to decay through an M4 transition. An isomeric state corresponding to this, but decaying by some other means so as to produce in the most likely instance a shorter half life, is not ruled out by these experiments.

IX. DECAY PROCESS

A. Decay Energy

In any attempt to unravel a decay scheme, the decay energy available is an important factor. It becomes especially vital in electron-capture decay, since the decay process involved is not as energy-dependent as beta or alpha decay. The possibility then exists energetically of populating, to some extent, all spin-available states up to the decay energy minus the binding energy.

The decay energy in electron capture is not simply determined experimentally, as is beta or alpha decay, since the energy is carried off by undetectable neutrinos. However, one is able to get a rough value for it by means of an examination of the nuclear energy surface. Glass, Thompson, and Seaborg[52] have constructed a set of self-consistent closed cycles based on experimental results together with nuclear systematics for the heavy-element region.

A value for the decay energy can be obtained directly up on extrapolating the curve of decay energy versus mass number, and these are

Bi^{205},	3.0 Mev;
Bi^{204},	4.7 Mev;
Bi^{203},	3.7 Mev.

A somewhat better value for the decay energy can be obtained if one constructs a series of closed cycles in order to extend the reported cycles into the region of interest. The experimental values available are the decay energy of Bi^{206}, which is 3.7 Mev, and the neutron-binding energy of $Pb^{206-205}$, which has been reported as 8.1 Mev. Extrapolation of the curves of the neutron-binding energy yields the following values:

$Bi^{206-205}$,	7.1 Mev;
$Bi^{205-204}$,	8.5 Mev;
$Bi^{204-203}$,	7.2 Mev;
$Pb^{205-204}$,	6.7 Mev;
$Pb^{204-203}$,	8.6 Mev.

(The choice of 6.7 Mev as the binding energy of $Pb^{204-205}$ will be discussed in connection with Pb^{205} decay.) Using these values, one obtains for the decay energies:

Bi^{205},	2.7 Mev;
Bi^{204},	4.5 Mev;
Bi^{203},	3.1 Mev.

These agree with the previous results within the limits of error, which increase somewhat as one gets away from the known values and relies on extrapolated values.

The results clearly indicate an increase in decay energy with a decrease in neutron number, which seems to insure a greater relative complexity in the energy levels involved. Another means of obtaining an approximate value for the decay energy has not been included here. This is the Bohr-Wheeler parabolas, whose chief success is in the between-shell region, since various parameters need to be assumed. The parameters involved are rather smooth constants except near a closed shell, where there is an abrupt change. Since there were no good means available by which to arrive at these parameters, the method was not successful in application.

B. Log Ft Values

Although log ft values obtained for beta decay are not precise values, for a given spin and parity change, they are helpful in giving an approximate idea of the nature of the states involved. Since it is necessary in arriving at a log ft value to know the decay energy to a particular state and the percent population of that state, one is somewhat at a loss in studying electron-capture decay, in which these values usually are obtainable only after one has arrived at a decay scheme.

However, a more or less average maximum value may be arrived at if the assumptions are made that the decay process populates the ground state of the daughter nucleus 100%. The values one can use for the decay energy of Bi^{203}, Bi^{204}, and Bi^{205} are those obtained from the energy surface. The error involved in using this decay energy is not great, because the electron-capture decay process is rather insensitive to small percentage energy changes. The resulting log ft values, based on the foregoing assumptions are:

	log ft
Bi^{205},	8.5;
Bi^{204},	7.5;
Bi^{203},	7.1.

It must be realized that these represent a sort of average minimum that the log ft values can approach in the particular decay.

Comparison of the known log ft values obtained in the Bi^{206} and Bi^{207} decay with the values obtained for Bi^{203}, Bi^{204}, and Bi^{205} can be fruitful. The decay energies reported for Bi^{206} and Bi^{207} are 3.4 to 3.7 Mev[6] and 2.36 Mev.[8] These are based on the last excited state in the decay scheme. The log ft values are:

	Energy excited state populated (Mev)	Spin	Percentage population	Total decay energy (Mev)	Decay energy to state (Mev)	log ft
Bi^{206}	3.40	5-	55	3.7	0.30	6.4
	3.28	5-	45	3.7	0.42	6.9
Bi^{207}	1.63	13/2+	90	2.36	0.73	10.0
	2.35	7/2-	10	2.36	0.01	7.5

The log ft values obtained in all these cases seem to fall into the first-forbidden group.

The Bi^{206} value can be explained by a spin change of 0, or 1 and a change in parity occurring during the decay process. This would mean that the ground state of Bi^{206} has spin 4+, 5+, or 6+. Pryce and Alburger seem to favor 6+ because of other decay-scheme considerations. The single-particle configuration that one is most likely to attribute to Bi^{206} is

$$(f^{-1}_{5/2}\, p^{-2}_{1/2})_n \;\; (h^{1}_{9/2})_p.$$

This can have spin values of 2, 3, 4, 5, 6, or 7+. The Bi^{204} log ft value of 7.5 is not too very different from the Bi^{206} values, so that a spin change of 0, 1 with a change of parity might be expected in the decay. Since we have no knowledge of the particular states populated

in the decay, one is unable to make a spin assignment for the ground state of Bi^{204}. The particle configuration to be expected is

$$(f^{-3}_{5/2}\, p^{-2}_{1/2})_n\, (h^{1}_{9/2})_p .$$

The spins available are the same as for Bi^{206}, although there is no reason to expect the ground state to have the same spin.

The log ft values obtained for Bi^{207} indicate a spin change of 0, 1 with change of parity occurring in the population of the 7/2- state, which is usually accorded in single-particle terms an $f_{7/2}$ configuration. The population of the 13/2+ state, attributed to $i_{13/2}$, seems to be occurring through a spin change of 2 and a parity change, since its somewhat higher log ft of 10.0 would fall into this class. If one assumes the ground-state spin of Bi^{207} to be the same as Bi^{209}, one arrives at a $(h_{9/2})_p$ configuration. Decay to the $i_{13/2}$ state then is [$\Delta I = 2$, yes]. However, one would expect that the decay of the $f_{7/2}$ state should be allowed, that is 0, 1 spin change and no parity change, and not first-forbidden as the log ft value indicates. This discrepancy can be explained if one realizes that the decay energy is approaching zero, and small errors in the estimate of decay energy greatly affects the calculated ft value. In view of the uncertainty involved in a decay energy for electron capture, this is not too unreasonable.

Examining the log ft values of 8.5 and 7.1 obtained for Bi^{205} and Bi^{203}--on the basis that the ground-state spins of Bi^{205} and Bi^{203} are analogous to Bi^{209}, $(h_{9/2})_p$--one can make a crude prediction as to the states populated. The log ft of 8.5 for Bi^{205} is in the range of first-forbidden values ($\Delta I = 0, 1, 2$, yes). Conceivably an allowed transition can take place, but the energy involved must be very small--on the order of 100 kev or less--similar to that in Bi^{207}. The states one might expect to see populated are those of spin 7/2, 9/2, and 11/2+, and possibly 13/2+. Allowed transitions would involve high-lying excited states of 7/2, 9/2, and 11/2-.

The difference in the Bi^{203} decay, as shown by the log ft value of 7.1, is the possible absence of decay by spin-change 2 and parity change. The possibility is also somewhat greater here for

allowed transitions. The decay energies here can be as large as 1 Mev. The possible states that could be populated would then be 7/2, 9/2, and 11/2+ for the first-forbidden transitions and 7/2, 9/2, and 11/2- for the allowed transitions.

One can expect in Bi^{203} and Bi^{205}--providing the ground states are similar to those of Bi^{207} and Bi^{209}--that a measurable percentage of the population will go to the $f_{7/2}$ state or a state of proper spin which has a considerable fraction of $f_{7/2}$ character. It is important to realize that the population by decay of any particular energy level so close to the closed shells of 82 protons and 126 neutrons is not just a matter of spin and parity. The particular configurations involved for each level become important, since the log ft values should only be adhered to in cases where a one-particle change takes place between the two configurations. When two particles of the configuration are involved in the decay process, one expects it to be hindered. The actual amount that it would be slowed down is difficult to predict. An interesting case that would lie between the two extremes of one- and two-particle changes would be one in which the spin and parity were proper, but the one-particle change required a high spin state such as $h_{9/2}$ to change to a $p_{1/2}$ state. As, for example, a

$$(f^{-2}_{5/2}\, p^{-2}_{1/2})_n\ (h_{9/2})_p,\ I = 9/2- \text{ state to decay to a}$$

$$(f^{-2}_{5/2}\, p^{-1}_{1/2})_n\ \ I = 9/2- \text{ state.}$$

In this instance a hindrance would again be expected, but perhaps to a somewhat smaller extent than in the two-particle case.

C. Lead-205 Decay

On the basis of closed cycles, involving experimentally measured neutron-binding energies and decay energies, it has long been thought that Pb^{205} should decay to Tl^{205}. Glass et al.[52] have reported a calculated decay energy of 440 kev. Measurements of the decay, in which the presence of thallium x-rays was sought, enabled Huizenga and Stevens[53] to set limits upon the half life of more than 6×10^7 yr on the basis of a search for K x-rays. Recently Huizenga and Wing[54] reported a half life of 5×10^7 yr based on observation of

thallium L x-rays of Pb^{205}. Such an extremely long half life is incompatible with a decay energy of almost 500 kev. The log ft value for this would be 15.5 or greater.

If one accepts this half life and decay energy, an explanation of the slowness of decay must be sought in terms of the configurations of the states involved. From the experimental work, which has shown the ground state of Pb^{207} to be $(p^{-1}_{1/2})_n$, Pb^{206} to be $(p^{-2}_{1/2})_n$, and Pb^{203} to be $(f^{-3}_{5/2}\, p^{-2}_{1/2})_n$, it seems almost necessary to accept the ground-state configuration of Pb^{205} as $(f^{-1}_{5/2}\, p^{-2}_{1/2})_n$. The spin of the ground state should then be 5/2. In analogy to Tl^{203}, the expected levels of Tl^{205} should be $s_{1/2}$ ground state, and excited states of $d_{3/2}$ and $d_{5/2}$. The measured spins for Tl^{203} and Tl^{205} ground states are indeed 1/2. On the basis of these configurations perhaps one would expect the decay process to be first-forbidden, with a log ft of about seven, and to populate the excited states of 3/2+ and 5/2+ as in Pb^{203} decay.

A feasible explanation for a log ft of 15.5 does not seem to be provided by the above considerations. One alternative is that the configurations of the states are incorrectly assumed, but this hardly seems likely, since other particle states are energetically unavailable. However, the configurations of these states are not expected to be pure, since mixing can always occur. The second alternative is to assume that the neutron or proton core is involved in the transitions and that the core differs greatly between Pb^{205} and Tl^{205} ground state. This again seems to be a poor solution, since one would not expect such a large core change so close to the closed shell.

The decay of Pb^{205} might be best explained, not by a log ft of 15.5 but by a third alternative, a very low decay energy, which is also suggested by the observed L-capture electron decay and the absence of K capture. To account for this low decay energy a new closed cycle must be constructed for this region. The values reported for the neutron binding energies are:

$Pb^{205-206}$,	8.10 ± 0.10 Mev;[55]
$Pb^{204-205}$,	none;

$Tl^{205-206}$,	6.23 ± 0.05 Mev;[56]
$Tl^{204-205}$,	7.48 ± 0.15 Mev;[57]
$Tl^{203-204}$,	6.54 ± 0.05 Mev.[55]

The reported beta-decay energy of Tl^{206} to Pb^{206} is 1.51 Mev, and that of Tl^{204} to Pb^{204} is 0.77 Mev. A cycle constructed on this basis yields the values of 360 ± 150 kev for the decay energy of Pb^{205} and 6.35 Mev for the neutron-binding energy of $Pb^{204-205}$, as shown in Fig. 10. If one constructs a plot of odd neutron-binding energies as in Fig. 11, one observes that this calculated value seems much too low in comparison with the thallium values.

The problem can be completely resolved if we assume that the binding energies for $Tl^{203-204}$ and $Tl^{205-206}$ are reversed. Their original assignment was made by Harvey[55] on the basis of (d, t) reactions using only one sample, which was 70% Tl^{205} and 30% Tl^{203}. Harvey noted that the expected peaks should be equally intense, but no mention was made of how a specific assignment was reached. The values used are those obtained by Kinsey[56] in his (n, γ) work, in which he apparently accepted Harvey's initial assignments. Because there seems to be no reason why the assignments cannot be reversed, we have recalculated the energy cycle, using the reversed thallium binding energies (i.e., $Tl^{205-206}$ = 6.54 ± 0.05). The closed cycle obtained is also shown in Fig. 10.

The decay energy of Pb^{205} then is 50 ± 150 kev, while the binding energy has increased to 6.66 Mev. This binding energy results in identical slopes for the thallium and lead odd-neutron binding energy curves, as shown in Fig. 11, which would seem more satisfactory on systematic grounds.

The results of Huizenga and Wing[53] are in agreement with this low decay energy obtained. If one accepts these results it would seem that the decay energy must lie between 85.5 and 12.7 kev, corresponding to the K and L_{III} binding energies.

A low decay energy such as this implies that Pb^{205} can decay only to the ground state of Tl^{205}, since the first excited state analagous to Tl^{203} probably lies at 280 kev. As the ground state of Pb^{205} is thought to be 5/2- and that of Tl^{205} to be 1/2+, the decay must occur

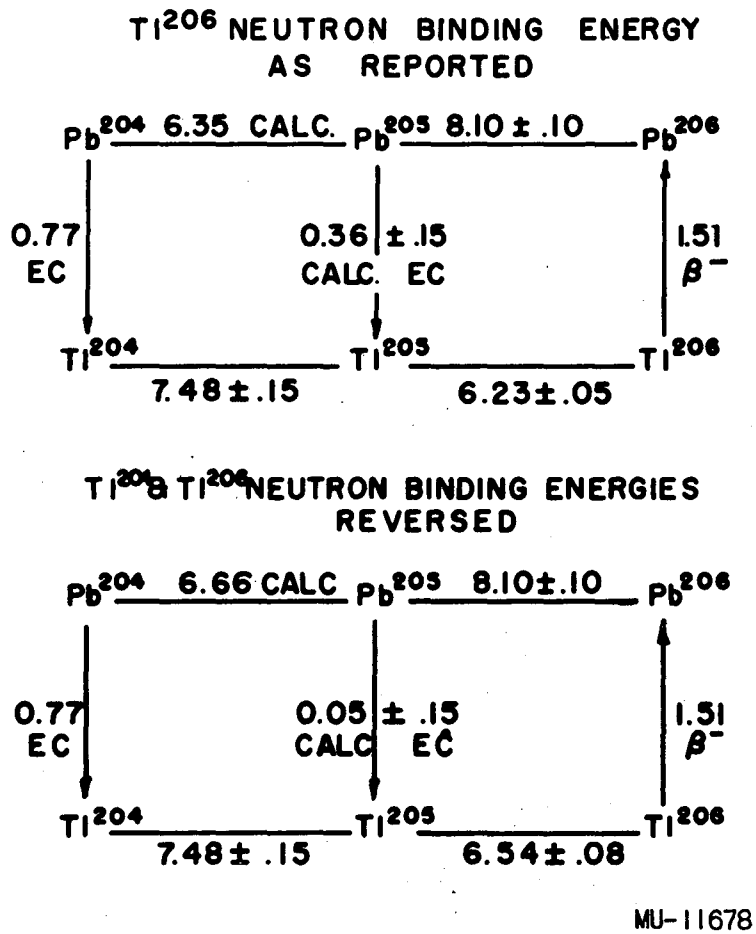

Fig. 10. Pb and Tl closed cycles.

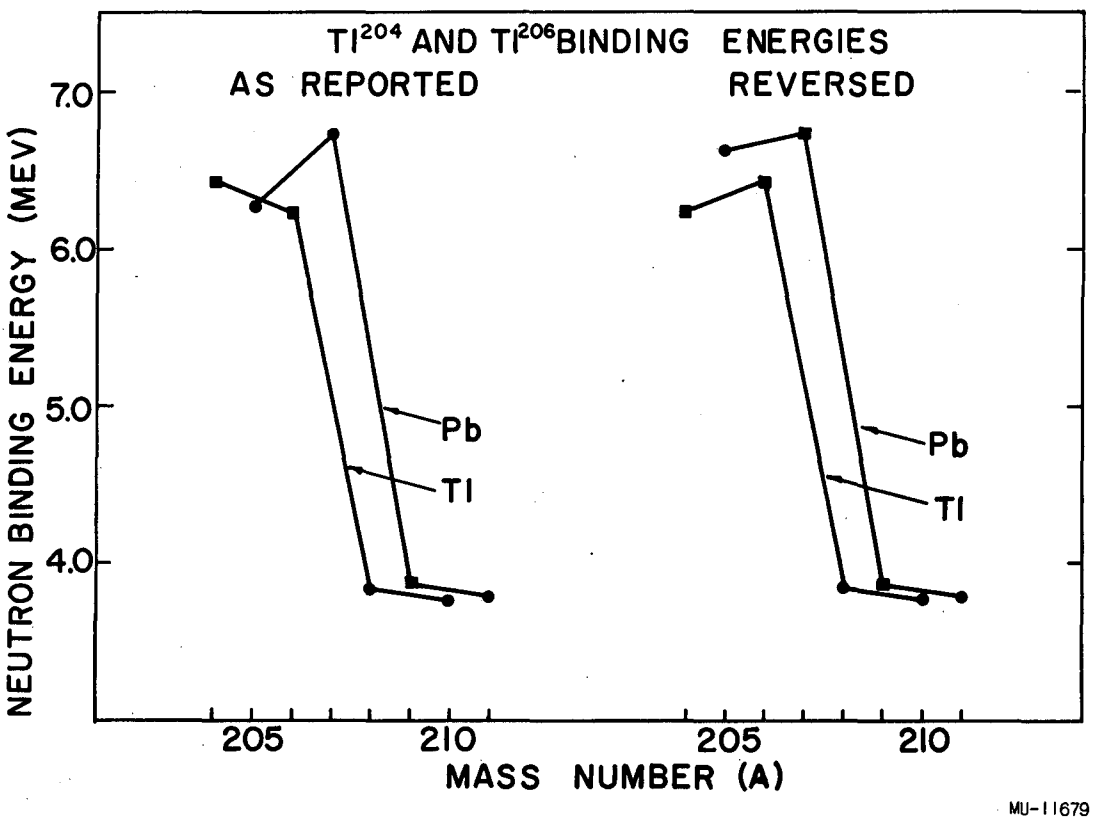

Fig. 11. Pb - Tl odd-neutron binding energies.

through a [$\Delta I = 2$, yes] transition-- a unique first-forbidden. This would mean that the log ft to be expected should be 9 or 10. From the work of Brysk and Rose[58] and that of Hoff and Rasmussen[59] it is possible to show that for L electron-capture of Pb^{205} the decay energy must be of the order of 16 kev to explain both the 5×10^7-yr half life and a log ft of 9 or 10. This value of the decay energy is within the limits of error of the closed cycles, and also satisfactory in the light of the L capture observed by Huizenga and Wing.

The experimental observance of L electron-capture decay clearly indicates that the binding energies of Tl^{204} and Tl^{206} had heretofore been reversed. The long half life of Pb^{205}, and the ground-state assignments of $f_{5/2}$ to Pb^{205} and $s_{1/2}$ to Tl^{205}, are now acceptable if one assumes that decay energy is about 16 kev.

X. CONCLUSIONS

A. General Discussion

The three most striking observations in the experimental work on the levels of the light lead isotopes are the complexity of levels, the presence of the long-lived isomeric states, and the trend for the transitions to group more or less about certain preferred energies. All three results can be explained in terms of a modified single-particle shell-model theory. The application of this theory as presented by Pryce and applied by him to the Pb^{206} energy levels has been extended by W. W. True to Pb^{204}. No theoretical work to date has been reported on the Pb^{205} and Pb^{203} energy levels, although Pb^{205} should be susceptible to treatment, whereas Pb^{203} should be somewhat more difficult because of the five neutron holes involved in the configurations.

The single-particle states dealt with here are shown most clearly in the energy levels of Pb^{207}. From the interpretation of the experimental results the following spacings are indicated:

Single-particle excitations	Energy (kev)
$p_{1/2} \rightarrow f_{5/2}$	570
$f_{5/2} \rightarrow p_{3/2}$	~ 300
$f_{5/2} \rightarrow i_{13/2}$	1060
$f_{5/2} \rightarrow f_{7/2}$	1780

These are by no means the precise values to be expected throughout this region, but they will serve as approximate values for any of the nuclides in question.

In more general terms, however, the theory predicts a large number of levels, as in Pb^{206} and Pb^{204}, although the Pb^{206} experimental work showed that many of the levels predicted theoretically are not populated. The factors that give rise to this complexity--in addition to the a priori existence of the levels--are the mode of decay, the decay energy, and the transitions between

the levels. Since decay proceeds almost entirely by electron capture, population of the higher excited states is possible. This is a direct result of the fact that electron-capture decay depends only on the square of the neutron energy, and therefore is rather insensitive energywise. For example, if the decay energy to two states were 5 Mev and 1 Mev, the former would be only 25 times as fast as the latter if the decay proceeded by electron capture. The factor would be 1000 if it were beta decay. Of course, a necessary requirement is that the decay energy be large and permit a population of higher excited states. In Bi^{203} and Bi^{205} the energy is about 3 Mev, while in Bi^{204} the decay energy is even greater, 4.5 Mev. These factors by themselves contribute to the complexity.

The complexity is also enhanced to some extent by the nature of the transitions involved between the levels. Since the nuclides are so close to the closed shells, the configurations involved in a transition between two levels become an important consideration. Two-particle changes or large Δj changes in configuration would mean that the transition is slowed, even if permitted by the spin and parity selection rules. Because there is a mixing of configurations in most states the amount of this hindrance cannot easily be estimated. However, the possibility arises of observing lower-energy transitions, which would normally not be seen, in competition with a higher-energy transition if the higher energy one is slowed by a sufficiently large factor. This process would of course work both ways, so that some expected lower-energy transitions would not be seen because of configurational hindrance.

The presence of long-lived isomeric states in the lead levels is a result of the proximity to the closed shell, since it is here that one finds particle states of greatly different j lying close to one another. In the lead isotopes the states involved are the $I_{13/2}$ and $f_{5/2}$ states. For single-particle states an M4 transition would be predicted, and experimentally such isomeric transitions are found in the even-odd isotopes of lead, where the lower excited states closely approximate the single-particle states. (The absence of an isomer in Pb^{205} is discussed in the section on the Pb^{205} energy levels.)

The even-even isomeric states can be interpreted according to Pryce in terms of configurational interaction, which predicts that levels whose configuration involves single-particle states of $\ell + 1/2$ and $\ell - 1/2$ will have their odd spin levels lying in descending order; that is, the highest odd spin state will lie lowest.[60] The experimentally observed isomeric states are a direct result of this, as the following shows:

Isotope	Unpaired single-particle states responsible for configuration	Possible spins	Experimental spin of isomeric state
Pb^{206}	$p^{-1}_{1/2}\, i^{-1}_{13/2}$	6-, 7-	7-
Pb^{204}	$f^{-1}_{5/2}\, i^{-1}_{13/2}$	4-, 5-, 6-, 7-, 8-, 9-	9-
Pb^{202}	$f^{-1}_{5/2}\, i^{-1}_{13/2}$	4-, 5-, 6-, 7-, 8-, 9-	9-

The odd parity of the isomeric level can be explained only by the presence of the $i_{13/2}$ state. The spins observed are also in agreement with the expected values. The isomers decay by E5 and E3 in Pb^{206} transitions because of the absence of any high spin states that can favorably compete with the 4+ state, to which all these isomers decay.

The trend observed for the transitions to group about certain preferred energies is apparent consequence of the single-particle states involved. This is a result of an averaging effect in which the level spacings of the single-particle model are roughly approximated. Theoretically this can be considered as the outcome of a large number of different base configurations in which one of the particles in the base configuration undergoes the single-particle excitations of which it is capable. Figure 12 of the Pb^{204} and Pb^{205} transitions is illustrative of this trend. In each case the total number of transitions were considered and then plotted versus energy, in intervals of 50 kev. The results can be interpreted in an approximate manner, since one does not regard these curves as precise. In each case a

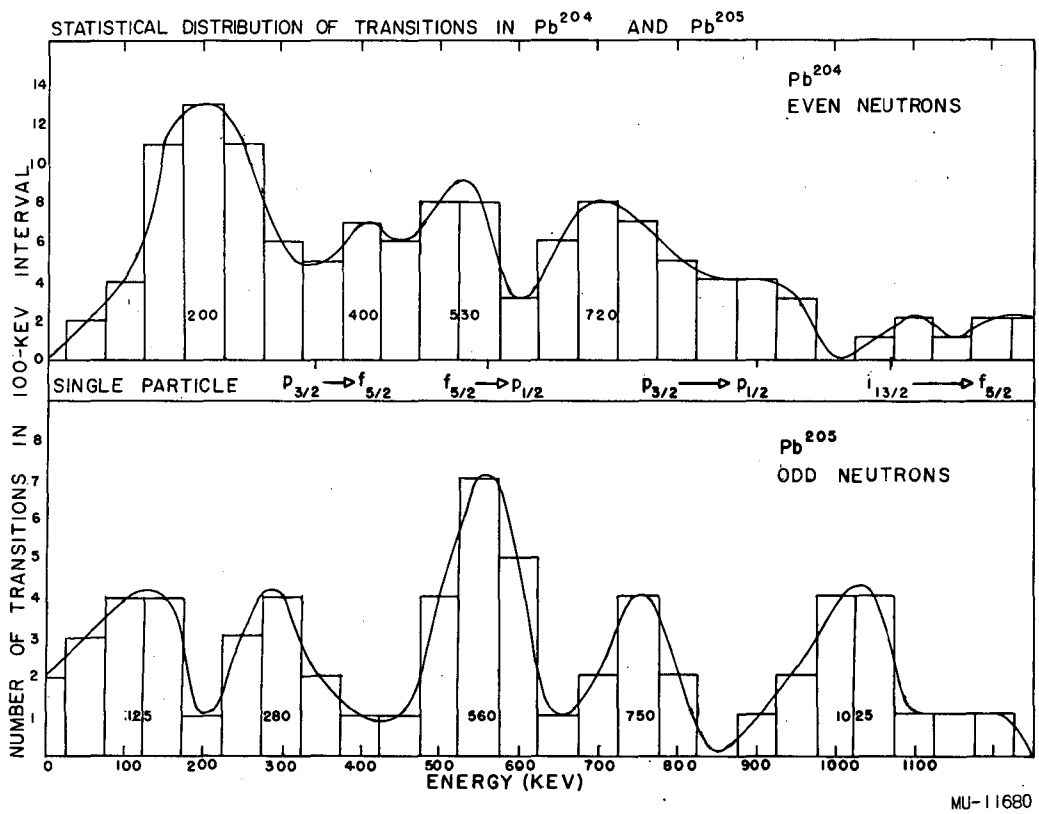

Fig. 12. Statistical distribution of transitions in Pb^{204} and Pb^{205}.

peak corresponding to the $p_{3/2} \rightarrow f_{5/2}$ and $f_{5/2} \rightarrow p_{1/2}$ transitions can be found at 200 to 300 kev and 500 to 600 kev respectively. In Pb^{205} there is also a peak that would indicate the $i_{13/2} \rightarrow f_{5/2}$ transitions at 950 to 1050 kev. However, there is no reason to believe that all the transitions corresponding to the above energy ranges are of this nature, and it is reasonable that some other transitions should accidentally lie in these intervals.

Parity--or, more precisely, the change in parity between two levels--can be considered from a qualitatively theoretical viewpoint. The parity of the single-particle states considered is odd for the $p_{1/2}$, $f_{5/2}$, $p_{3/2}$, $f_{7/2}$, and $h_{9/2}$ states, and even only for the $i_{13/2}$ state. This means in Pb^{205} that all the levels will be odd, except those which contain one $i_{13/2}$ in addition to two odd states or three $i_{13/2}$ states in their configuration. Pb^{204}, on the other hand, will have even states excepting that again the states containing one or three $i_{13/2}$ configurations will be odd. The only other means by which a state may have odd parity conforming to the $i_{13/2}$ configuration is by excitation of the proton levels. But this, because of the closed shell, requires about 3 Mev excitation energy, as in Pb^{206}. Therefore, one can clearly see that transitions that involve parity changes must in most cases also involve large changes in Δj, since the single-particle states lying below the $i_{13/2}$ and the $f_{5/2}$, $p_{3/2}$, and $p_{1/2}$. The transitions between an $i_{13/2}$ state and an $f_{5/2}$ state, which is the most likely, should then be M4, as is observed in the even-odd nuclides. However, if the spins of the levels are such that an E1 is permitted and experimentally observed, it is also very likely that it will be slow because of the large change in Δj. One can conclude that all E1, M2, and E3 transitions should be affected by this to some extent.

B. Lead-205

As indicated previously, the ground state of Pb^{205} is most likely a $f_{5/2}p_{1/2}{}^2$ configuration, which means that its spin is 5/2-. Using this as a premise, Harvey[61] studied the levels of Pb^{205} by means of a (d,t) reaction on Pb^{206}. His results were

Level energy (Mev)	Level assignment
0.00	$f_{5/2}$
0.27	$p_{3/2}$
0.84	$i_{13/2}$
1.79	--

The assignment of $i_{13/2}$ to the 0.84-Mev level may now be questioned, as the experimental work described herein indicated the absence of an isomeric state. However, the existence of a level at about 270 kev is corroborated by Frank Asaro's work upon the alpha decay of Po^{209}, in which an excited state of Pb^{205} is shown to occur at 260 kev.[66] The 260.5-kev M1 transition, which we have found in Bi^{205} decay, would then explain this first excited state. The level using Harvey's assignment would have a $p_{3/2}p_{1/2}^{2}$ configuration and therefore 3/2- spin and parity.

The 1.79-Mev level found by Harvey is interesting since there are two possible transitions, the 1766.4- and 1777.4-kev gamma rays, which could depopulate such a level. The coincidence work on Bi^{205} indicated that the 703-kev transition was in coincidence with one of 1770 kev. This would mean that one of these transitions goes to ground and the other is in coincidence with the 703-kev gamma ray. The related gamma ray intensities are 1.0 for the 703- and 2.0 for the combined 1770-kev peak. From the K-line electron intensities measured by the Swedish group and listed in Table V, the 703.3-kev transition is 1000, the 1766.4 is 436, and the 1777.4 is 52.[26] On the basis of L-subshell conversion ratios and K/L ratio, the 703.3 is an E2 transition, and we can therefore assign the 1700's on the basis of intensity. The K-conversion coefficients of interest are:[62]

Multipole order	at 1700 kev	at 703 kev
M1	3×10^{-3}	---
E1	8×10^{-4}	---
E2	1.7×10^{-3}	1.0×10^{-2}

With these values one can compare the various values of the transition intensities one obtains for the different multipole orders with those obtained from the gamma intensities. This is done in Table XIII. The results are clearly indicative of the 1766.4-kev transition's being an M1 transition. Also, the fact that it is the most intense gamma ray in the spectrum indicated that it depopulated directly to ground, and explains the 1.79-Mev level observed by Harvey. This would be quite analogous to Pb^{207}, where a 1780-kev level is seen assigned as the $f_{7/2}$ state, and one might expect the $p^2_{1/2}f_{7/2}$ configuration to account for this level. The coincidence work would then be explained by the 1777.4-kev transition in coincidence with the 703.3, although no unambiguous multipole order assignment can be made to the 1777.4-kev transition. From the results in Table XIII, the most probable assignment would be an E1. In the above argument the 703.3-kev transition has not been considered to precede the 1766.4-kev gamma ray because, as will be shown, the 703.3-kev transition probably goes directly to ground.

The only level reported by Harvey that is yet to be explained is the 840-kev $i_{13/2}$ level. It is in the explanation of this result that the 703.3-kev E2 transition is required. On the basis of the sum 703.3 + 284.0 = 987.5, levels can be assigned at 703.3 and 987.5 kev with the 284.0-kev M1 and the 703.3-kev E2 transitions in cascade. The average energy of these two levels, which would be unresolved in Harvey's work, would explain his result of 0.84 Mev. Also, from the Swedish work in which a K/L ratio of 4.2 ± 0.8 is reported for the 987.5-kev transition, it would seem that this is an E2 transition.[26,63]

Table XIII

Multipole order of 1766.4- and 1777.4-kev transitions in Pb^{205}

1766.4-kev multipole order	Relative transition intensity	1777.4-kev multipole order	Relative transition intensity	Ratio of $\frac{1766.4 + 1777.4}{703.3}$
M1	1460	M1	175	1.68
M1	1460	E1	650	2.11
M1	1460	E2	310	1.77
E1	5450	M1	175	5.6
E1	5450	E1	650	6.1
E1	5450	E2	310	5.8
E2	2670	M1	175	2.8
E2	2670	E1	650	3.3
E2	2670	E2	310	3.0

Relative transition intensity of 703.3 is $\frac{1000}{1.0} = 1000$

Experimental ratio of $\frac{1766.4 + 1777.4}{703.3} = 2.0$

The presence of these two levels at 703.3 and 987.5 kev plays an important part in explaining the absence of the isomeric state, since either or both have a spin of 9/2-. The high spin is also shown by the absence of a transition between these levels and the 3/2-level at 260.5 kev. A 9/2-level at this point in competition with a possible $i_{13/2}^{+}$ level at about 950 kev could be the reason for the failure to find an isomeric state.

The only other experimental result yet to be used is the coincidence of the 570-kev with the 1044-kev transition. The energies of these two gamma rays total to those of the 1614-kev gamma ray, as do numerous others, which suggests a level at 1614 kev, probably populated directly in the decay. From this point on, the further addition of levels to this scheme must be done on the basis of numerology alone. The decay scheme shown in Fig. 13 presents one of the most likely schemes which can be constructed. This is a partial scheme in that only about two-thirds of the transitions have been assigned. Those levels which seem certain have been drawn in solid lines, while the levels that are of a more questionable nature are indicated by dashed lines.

All energy sums are within 0.1% except the 1351.5- and 260.5-kev, summing to 1614 kev, and those sums adding to the 2126.0-kev level. In these cases the agreement is within 0.2%, which is still within the limits of error. On the basis of electron intensities the only manner in which the 758.3-kev level can be present is for the 758.3-kev gamma ray to be an E2 and the 579.7- and 745.0- gamma rays populating the level to be M1 transitions. Tentative spins and parities are indicated at the left in Fig. 13. Those which are highly uncertain are in parentheses.

The order of the 570.7-kev and 1043.5-kev sum has been determined solely on the basis of the other sums one is able to construct with the 570.7-kev gamma ray in that position. A reversal of this order would not be improbable. Another ambiguity lies in the placement of the 1766.4-kev and 1777.4-kev gamma rays. If the electron intensities measured by the Swedish group were off by 30% or so it is possible that the 1766.4-kev would be in coincidence with

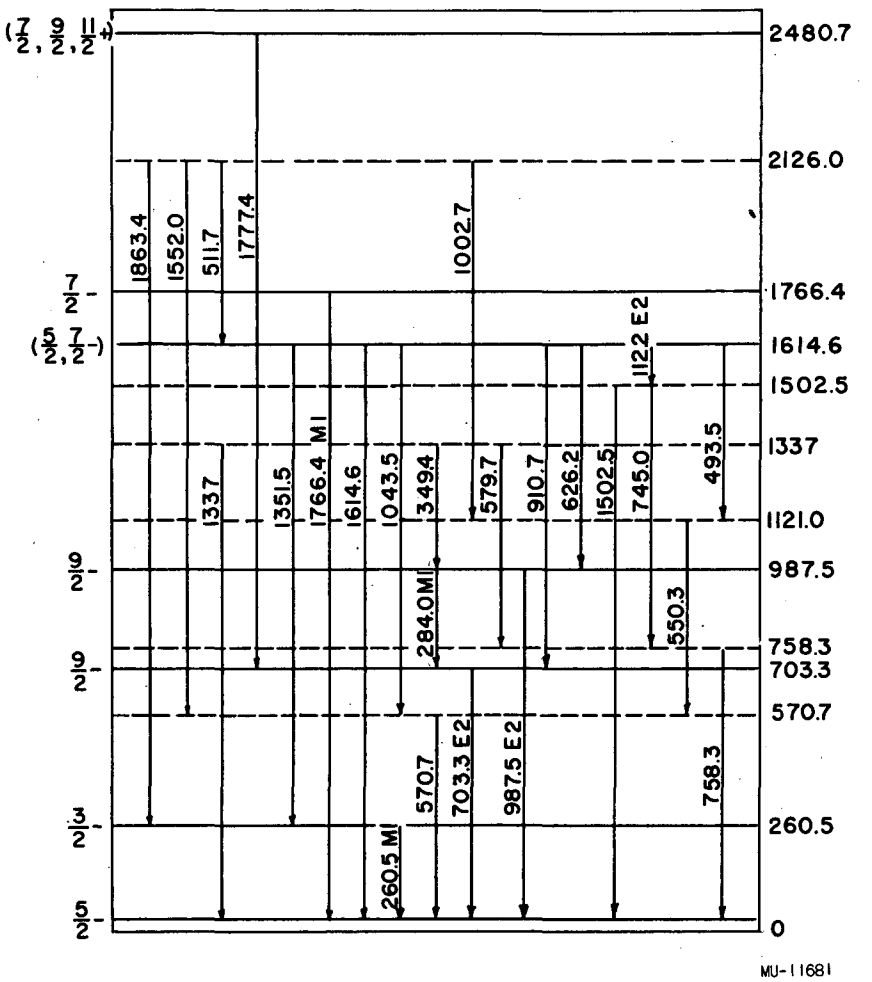

Fig. 13. Proposed energy-level diagram - Pb^{205}.

the 703.3, and that the 703.3- plus 1073.3-kev sum (1777.4 kev) would be significant, indicating a level at 1777.4 kev. However, it is unlikely that the Swedish measurements are in error by so large an amount.

Clearly, further levels may be postulated to explain the missing gamma rays. It is quite possible that, for the higher-energy transitions, the level indicated by them decays directly to ground. Because of the limitations imposed by the decay energy, these higher-energy transitions, if they do not go directly to the ground state, must at least populate one of the lower excited states. Further than this, the levels that might be defined from a strictly numerological approach are too uncertain to warrant inclusion.

The absence of an isomeric state is probably due to levels of spin of 7/2 or 9/2 at 703.3 and 987.5 kev in competition with the $i_{13/2}$ level. The Swedish investigators, Bergstrom et al., have also considered this problem.[26] They consider three possible explanations. The first is that the spin of the 15-day Bi^{205} is not 9/2-, analogous to Bi^{207} and Bi^{209}. They dismiss this explanation as improbable because the isomeric state appears again in Pb^{203}. The second possible explanation is that the ground-state spin of Pb^{205} is not 5/2-, but some higher spin, to account for the long half life of Pb^{205}. On the basis of the present work on Pb^{205}, it has been shown that an extremely low decay energy is the probable reason for the long half life. The third suggestion considered by Bergstrom etal. is that there exists a level of intermediate spin between the $i_{13/2}$ and $f_{5/2}$ levels such that the cross-over transition would be much faster than the M4 isomeric gamma ray.

From the decay scheme proposed (see Fig. 15) one can see that there is no level satisfying the suggested requirements. The levels occurring at about the energy where the isomeric level might be expected, all deexcite directly to ground state. If the ground state has a spin of 5/2-, none of these excited levels can have a spin $i_{13/2+}$. The proposed decay scheme would seem to indicate that the isomeric level expected is not populated appreciably and the most

likely reason for this lack of population is that other levels exist which are able to compete. The E2 multipole order assignments to the 703.3- and 987.5-kev transitions uphold this idea, providing levels of spin 7/2- or 9/2-.

From theoretical considerations, it is reasonable that other high-spin levels exist which contain the $i_{13/2}$ single-particle state in their configuration. The 1121.0-kev level might be such a case, since the lack of a transition directly to ground state would suggest a spin of 11/2 or greater. If the parity of this state could be determined, the presence of $i_{13/2}$ character in the configuration could be definitely decided.

In this discussion of the absence of the M4 isomeric transition in Pb^{205}, the greatest difficulty is encountered when one must explain the recurrence of the isomeric transition in Pb^{199}, Pb^{201}, and Pb^{203}. If the premise is accepted that the isomeric state is missing in Pb^{205} because of competition of other levels, it is not clear why this competition is not present in the lighter, even-odd lead isotopes, since in all cases the ground state assumed is one containing $f_{5/2}$ and $p_{1/2}$ single-particle states. Perhaps an explanation will be related to the fact that the ground state of $Pb^{205}(f^{-1}_{5/2}p^{-2}_{1/2})$ has only one $f_{5/2}$ hole, whereas the configurations of the lighter lead isotopes have three or more holes.

Thus, an understanding of this situation would require knowledge of the configurations involved in the making up of the levels of 1 Mev or less in Pb^{205}. Unfortunately one can only guess what these might be; however, the choices available are so limited that the result cannot be too incorrect. The first excited state clearly is the $p^{-1}_{3/2}\,p^{-2}_{1/2}$ configuration. The 570.7-, 703.3-, 758.3-, and 987.5-kev levels probably all contain some, if not all, of the $f^{-2}_{5/2}\,p^{-1}_{1/2}$ configuration. The levels available from such a configuration are those of spins 1/2, 3/2, 5/2, 7/2, and 9/2, -. These correspond to the values of the $p_{1/2}$ state together with values possible for the $f^{-2}_{5/2}$ configuration (0, 2, and 4+.)

The 570.7-kev transition is interesting since it is the same within a kilovolt as the 569.7-kev E2 transition in Pb^{207}, which

corresponds to a single nucleon changing from $f_{5/2}$ to $p_{1/2}$ states. A reasonable guess then might be that such is the case in Pb^{205} and that the 570.7-kev level is the lowest state of the $f^{-2}_{5/2}\, p^{-1}_{1/2}$ configuration. This would have the interesting theoretical implication that the pairing energy of a $p^{-2}_{1/2}$ pair is almost the same as that of a $f^{-2}_{5/2}$ pair.

Supposedly the 703.3-, 758.3- and 987.5-kev levels then correspond to states of higher spin of the $f^{-2}_{5/2} p^{-1}_{1/2}$ configuration. For one or more of these levels to have a 9/2- spin, the configuration would be $f^{-2}_{5/2}(J = 4)\, p^{-1}_{1/2}$. This would imply that the $f_{5/2}$ holes are arranged in one extreme, opposite to the J = 0 arrangement. It is not difficult to see from a qualitative viewpoint how this might occur, since the spin values available are somewhat limited.

It is this limitation on spins which seems to provide a possible clue to the absence of these 7/2- and 9/2- spin states in the lighter lead isotopes, which would compete with the $i_{13/2}$ level. If Pb^{203} is used as an example, the levels analogous to the Pb^{205} case would have the configuration $f^{-4}_{5/2} p^{-1}_{1/2}$. The spins available are 1/2 through 21/2- corresponding to

$$J_{(f_{5/2})^4} = 0, 2, 4, 6, 8, 10+.$$

A much larger number of levels is possible in Pb^{203} than in Pb^{205}. Qualitatively, then, it may be less probable to find a 7/2 or 9/2-level in Pb^{203} than in Pb^{205} because of the rapid increase in the number of orientations available.

That the $i_{13/2}$ level is decreasing in energy with respect to the $f_{5/2}$ level, as shown in the increasing half lives for the isomers may also be a contributing factor. The competition involved may be changing in favor of populating the isomeric state. From these considerations it is obvious that no clear reason can be given for the absence of the isomer in Pb^{205}.

C. Lead-204

Previous work on the Pb^{204} isomer provides a substantial framework on which the level scheme of Pb^{204} can be constructed. The levels obtained from studies on the isomer are shown in Fig. 14,

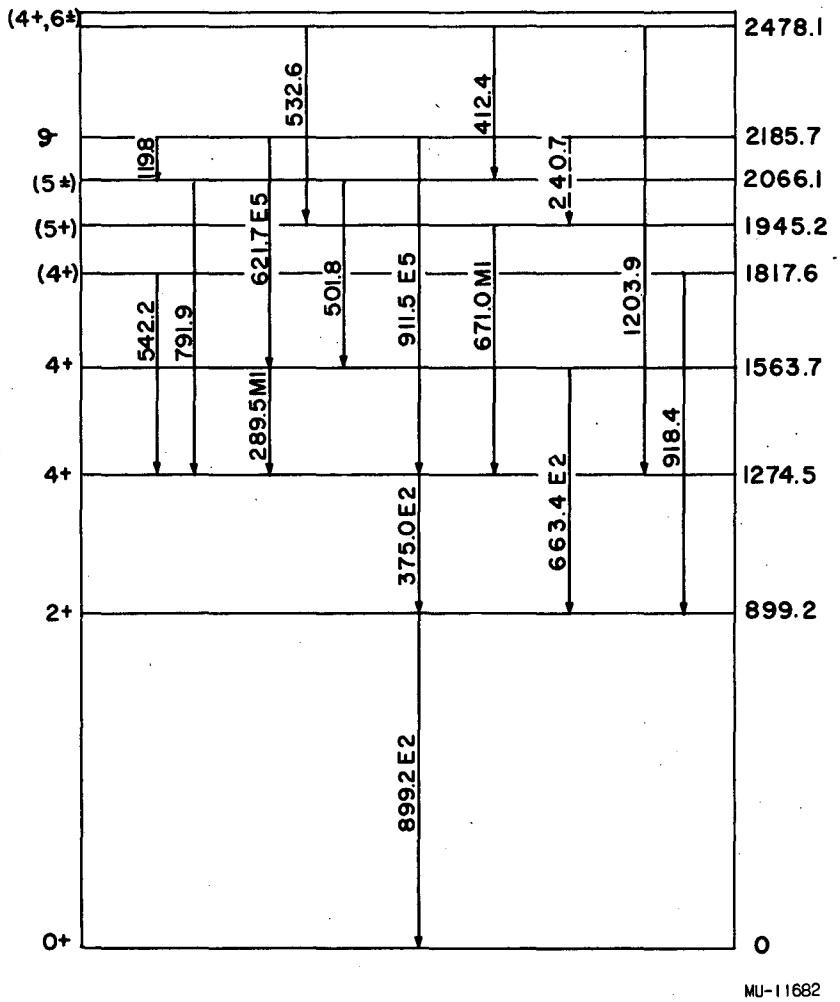

Fig. 14. Proposed energy-level diagram - Pb^{204}.

and occur at 899.2, 1274.2, 1563.7 and 2185.7 kev. The other basis for the construction of a decay scheme is the theoretical work of W. W. True, which applies configurational interaction theory to the levels of Pb^{204}. The theoretical results give the positions of possible levels only within a few hundred kev. It is therefore not possible to construct a decay scheme directly from the theoretical work and the list of transitions. As the present coincidence and scintillation gamma work were unsuccessful, there are no additional experimental data other than information on the isomer. This leaves only the numerical work on the sums and differences of the accurately measured transition energies as the means to construct a level scheme. Since there are some 10,000 sums to work with, it is apparent from the start that very little can be done in a decisive manner, even with the theoretical levels as a guide. In order to avoid a great deal of uncertainty, only the sums of two transitions compared to single transitions, as listed in Table VIII, are considered.

One of the important features of the sums is that the 911.5-kev E5 isomeric transition occurs as a cross-over transition six times. In terms of a probability picture, one would expect this to occur in only one out of ten thousand cases, if the agreement in energy were coincidental. This indicates that some of the sums involved are significant. It is of interest, then, to know what type of transitions (energy, multipole order, etc.) might compete with the 911.5-kev gamma ray. If one defines such competition to mean that the competing transition is about one one-hundredth as intense as the E5 isomeric transition, the following ranges of energy are involved:

Competing transition	911.5 E5 Transition 1/1	1/100
M4	500	240 kev
E4	220	120 kev
M3	85	35 kev
E3	40	15 kev

These results are only approximate; they are taken from Montalbetti's nomogram,[65] and assume no hindrances. Obviously if these weaker transitions are to compete with the 911.5-kev E5 and be observed, then

the isomeric level must be populated in Bi^{204} decay to a reasonable extent. The population of the isomeric state has been calculated to be 11 to 12% on the basis of the magnetic-lens electron spectrometer work. From the permanent-magnet spectrograph results, after making the proper corrections, one finds the average ratio of the intensities of the K-conversion lines of the 899.2-kev E2 depopulating the first excited state to the 911.5-kev isomeric transition to be

$$\frac{K\ 911.5}{K\ 899.2} = 1.31.$$

Again assuming that there is no direct population for the ground state in Pb^{204} and that all decays go 100% through the first excited state, one is able to obtain a population of the isomeric state, using conversion coefficients of 6.8×10^{-3} for the 899.2-kev E2 and 6.0×10^{-2} for the 911.5-kev E5 transition. On this basis, the isomeric state is populated about 15%. This is in good agreement with our previous results (which, were less certain). Of course, this population of the isomeric state is probably not direct, but involves higher-lying excited states in a cascade. Now if the isomeric state is present in fair abundance, then, according to the theoretical work of True, other cross-overs are quite probable. From the five or so sums available for the 911.5-kev transition, listed in Table VIII, the ones involving 671.0-kev M1 and the 791.9-kev transitions seem to be the most likely. The 791.9-kev sum would require that the 119.8-kev transition be an E4 or possibly an M4. Neither of these multipole orders seems to be fit by the conversion-line data; but the data in question are based on very weak lines.

Considering the analogy with the other even-even lead isotope, Pb^{205}, it is interesting to note that the 671.0-kev transition placed in the Pb^{204} scheme is almost the same as the 657.3 in Pb^{206}. One difference is the fact that in Pb^{206} the spin sequence is 4+ to 3+, and in Pb^{204} it is 5+ to 4+, although both are M1 transitions. In Pb^{206} the isomeric level that lies above de-excites to some extent through this level. This placement of the 671.0-kev transition as depopulating through the second excited state also agrees with the electron-electron coincidence work, in which it was observed to be in coincidence with

the 375.0-kev and 899.2-kev transitions. Furthermore, from intensity considerations, it must populate either the first or second excited state.

Although the position of the 671.0-kev gamma ray seems fairly well established, the sum of the 671.0-kev and 240.7-kev transitions equal to the 911.5-kev gamma ray presents a dilemma indicative of the type encountered in this complex region. In the work on Pb^{204m} it was established that the 289.5-kev K line was present to the extent of about 2.5% of the 911.5-kev K line. Since the normalized value of the 911.5-kev K line in the Bi^{204} spectrum is about 1300, this would require a line to have an intensity of less than 2.5% of this value which is (30) in the low-energy Bi^{204} spectrum in order not to have been observed in the isomeric work. From Table AV in the Appendix the following results were obtained:

	E (kev)	I_s
K line	911.5	1300
K line	119.8	too weak to be measured
K line	240.7	290
K line	621.7	too weak to be measured

Since an upper limit of $I_s = 30$ has been established for the absence of the K line of any competing isomeric transition in the Pb^{204m}, it would seem that the origin of 240.7-kev gamma ray from the isomeric level is ruled out. The 621.7-kev and 119.8-kev transitions, because of their low intensities, are in agreement with what one might expect from the decay scheme, although this by no means proves that they actually are parallel with the 911.5-kev transition.

Therefore, the 240.7-kev transition does not seem to originate at the isomeric level with the 911.5-kev gamma ray, if the intensity measurements are good within a factor of 10. This result illustrates the problems that confront an experimenter in this region. Until one considers the intensity, it seems almost certain that the 240.7-kev transition should be competing with the E5 gamma ray, as indicated by the sum of 240.7 plus 671.0, which equal 911.5 within 0.02%.

With this result in mind it is apparent that the use of only the sums and isomeric data as a basis for constructing an energy level diagram permits very little more to be accomplished by a numerological approach before a great deal of uncertainty occurs in the assignments. The levels that can be assigned with some degree of certainty are shown in Fig. 14. All the sums used agree within 0.1%, with the exception of the 542.2-kev and 663.4-kev transitions. The 663.4-kev has been placed in the scheme, because it is abundant and therefore should lie low; and it is clearly an E2 transition, from the conversion-line data. The placement of the 542,2-kev transition is dependent upon the position of the 918.4-kev gamma ray. In turn, the 918.4-kev has been placed in analogy with the 880.5-kev transition in Pb^{206}; both de-excite the 4+ third excited state to the 2+ first excited state.

The spin and parities are indicated to the left in Fig. 14. Those in paraentheses are based on W. W. True's theoretical work alone; the spin assignments are of course not certain, although the third 4+ state would be the only choice possible from True's work.

Recently a tentative partial decay scheme for Pb^{204} has been offered in a paper by Wertheim and Pound.[27] They report the observation of the following transitions:

Internal conversion: 371, 668, 895, 910, 982 kev;

External conversion: 372, 895, 891 kev.

The conversion-line measurements were carried out by Bainbridge and Marcisi on a sample of Bi^{204} provided by Wertheim and Pound. The external conversion lines were obtained by use of a uranium converter. Within the limits of error involved, the observed 371-, 668-, 895-, and 910-kev transitions clearly correspond to the 375.0-, 671.0-, 899.2-, and 911.5-kev gamma rays obtained in this work. The 982-kev gamma ray reported by Wertheim and Pound does not correspond to any transition assigned in this work.

Gamma rays of 1200, 1730, and 2100 kev are also reported by Wertheim and Pound. These were found in the scintillation spectrum. The gamma-ray spectrum analyzed in the course of this work, as previously discussed, did not show any clear indication of any of the

reported gamma rays, although transitions at 1203.9 and 1211.5 kev were found in the electron spectrum, and these could possibly correspond to the 1200-kev gamma ray of Wertheim and Pound. The 1730- and 2100-kev transitions remain unexplained even when the very weak lines observed in the magnetic-lens spectrograph work are considered. An interesting explanation for the three gamma rays seen--the 1200-, 1730-, and 2100-kev-- is that they are the results of the more intense transitions, such as the 375-, 671-, 895-, and 912-kev gamma rays, summing up in the crystal to give a much higher-energy pulse. The mathematics involved makes this a tempting explanation. However, since their exact experimental procedures were not mentioned by Wertheim and Pound, this remains a conjectured explanation.

The 981-kev transition reportedly found in the conversion-line work on Pb^{204} requires a definite explanation, for Wertheim and Pound report its transition intensity to be 75% of the total decays. The 75% value was arrived at by measuring the combined delay coincidences of the 981- and 898-kev and the 910- and 895-kev gamma rays. From the time-dependent coincidence rate obtained, they were able to conclude that the fraction of decays going through the 981-kev gamma ray was 75%.

Such an intensity is entirely inconsistent with the results of our work. The gamma-ray spectrum obtained in the course of this work all showed a broad peak at about 900 kev, attributable to the 899-plus 912-kev gamma rays and a small high-energy shoulder. The shoulder was explainable by the K x-ray stack-up with the 900-kev peak, since the complexity of the Bi^{204} decay provides a large number of K x-rays. This small shoulder is not explainable in terms of a transition that occurs in 75% of the decays.

The conversion lines obtained from the permanent-magnet spectrographs are ambiguous as to the 981-kev transition. A possible assignment is:

VVS	896.1		W-VW	968.7
	88.0 K			15.2 L_2
	984.1			983.9

Av = 984.0.

There are other difficulties resulting from this assignment, outside of the apparent intensity discrepancy. The 968.7-kev electron line has been assigned as the K line of a 1056.7-kev transition. The intense 896.1-kev line is of course the L_2 line of the 911.5-kev isomeric transitions. The sums in that case are:

VVS	823.0	VVS	896.1	W	898.4	M	908.0	W	910.4	
	88.0		15.2	L_2	13.0	L_3	3.6	M_2	0.8	N_2
	911.9,		911.3,		911.4,		911.6,		911.2,	

Av = 911.5 kev.

The alternative solution available is that both transitions are present, and that the 896.1-kev line is both a K and an L_2 line.

In order to examine this solution, the intensities of the various lines were studied. If the 968.7-kev line is the L_2 of the 984.0, it is possible to obtain the intensity of the associated K line from an assumed K/L ratio. The K/L ratio chosen was 5. This choice would include E1, E2, M1, and M2 transitions. With the K-line intensity for the assumed 984.0-kev gamma ray one can then compare its effect upon the K/L ratio for the 911.5-kev E5 transition. The theoretical value for this K/L ratio is 1.7_5. The experimental K/L ratios obtained, assuming the absence and the presence of a 984.0-kev transition, are as follows:

	984.0 not real	984.0 real
1.	1.6_9	2.0_5
2.	1.6_6	2.0_1
Av K/L	1.6_8	2.0_3

Theoretical K/L = 1.7_5 .

From these results one is not completely certain of the true state of affairs because the errors in the measurements are about 25%. However, one can say that it seems more reasonable to assume that the 984.0-kev transition is not real. If it were not real, it would be an excellent example of the difficulty involved in making assignments to conversion lines when there is a large number involved. It also would point out the problems encountered with coincidence, which are multiplied manyfold in the pure numerical correlations of the transitions.

The one clear result from both the gamma spectra and the conversion-line data is that if the 984.0-kev transition does exist, it is not present 75% of the time, but about 10% at the most. From this it would seem that Wertheim and Pound were not cognizant of the low K/L ratio accompanying an E5 transition, and assigned the 911.5-kev L_2 line almost completely to their 981-kev gamma ray, since no mention is made of the unreasonably high transition intensity given to the 981-kev line.

The most reasonable conclusion to reach upon the actuality of the 984.0-kev transition is that possibly it is not present, but coincidental. This has not been conclusively shown, however, and the possibility of its existence always should be recognized.

The scintillation spectrum indicated that about 60% of the total decays to excited states depopulated through the first excited state but not through the second excited state. The value one obtains from the conversion-electron spectrum is in agreement if one uses Rose's values of the conversion coefficients as given by Nijgh.[16]

375.0 kev	E2	$\alpha_K = 4.4 \times 10^{-2}$
899.2 kev	E2	$\alpha_K = 6.9 \times 10^{-3}$

Since the 375-kev K line is about four times as intense as the 899.2-kev K line, about 40% of the decays to the excited states on this basis go through the 899.2-kev transition but not through the 375.0-kev transition. If the errors involved in the electron intensity measurements are recognized (taken into account) this is in agreement with the 60% value found in the scintillation spectrum work. The question of where this additional intensity in the 899.2-kev gamma ray arises is left unanswered. The 918.4-kev transition postulated in the energy-level diagram, Fig. 14, could provide about 10% of the 40 to 60% required if it were an E2 transition. The remainder of the intensity must come from a number of levels which de-excite directly to the 2+ state or from direct population of this state in the decay of Bi^{204}.

One is forced to conclude that little can be done in the way of a decay scheme on the basis of the known experimental results. The uncertainty one finds in assigning levels becomes almost exponential in nature as one gets further from experimental fact into pure

numerology. This curtain of uncertainty is reached much sooner in the Pb^{204} than in Pb^{205}, and it is therefore possible to assign a correspondingly greater fraction of the transitions found in Pb^{205}. This is due mainly to the very nature of the difference between even-even and even-odd nuclides and is manifested most strongly in the 0+, 2+, 4+ sequence of excited states in even-evens, as compared with the essentially random assignments in even-odds. Because of the almost sacred nature of the first excited state in even-evens through which almost all the decay from higher states must go, Pb^{204} becomes more difficult to approach than Pb^{205}, since in Pb^{205} there are a large number of gamma rays de-exciting directly to the ground state and thus providing a good means of solution. In the Pb^{204} case, a large amount of uncertainty is initially introduced, because one can never be sure, except by experimental coincidence results, whether a particular transition goes through only the first or both the first and second excited states. This initial handicap is one of the main reasons for the inability to arrive at a larger number of levels for Pb^{204}.

Another factor that enters into the Pb^{204} problems is the lack of data on high-energy transition, which was available for Pb^{205}. Attempts were made to observe high-energy transitions by means of the double-focusing beta spectrometer. The instrument has a variable resolution of from 0.3 to 1.0%. The results obtained were negative, probably owing to the lack of transition intensity of the higher-energy transitions and the accompanying decrease in conversion coefficients as the energy of a gamma increases. Perhaps with the use of a much larger amount of activity the high-energy lines may be clearly established. Of course, the uncertainty inherent in even-even nuclei will still be present.

D. Lead-203 Energy Levels

On the basis of the experimental work of Prescott[36] based on Pb^{203}, which indicated that the ground state of Pb^{203} was $f_{5/2}$, it is reasonable to assume the ground-state configuration to be $(f^{-3}_{5/2}\, p^{-2}_{1/2})$ with a closed proton shell. The expected energy levels, then, especially those less than a few Mev, should be indicative of the odd-neutron excitations.

This is the same situation as exists in Pb^{205}, where the ground state is postulated to be $(f^{-1}_{5/2}\, p^{-2}_{1/2})_n$. One should therefore be able to construct an energy-level diagram analogous to the one for Pb^{205}. The similarity is shown in a comparison of a number of transitions in both nuclides as follows:

Pb^{203}	Pb^{205}	Transition Assignment
126.4	112.2	Both E2
264.0	260.5 or 284.0	Both M1
381.5	383.3	
625.0	626.2	
708.4	703.3	
1033.7	1043.5	

However, differences exist between the two isotopes other than the differences in isomeric behavior. Firstly, Pb^{205} seems to have about twice the number of transitions that have been found for Pb^{203}. The explanation for this seems to lie in (α, 4n) cross-section curves, which indicates that the maximum-energy bombardments carried out were still somewhat below the peak cross section, and therefore it is very likely that the atom yield of Bi^{203} was less than that of Bi^{204} or Bi^{205}. This would result in relatively less activity for the Bi^{203} fraction, and only the stronger transitions associated with Pb^{203} could be observed. The second difference lies in the absence of any strong transitions in the 570-kev region, comparable to the 570.7 and 579.7 in Pb^{205}. Explanation here is not clear, but perhaps it is in some way related to the absence of the isomeric level in Pb^{205}.

The best approach would seem to be to construct a decay scheme from the transition sums and then relate it to Pb^{205} energy levels. The experimental evidence on the Pb^{203m} isomer clearly indicates a level at 824.9 kev. Since the ground-state configuration is 5/2- and the isomeric transition--on the basis of K/L ratio, half life, and L-sub-shell conversion ratio--is an M4 state, one can assign a spin of 13/2+ to the 824.9-kev level. No other levels can be assigned at this time by purely experimental means.

It is necessary to consider the sums of two gamma rays that one can obtain from the Pb^{203} transitions. These are listed in Table VIII. The sums listed are all within the limits of error, with the exception of the 824.9- and 708.4-kev transitions, totaling 1533.3 kev. Since our absolute energies are good to within 0.1%, it is felt that the relative values should be somewhat better, and therefore a 0.2% or greater error seems outside the allowable limits. In addition to this, the sums-of-two with other sums-of-two give strong indication that the 708.4-kev transition is not in coincidence with the 824.9-kev transition, but rather that it represents the first excited state.

From the numerology of the transitions, a probable energy-level diagram (but by no means the only one) would have levels at 708.4, 824.9, 1089.4, 1430.7, 1528.1, 1536.4, 1588.2 or 1654.5, and 1714.4 kev, as shown in Fig. 15. The transitions not included in this scheme are the 465.4- and 1033.7-kev gamma rays. The 1033.7-kev gamma ray could possibly be fitted into the scheme by having it de-excited to the ground state directly. Placement of a level at 1536.4 kev above ground is reasonable if one assumes its configuration to be analogous to the levels on Pb^{205} and Pb^{207} de-excited by 1766.4-kev and 1780-kev transitions respectively. This configuration in the Pb^{203} case would be $f^{-2}_{5/2}\, p^{-2}_{1/2}\, f^{-1}_{7/2}$, and would be expected to recieve a moderated fraction of direct population by Bi^{203} decay. The difficulty in using this level is the presence of the possible level at 1528.1 kev suggested by the numerology of the sums. Energy levels lying this close have not been experimentally observed in this region. However, the 1528.1-kev level is uncertain, and it is as likely that a level at 894.9 kev, resulting from a reversal of the 819.7-kev + 186.5-kev transition sequence, could occur. If the 1536-kev level is accepted, then in analogy to Bi^{205} and Bi^{207} the 1536.4-kev transition might possibly be an M1.

Again one is forced to realize the uncertainty of an energy-level diagram obtained solely from numerology. Unfortunately Pb^{203} does not have the higher-energy transitions reported as in Pb^{205}, and the instrumentation and source activity available were insufficient to obtain them. This results in a less certain decay scheme than the Pb^{205} scheme.

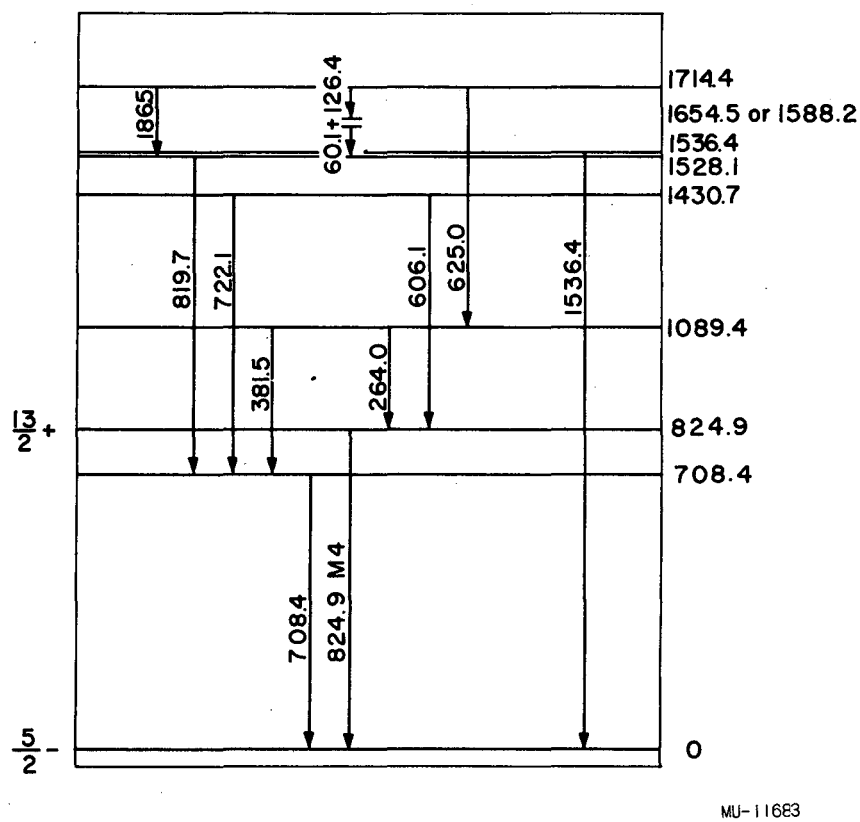

Fig. 15. Proposed energy-level diagram - Pb^{203}.

One is able, however, to give some credence to certain features of the decay scheme on the basis of the Pb^{205} results. The level at 708.4 kev in Pb^{203} seems to be similar to the 703.3-kev level in Pb^{205}, although nothing can be said about the 708.4-kev transition's depopulating, so that comparison with the 703.3-kev E2 multipolarity cannot be made. The fact that the 708.4 does not clearly evidence itself as an E2 transition perhaps ties in with the absence of any lower excited state such as the 260.5- and 570.7-kev levels in Pb^{205}. The $p_{3/2}$ level in Pb^{203} which, analogous to the 260.5-kev level in Pb^{205}, is probably missed because of the lack of low-level population brought about by competition with high spin levels such as the 13/2+. This is a natural result here, since the ground-state spin of Bi^{203} is probably 9/2-.

The absence of the analogous 570.7-kev level in Pb^{203} is somewhat more difficult to explain. The level has been discussed for Pb^{205} in relation to the absence of the isomer and assigned an $f^{-2}_{5/2}\, p^{-1}_{1/2}$ configuration. The reason given in the Pb^{205} discussion for the reappearance of the isomeric state in Pb^{203} is that the analogous configuration $f^{-4}_{5/2}\, p^{-1}_{1/2}$ has so many more possible spin orientations that, at least qualitatively, the probability of populating any particular orientation should be less in Pb^{203} than in Pb^{205}. This could explain not only the absence of the 570.7-kev level but also the absence of strongly populated 987.5-kev Pb^{205} level in Pb^{203}.

E. Thallium-203

The energy levels of Tl^{203}, populated in the decay of 52-hr Pb^{203}, have been clearly established by Prescott[36] to be 0, 279, and 680 kev. It was on the basis of the established spin sequences of 1/2+, 3/2+, and 5/2+ for these levels that Prescott was able to assign the ground-state spin of Pb^{203} to be 5/2-, from the direct level population observed in the decay. In terms of single-particle states, the ground state of Pb^{203} has been interpreted as an $f_{5/2}$ odd neutron, while the odd-proton states of Tl^{203} are the $s_{1/2}$ ground state and the $d_{3/2}$ and $d_{5/2}$ excited states.

The transitions seen in the decay of Pb^{203} in this work have been the 279.1-kev M1-E2 transition and the 400.6-kev M1 transition. The 680-kev E2 transition was not seen, probably owing to the low conversion coefficient. On the basis of these transition energies it is possible to define the levels somewhat more accurately at 0, 279.1, and 679.7 kev.

Since in our photographic plates the 279.1-kev transition is dominant it was quite convenient to measure the M1-E2 mixing associated with it. The M1-E2 mixing has interested a large number of investigators, because the 279.1-kev transition in Tl^{203} is not only a prominent line in Pb^{203} electron-capture decay, but it is also the only transition observed in Hg^{203} beta decay. The K/L ratio obtained in this work once again indicated the uncertainty involved in the intensity of low-energy conversion lines. Our value for the K/L ratio was 2.1. Nijgh,[16] in his compilation of the reported experimental data on the 279-kev transition, clearly indicates that the K/L ratio is 3.3. It is apparent that the K/L ratio obtained in our work, which indicates a mixing of M1/E2 ~ 0.1, is far different from Nijgh's values that give an M1/E2 mixing of about 0.33. Nijgh also obtains agreement with this mixing ratio from the conversion coefficient of the 279.1-kev gamma ray.

In our case a good value for the mixing could be obtained from the L-subshell conversion ratio. The experimentally observed ratio agrees quite well with that reported by Swan and Hill:[64]

	This work	Swan and Hill
L_1	3.28	2.85
L_2	1.86	2.08
L_3	1.00	1.00

The theoretical values from Rose, as given by Nijgh, for the M1 and E2 conversion coefficients of a 279-kev transition are:

	M_1	E_2
L_1	0.0826	0.0116
L_2	0.0072	0.0224
L_3	0.00045	0.0122

When the values of the conversion coefficients were used, the M1-E2 mixing obtained from the L-subshell ratio was

$$\frac{M1}{E2} = 0.29.$$

This is in good agreement with the previously reported results.

The problems associated with intensity comparisons over a large portion of the electron spectrum still remain, as shown by the low K/L ratio. However, intensity comparisons of close-lying electron lines, as in L subshells, are fairly accurate.

ACKNOWLEDGMENTS

I would like to express my gratitude to Dr. Jack M. Hollander, whose continued help and guidance have made this work possible. I would also like to thank Professor John O. Rasmussen for his cooperation and many helpful comments. The assistance and discussions with Frank Asaro, Frederick L. Canavan, Charles Gallagher, Richard A. Glass, Marvin I. Kalkstein, Jose Juliano, Frank Stephens, Donald Strominger, Allan W. Stoner, Warren Smith, and Sigvard Thulin are appreciated. I would also like to thank Professors Isadore Perlman, Glenn T. Seaborg, and David H. Templeton for their helpful comments.

The cooperation of the late G. Bernard Rossi, William B. Jones, and the crew members of the 60-inch cyclotron is gratefully acknowledged. I would like to thank Mrs. Thérèse Pionteki for the counting of samples and Mrs. Eleanor Potter for her aid in drawing figures. Finally I would like to express my appreciation to the Health Chemistry Group, who have made it possible to carry out this work safely.

This work was performed under the auspices of the U. S. Atomic Energy Commission.

Table AI

Bismuth-203 and Bismuth-204 Conversion Lines
from Permanent-Magnet Electron Spectrographs

Isotope Present											
203	203			203		203		203			
204	204	204	204	204	204	204	204	204			
Plate Number											
180	215	148	162	179	194	178	147	178			
Spectrograph									Average Energy	Transition Energy	
PMI	PMI	PMII	PMII	PMII	PMIII	PMIII	PMIV	PMIV	$\bar{E}$	E_γ	Nuclide
	28.67^{vw}		27.59^{vvb}	22.92^{vw}							
	29.61^{vw}								29.61	117.7K	203
	35.79^{vvw}										
			31.75^{vvvw}	31.75^{w}					31.75	119.8K	
	38.50^{vw}								38.50	126.4K	203
44.17^{vvw}	44.19^{vw}			44.23^{ms}					44.23	$60.08L_1$	203
	49.14^{vvw}										
52.72^{w}	52.67^{m}	52.90^{w}	52.82^{m}	52.82^{s}					52.78	140.9K	
	53.48^{vvw}										
	54.07^{vvw}										
	55.02^{vvw}										
	55.92^{vw}	56.16^{vvw}							56.16	60.08M	203
									56.04	KL_1L_1 auger	

Table AI continued

180 I	215 I	148 II	162 II	179 II	194 III	178 III	147 IV	178 IV	$\bar{E}$	E_γ	Nuclide
			56.50^{vw}	56.50^{m}					56.50	144.5K	
	56.63^{vw}		56.72^{vvw}	56.72^{ms}					56.68	KL_1L_2	Auger
		56.95^{vwb}									
			57.15^{vvw}	57.15^{w}					57.35	KL_2L_2	Auger
	57.54^{vvw}										
				57.72^{w}							
	58.80^{vvw}	58.97^{vvw}	59.00^{vwb}	59.00^{w}					58.93	KL_1L_3	Auger
	59.18^{w}								59.18	60.08N	203
		59.67^{vwb}	59.67^{wb}	59.54^{s}					59.60	KL_2L_3	Auger
	60.31^{vvw}			60.58^{w}							
			61.68^{vvw}	61.68^{wm}					61.68	KL_3L_3	Auger
63.37^{s}	63.31^{s}	63.58^{m}	63.44^{s}	63.44^{vs}					63.43	$78.60L_2$	
64.38^{m}	64.24^{m}	64.47^{m}	64.40^{m}	64.40^{s}					64.37	$80.22L_1$	
			65.03^{vvvw}	65.03^{vw}					65.03	$80.22L_2$	
65.55^{m}	65.59^{m}	65.78^{m}	65.61^{ms}	65.61^{vs}					65.63	$78.60L_3$	
				68.18^{w}					68.18	KL_1M_1	Auger
				68.56^{vw}					68.56	KL_1M_2	Auger
				69.04^{w}					69.04	KL_1M_3	Auger
				69.60^{w}					69.60	KL_1M_5	Auger
			71.11^{vw}						71.11	KL_3M_1	Auger
				71.29^{wb}					71.29	KL_3M_2	Auger

Table AI continued

180 I	215 I	148 II	162 II	179 II	194 III	178 III	147 IV	178 IV	$\bar{E}$	E_γ	Nuclide
			71.56^{vvw}								
			71.91^{vwb}	71.91^{w}					71.91	KL_3M_3	Auger
			72.22^{vvw}	72.22^{vw}					72.22	KL_3M_4	Auger
			72.89^{vwb}	72.89^{vwb}							
			73.88^{vvw}								
			74.30^{vvw}						74.30	KL_3N_3	Auger
			74.69^{vw}						74.69	$78.60M_1$	
74.97^{w}	74.95^{w-m}	75.12^{vw}	75.01^{m}	75.01^{s}					75.01	$78.60M_2$	
75.15^{w}											
	75.40^{w}	75.59^{vw}	75.54^{wm}	75.54^{s}					75.51	$78.60M_3$	
76.30^{vw}	76.27^{w}	76.35^{vw}	76.31^{w}	76.31^{s}					76.31	$80.22M_1$	
		76.92^{vvw}	76.87^{vvw}	76.78^{w}					76.9	164.9K	
77.91^{vw}	77.81^{vw}								77.92	$78.60N_3$	
		78.05^{vwb}	78.00^{vwb}	78.00^{ms}							
				78.57^{vw}							
	79.18^{vvw}										
		79.46^{vvw}	79.35^{vvw}	79.30^{wm}					79.37	$80.22N_1$	
		80.87^{vvw}	80.81^{vw}	80.80^{vw}	80.8^{w}				80.83	168.8K	
81.91^{vw}	81.85^{vw}	82.07^{vw}	81.83^{w}	81.83^{ms}	81.8^{s}				81.9	170.0K	
			83.12^{vwb}								
			84.13^{vvw}								

Table AI continued

180 I	215 I	148 II	162 II	179 II	194 III	178 III	147 IV	178 IV	$\bar{E}$	E_γ	Nuclide
	84.34^{vw}										
		84.64^{vw}	84.58^{vw}	84.58^{m}	84.8^{s}				84.6	$100.4L_1$	
				85.20^{vw}					85.2	$100.4L_2$	
			85.77^{vvw}								
88.08^{s}	88.00^{s}	88.11^{m}	88.00^{vs}	88.00^{vvs}	88.1^{vvs}	88.1^{s}			88.05	172.2K	
			89.57^{vwb}	89.57^{vwb}					89.57	$105.5L_1$	
				93.24^{vw}					93.24	$109.1L_1$	
			93.90^{vw}	93.90^{vw}					93.90	$109.1L_2$	
		96.10^{m-s}	95.94^{s}	95.94^{vvs}	96.1^{vvs}	96.1^{s}			96.0	184.2K	206
				96.52^{vw}					96.5	$100.4M_1$	
				97.40^{vw}					97.4	$112.5L_2$	205
				98.47^{vs}		98.4^{vs}			98.4	186.5K	203
				99.37^{vw}					99.4	$112.5L_3$	205
				100.56^{vw}						$117.7L_1$ or $100.5M_1$	203
				101.84^{vw}					101.84		
			$103.96^{vvw?}$	103.96^{vw}	103.8^{w-m}				103.96	$119.8L_1$	
				105.75^{vw}					105.75	$109.1M_2$	
			106.80^{vw}								
				107.56^{vw}					107.8	$123.7L_1$	206
			107.99^{vw}								

Table AI continued

180 I	215 I	148 II	162 II	179 II	194 III	178 III	147 IV	178 IV	$\bar{E}$	E_γ	Nuclide
				111.21^{s}		111.2^{s}			111.21	$126.4L_2$	203
				113.39^{ms}		113.2^{s}			113.39	$126.4L_3$	203
				$113.82^{vw?}$					113.82	$117.7M_1$	203
				$114.28^{vw?}$					114.3	202.4K	206
				115.45^{vw}							
				116.94^{vw}					116.94	$117.7N_1$	203
				117.21^{vw}							
				119.15^{vw}							
				121.08^{vwb}	121.2^{vw}				121.1	209.1K	
				122.86^{wm}					122.86	$126.4M_2$	203
			123.22^{vw}	123.27^{w}		123.1^{wm}			123.27	$126.4M_3$	203
				124.06^{vw}							
			124.40^{vw}						} 124.5	212.7K	
				124.63^{w}	124.6^{vvs}	124.6^{s}					
		125.02^{vw}	124.97^{vw}	124.97^{m}					125.0	$140.9L_1$	
				125.58^{w}	125.5^{vw}	125.5^{wm}			125.5	213.5K	
				126.13^{vw}					126.13	126.4N	203
			126.70^{vw}								
			127.34^{vw}								
		128.18^{w-m}	128.19^{m}	128.10^{vs}	128.2^{vvs}	128.2^{vvs}			128.2	216.2K	
			128.68^{vw}	128.60^{wm}	128.7^{vw}				128.6	$144.5L_1$	

Table AI continued

180 I	215 I	148 II	162 II	179 II	194 III	178 III	147 IV	178 IV	$\bar{E}$	E_γ	Nuclide
			129.96^{vvw}								
			130.70^{vvw}								
				131.41^{m}	131.4^{s}	131.4^{s}			131.4	219.5K	
		131.62^{vvw}	131.70^{vw}								
			132.40^{vvw}								
			133.84^{vvw}								
		134.49^{w}	134.48^{m}	134.48^{s}	134.4^{vvs}	134.4^{vvs}			134.4	222.5K	
			135.59^{vvw}								
				136.95^{w-vw}	137.0^{w-m}	137.0^{w-m}			137.0	$140.9M_1$	
			137.36^{vvvw}								
				139.06^{w-vw}	139.0^{w}	139.0^{w}			139.0	227.1K	
			139.47^{vvw}								
					139.8^{vw}						
				140.63^{vw}					140.6	$144.5M_1$	
				143.20^{vvw}		$143.2^{vw?}$					
				143.79^{vvw}	143.9^{vvw}				143.8	$144.5N_1$	
				146.40^{vw}	146.3^{vw}	146.3^{w}			146.4	234.4K	206
				147.79^{vvw}							
			149.12^{vvw}	149.12^{w}	148.9^{vw}	148.9^{vw}			149.0	$164.9L_1$	
		152.84^{vvvw}	152.60^{vw}	152.63^{ms}	152.7^{s}	152.7^{s}			152.7	240.7K	
			153.28^{vvw}								

Table AI continued

180 I	215 I	148 II	162 II	179 II	194 III	178 III	147 IV	178 IV	$\bar{E}$	E_γ	Nuclide
				154.21^{vw}	154.3^{w}	154.3^{w}			154.2	$170.0L_1$	
				154.95^{vvw}							
					156.9^{vvw}						
		160.44^{vw}	160.46^{vvw}	160.33^{ms}	160.5^{vs}				160.4	$176.2L_1$	
		161.31^{w}	161.28^{m}	161.28^{vs}	161.2^{vvs}	161.2^{vvs}			161.3	249.1K	
				164.48^{vw}	164.3^{w}	164.3^{vw}			164.4	252.4K	
				165.88^{vw}					} 166.1	$170.0M_1$	
			166.65^{vvw}		166.3^{vw}	166.3^{vw}					
		168.47^{vw}	168.52^{w}	168.52^{s}	168.3^{vvs}	168.3^{vvs}			168.5	$184.2L_1$	206
				169.04^{vw}	168.9^{vw}				169.0	$184.9L_1$	
				169.70^{vw}	169.7^{vw}				169.7	$184.9L_2$	
			170.33^{vw}								
				170.81^{ms}		170.6^{s}			170.7	$186.5L_1$	203
			172.54^{vw}	172.54^{wb}	172.4^{w-m}	172.4^{m}			172.4	176.2M	
		175.10^{vvw}	175.09^{vw}	175.04^{m}	174.8^{s}	174.8^{s}			175.1	263.8K	206
					176.0^{vw}						
				176.19^{vs}		176.0^{vs}			176.1	264.0K	203
				176.56^{vvw}							
			177.29^{vvwb}								
				180.42^{wm}	180.3^{ms}	180.3^{s}			180.4	$184.2M_1$	206
				181.86^{vvw}							

Table AI continued

180 I	215 I	148 II	162 II	179 II	194 III	178 III	147 IV	178 IV	$\bar{E}$	E_γ	Nuclide
				182.81^{w}		182.7^{vvw}			182.8	$186.5M_1$	203
				183.26^{vw}	183.1^{w}	183.1^{m}			183.2	$184.1N_1$	206
			183.67^{vvw}								
				185.45^{vw}					185.5	$186.5N_1$	203
				187.08^{vvw}	187.4^{vvw}				187.3	$202.4L_1$	206
				190.47^{vw}							
				191.92^{vvw}							
					193.6^{w}				193.6	281.6K	205
				193.84^{vvs}		193.7^{vvs}			193.7	279.1K	Pb^{203}
			194.80^{vvw}								
				196.24^{vw}	196.0^{w}	196.0^{m}			196.1	284.1K	205
					197.0^{vw}				197.0	$212.7L_1$	
				198.52^{vw}	198.3^{w}	198.3^{vw}			198.4	$213.6L_2$	
				199.22^{vvw}							
			200.47^{vw}	200.40^{m}	200.2^{s}	200.2^{wm}			200.4	$216.2L_1$	
		201.59^{w}	201.57^{m}	201.45^{s}	201.4^{vvs}	201.4^{vs}			201.5	289.5K	
		203.14^{vvw}	203.09^{vw}	203.09^{wm}	202.8^{ms}	207.8^{m}			203.0	291.0K	
		204.51^{vvw}	204.48^{vwb}	204.48^{wmb}	204.1^{s}	204.1^{sb}			204.3	$219.5L_2$	
			205.40^{vvw}								
		206.80^{vvw}	206.56^{vw}	206.56^{m}	206.4^{ms}	206.4^{ms}			206.6	$222.5L_1$ or $219.5L_3$	

Table AI continued

180 I	215 I	148 II	162 II	179 III	194 III	178 III	147 IV	178 IV	$\bar{E}$	E_γ	Nuclide
					208.3^{vw}						
				211.34^{vw}					211.3	$227.1L_1$	
				212.35^{vw}	212.2^{w}	212.2^{vw}			212.3	$216.2M_1$	
				218.50^{vw}							
				215.93^{vw}	215.9^{vvb}	215.9^{wmb}			215.9	$219.5M_2$	
				216.29^{vw}					216.3	$219.5M_3$	
				217.19^{vw}							
				218.56^{vwb}	218.6^{w}	218.6^{w}			218.6	$222.5M_1$ or $219.5N_1$	
				219.45^{vw}							
				221.57^{vw}					221.6	$227.5N_1$	
				224.63^{w}	224.7^{w}	224.4^{w}			224.6	$240.7L_1$	
				225.65^{vw}		225.4^{vw}			225.5	313.5K	
		233.21^{vw}	233.13^{vw}	233.13^{ms}	233.1^{s}	233.1^{vs}			233.1	$249.1L_1$	
					236.8^{vwb}				236.8	$240.7M_1$	
				241.21^{vw}							
				242.89^{w}	242.9^{w}	242.9^{wm}			242.9	330.9K	
				244.16^{vw}	244.0^{w}				244.1	332.1K	
				245.08^{w}	245.2^{vw-w}	245.2^{wb}			245.1	$249.1M_1$	
				246.73^{vw}	246.9^{w}	246.9^{w}			246.7	$262.8L_1$	206
				248.04^{m}		248.0^{m}			248.0	$264.0L_1$	203

Table AI continued

180 I	215 I	148 II	162 II	179 III	194 III	178 III	147 IV	178 IV	$\bar{E}$	E_γ	Nuclide
					248.2^{vvw}				248.2	$249.1N_1$	
				251.05^{vvw}							
			251.58^{vvw}			251.5^{vvw}					
				252.51^{vw}	252.6^{vw}	252.6^{vvw}			252.6	376.8K	
			253.50^{vvw}								
		255.74^{vw}	255.55^{m}	255.55^{vs}	255.4^{vvs}	255.4^{vvs}			255.6	343.5K	206
			257.09^{vvw}						257.1	$260.7M_2$	205
			258.20^{vvw}								
				258.92^{vvw}	259.0^{vw}	259.0^{vvw}			258.9	$262.8M_1$	206
				260.13^{vw}		260.1^{vvw}			260.1	$264.0M_1$	203
			260.80^{vvw}								
					261.6^{vvw}				261.6	349.6K or $262.8N_1$	205 206
				263.69^{s}		263.8^{vs}			263.7	$279.1L_1$	Pb^{203}
				264.30^{m}		264.3^{s}		264.1^{ms}	264.3	$279.1L_2$	Pb^{203}
				266.35^{w}		266.4^{ms}		266.1^{w}	266.3	$279.1L_3$	Pb^{203}
				273.13^{m}							
			273.50^{vw}		273.6^{m}	273.6^{wm}		273.2^{m}	273.5	$289.5L_1$	
					275.0^{vw}				275.0	$291.0L_1$	
				275.15^{w}		275.6^{s}			275.3	$279.1M_1$	Pb^{203}
					276.1^{vw}						
					277.2^{vw-vw}						

Table AI continued

180 I	215 I	148 II	162 II	179 III	194 III	178 III	147 IV	178 IV	$\bar{E}$	E_γ	Nuclide
						278.3^{w}			278.3	$279.1N_1$	PB^{203}
				280.00^{m}							
					280.4^{vwb}	280.4^{vwb}					
					283.1^{vvw}						
					287.0^{vvvs}	287.0^{vvvs}	287.0^{s-b}	287.0^{vvs}	287.0	375.0K	
					288.8^{w}	288.8^{w}	288.7^{w}	288.7^{w-m}	288.8	376.8K	
					290.9^{vvw}				290.9	$291.0L_1$	
						293.4^{wm}		293.6^{ms}	293.5	381.5K	203
					294.1^{vvw}						
					298.2^{vw}	298.2^{vw}			298.2	286.2K	206
					302.0^{vvw}						
					307.8^{vw}						
					310.1^{ms}	310.1^{s}	310.1^{vs}	310.1^{s}	310.1	398.0K	206
								312.0^{vw}			
					312.9^{vw-vvw}						
					314.9^{vw-vvw}				314.9	$330.9L_1$	
						315.6^{m}		315.1^{vw}	315.3	400.6K	Pb^{203}
					317.3^{w}	317.3^{vw}		317.7^{w}	317.5	405.5K	
					320.4^{vw}						
					324.5^{w}	324.3^{vw}		324.4^{w}	324.4	412.4K	
					327.6^{m}	327.6^{ms}	327.6^{s}	327.6^{m}	327.6	$343.5L_1$	206

Table AI continued

180 I	215 I	148 II	162 II	179 III	194 III	178 III	147 IV	178 IV	$\bar{E}$	E_γ	Nuclide
					333.7^{m}	333.7^{wm}	333.9^{m}	333.9^{vs}	333.8	421.8K	
					339.6^{w}	339.6^{w}	339.6^{w}	339.6^{vw}	339.6	$343.5M_1$	206
					342.6^{vvw}	342.6^{vvw}	342.2^{vvw}	342.2^{vw}	342.6	$343.5N_1$	
					344.6^{vvw}	344.6^{vvw}					
					350.9^{wm}	350.9^{wm}	350.8^{wm}	350.8^{ms}	350.8	438.8K	
					352.6^{vw}	352.3^{vvw}	352.2^{vvw}	352.2^{vw}	352.4	440.2K	
					359.0^{s}	359.0^{vsb}			359.1	$375.0L_1$	
					359.2^{s}		359.7^{vvsb}	359.7^{vvsb}	359.7	$375.0L_2$	
					362.1^{m}	362.1^{ms}		361.5^{s}	362.3	$375.0L_3$	
					363.8^{vvw}						
						365.2^{vvvw}					
					371.1^{m}	371.1^{s}	371.1^{s}	371.1^{vs}	371.1	$375.0M_1$	
					374.0^{w}	374.0^{wm}	374.5^{w}	374.5^{ms}	374.2	$375.0N_1$	
						377.6^{vvw}		377.2^{vvvw}	377.4	465.4K	203
					380.5^{vw}	380.5^{vw}	380.1^{vw}	380.1^{w}	380.3	468.3K	
					382.9^{w}	382.9^{w}	382.3^{vw}	382.3^{vw}	382.9	$398.0L_2$	206
					385.0^{vvw}	385.0^{vw}		385.3^{vw}	385.0	$398.0L_3$ or $400.6L_1$	206 Pb^{203}
					389.7^{vw}		389.9^{vvwb}	389.4^{w}	389.7	$405.5L_1$	
					394.2^{vvw}	394.2^{vw}	394.0^{vvw}		394.2	$398.0M_2$	206
								396.6^{vw-vvw}	396.6	$412.4L_1$	

Table AI continued

180 I	215 I	148 II	162 II	179 III	194 III	178 III	147 IV	178 IV	$\overline{E}$	E_γ	Nuclide
					397.8^{vw}		397.2^{vw}		397.2	$398.0N_1$	206
								402.2^{vw}			
					406.1^{vw}	406.1^{vw}		405.8^{w}	405.9	$421.8L_1$	
					409.1^{ms}	409.1^{s}	409.1^{vs}	409.1^{s}	409.1	497.2K	206
								410.0^{vw}			
					413.9^{w}	413.9^{w}	413.9^{n}	413.9^{vw}	413.9	501.8K	
					421.1^{vw-vw}						
								422.9^{vw}	422.9	$438.8L_1$	
					424.1^{vw}				424.1	$440.2L_1$	
					428.1^{s}	428.1^{s}	428.1^{vs}	428.1^{vs-s}	428.1	516.0K	206
					434.4^{vw}	434.4^{vwb}	434.3^{w-vw}	434.3^{m}	434.3	522.2K	
					444.6^{wm}	444.6^{wm}	444.6^{w}	444.6^{s}	444.6	532.6K	
					449.5^{s}	449.5^{vs}	449.5^{vs}	449.5^{vs}	449.5	537.5K	206
								450.3^{vw}			
					454.2^{vw}		454.1^{vw}	454.2^{vw}	454.2	542.2	
					458.0^{vw}			457.4^{vw}	457.7	545.7K	
						461.1^{vw}	460.5^{vw}	460.5^{w}	460.8	548.8K	
					464.4^{vw-vw}						
								476.1^{vw}			

Table AI continued

180 I	215 I	148 II	162 II	179 III	194 III	178 III	147 IV	178 IV	$\overline{E}$	E_γ	Nuclide
							480.3^{w}	480.3^{m}			
					481.3^{w}	481.3^{wm}	481.9^{vw}	481.9^{vvw}	481.6	$497.2L_1$	206
						482.3^{w}			482.3	570.3K	205
					486.1^{vvw}	486.1^{vvw}	485.6^{vvw}	485.8^{vw}	485.8	$501.8L_1$	
					489.1^{vvw}						
					493.2^{vw-vvw}	493.2^{vvw}	492.8^{vvw}	492.8^{vvw}	493.0	$497.2M_1$	206
					497.4^{vw}	497.4^{vvw}	497.7^{vvvw}	497.2^{w}	497.4	585.4K	
					500.9^{w-mb}	500.9^{msb}	500.9^{vs}	500.9^{s}	500.9	$516.0L_2$	206
					503.1^{vw}	503.1^{w}	502.7^{vw}	502.7^{vw}	502.9	$516.0L_3$	206
					507.0^{vvw}	506.7^{vvw}	506.3^{vvvw}	506.8^{vwb}	506.7	$522.2L_2$	
							509.2^{vvvw}	509.2^{vw}	509.2	$522.2L_3$	
					510.7^{vvw}						
					512.3^{vw-w}	512.3^{vvw}	512.5^{w-m}	512.5^{vw}	512.4	$516.0M_2$	206
					515.4^{vw}		515.8^{vwb}		515.6	$516.0N_2$	206
					516.8^{vw}	516.6^{vvwb}		516.4^{w}	516.6	$532.6L_1$	
						518.1^{vw}		518.1^{vvw}	518.1	606.1K	203
					521.7^{w}	521.7^{m}	521.7^{m}	521.7^{w}	521.7	$537.5L_1$	206
					524.4^{vvw}		524.0^{vvw}	524.0^{vw}	524.1	$537.5L_3$	206
					527.2^{vw}	527.2^{vvw}			527.2	615.2K	
					532.6^{vw-w}	532.6^{m}	532.6^{m}	532.4^{wb}	532.6	620.6K	206
						536.8^{vvw}	$537.1^{vvw?}$	537.1^{w-vw}	537.0	625.0K	203

Table AI continued

180 I	215 I	148 II	162 II	179 III	194 III	178 III	147 IV	178 IV	$\overline{E}$	E_γ	Nuclide
					540.0^{vw}						
					544.4^{vw}	544.4^{wm}	544.2^{wm}	544.2^{wb}	544.3	632.2K	206
								554.2^{vvw}			
					558.0^{vvw}		558.7^{vvw}	558.7^{vvw}	558.4	646.4K	
							562.3^{vvw}				
					563.0^{vvw}						
					567.4^{vvw}						
					569.6^{vvw}	569.6^{vvw}	569.3^{vw}	569.3^{vvw}	569.4	657.4K	206
					573.7^{w}	573.7^{wm}	573.3^{m}	573.3^{s}	573.5	661.5K	
					575.4^{vw}	575.4^{vw}	575.6^{vw}	575.6^{w}	575.5	663.4K	
					583.0^{ms}	583.0^{s}	583.2^{vs}	583.2^{ws}	583.1	671.0K	
					596.1^{vvw}	596.1^{vvw}	596.5^{vvw}	596.5^{vvw}	596.3	684.3K	
					603.2^{vw-vvw}						
							603.9^{vwb}	603.9^{w}	603.9	620.6 L_1	206
							607.6^{vvw}				
						612.2^{vvw}		611.7^{vvw}			
					615.3^{vvw}	615.3^{w}			615.3	703.4K	205
							617.0^{w}	617.0^{vvw}	617.0	632.2 L_1 or 620.6 M_1	206 206
						620.4^{w}		620.3^{m}	620.4	708.4K	
					621.5^{vw}						
					622.4^{vw}	622.4^{vw}	622.3^{wb}	$622.3D^{w}$	622.4	710.4K	

Table AI continued

180 I	215 I	148 II	162 II	179 III	194 III	178 III	147 IV	178 IV	$\bar{E}$	E_γ	Nuclide
					630.6^{vw}	630.6^{vwb}	630.3^{vw}	630.3^{w-m}	630.5	718.5K	
						634.5^{vw}		633.7^{w}	634.1	722.1K	203
					637.4^{vvw}	637.1^{vvw}	637.5^{vw}	637.5^{vw}	637.3	725.3K	
						645.5^{vvw}	645.8^{vw}	645.8^{vw}	645.6	$661.5L_1$	
					647.8^{vvwb} dart	647.8^{vvw}	648.4^{vw}	648.4^{vw}	648.1	$663.4L_1$	
						651.3^{vvw}			651.3	739.3K	206
					655.0^{w}	655.0^{w}	655.0^{w}	655.0^{ms}	655.0	$671.0L_1$	
						656.6^{vvw}					
							657.2^{vvw}	657.2^{w}	657.2	745.2K	
					657.7^{vvw}	657.7^{vvw}					
							660.4^{vvw}	660.6^{vvw}	660.5	748.5K	
						662.3^{vvw}					
							666.9^{vw}		666.9	$671.0M_1$	
					666.2^{vw}	666.2^{vvw}	666.9^{vw}	666.0^{m}	666.1	754.1K	206
						670.5^{vvw}	670.2^{vw}	670.5^{vvw}	670.4	$671.0M_1$	
					677.7^{vvw}		677.2^{vvvw}	677.2^{vw}	677.4	765.4K	
							683.7^{vvvw}				
								686.1^{vvw}			
						688.0^{vvw}			} 688.3	$703.4L_1$	205
							688.5^{vvw}				
							692.8^{vvw}				

Table AI continued

180 I	215 I	148 II	162 II	179 III	194 III	178 III	147 IV	178 IV	$\bar{E}$	E_γ	Nuclide
						695.7^{vvw}	694.6^{vvw}	694.6^{vvw}	694.6	$710.4L_1$	
					703.5^{w-vw}	703.5^{vvw}	704.4^{w}	704.4^{m}	704.4	791.9K	
						705.2^{vvw}					
							709.6^{vvw}	709.2^{vvw}	709.4	$725.3L_1$	
					715.3^{w-m}	715.3^{ms}	715.3^{s}	715.3^{m}	715.3	803.4K	206
						731.7^{w}		731.5^{m}	731.6	819.8K	203
					733.7^{vvw}						
							735.4^{vvwb}				
						736.5^{vs}		736.9^{vvs}	736.7	824.9K	203
								739.1^{vvw}			
					744.2^{vw-vvw}		744.4^{vw}	744.4^{vw}	744.3	832.3K	
					746.2^{vw-vvw}		746.4^{vw}	746.4^{vw}	746.3	834.3K	
							750.1^{vvw}				
							754.1^{vvw}		754.1	842.1K	206
					758.8^{vw-vvw}	758.9^{vw}	759.5^{vw}	759.5^{w-m}	759.1	844.1K	
							765.7^{vvw}				
							768.8^{vvwb}				
							775.9^{vvwb}	775.9^{vw}	775.9	$791.9L_1$	
					787.6^{vw-vvw}	787.6^{vw}	787.6^{w}	787.5^{vw}	787.6	$803.4L_1$	206
					792.5^{w}	792.5^{wm}	792.5^{m}	792.5^{w}	792.5	880.5K	206
							800.4^{vvw}		800.4	$803.4M_1$	206

Table AI continued

180 I	215 I	148 II	162 II	179 III	194 III	178 III	147 IV	178 IV	$\bar{E}$	E_γ	Nuclide
						804.3^{vvw}		803.9^{vvw}	804.1	$819.8L_1$	
					807.3^{vw}	807.3^{vw}	807.1^{w}		807.2	895.2K	206
						808.8^{m}		809.5^{vs}	809.1	$824.9L_1$	
					811.5^{ms}	811.5^{ms}	811.3^{vvs}	811.3^{vs}	811.4	899.2K	
							814.2^{vvw}				
						821.1^{vvw}		821.1^{w}	821.1	$824.9M_1$	
					823.9^{s}	823.9^{s}	824.0^{vvs}	824.0^{vvs}	823.9	911.5K	
					830.7^{w}	829.7^{vvw}	830.5^{w}	830.5^{wm}	830.3	918.4K	
							845.6^{vvvw}	845.6^{vvw-vw}	845.6	933.6K	
							853.3^{vvvw}				
							865.3^{vw}	865.3^{vvw}	865.3	$880.5L_2$	206
							879.3^{vvw}		879.3	$895.2L_1$	
					883.8^{w}	883.8^{w}	883.5^{w}	883.2^{ms}	883.5	$889.2L_1$	
							885.8^{vvw}	885.8^{vw}	885.8	$899.2L_3$	
							890.6^{vvvw}				
							896.1^{s}	896.1^{vvs}	896.1	$811.5L_2$	
							898.4^{vw}	998.4^{w}	898.4	$911.5L_3$	
							902.7^{vvw}	902.7^{vw}	902.7	$918.4L_1$	
							908.0^{w}	908.0^{m}	908.0	$911.5M_1$	
							910.4^{vw}	910.4^{w}	910.4	$911.5N_1$	
							914.3^{vvw}		914.3	$918.4M_1$	

Table AI continued

180 I	215 I	148 II	162 II	179 III	194 III	178 IV	147 IV	178 IV	$\bar{E}$	E_γ	Nuclide
							930.8^{vw}	930.8^{vw}	930.8	1018.8K	206
								945.5^{w-m}	945.5	1033.7K	
							956.1^{vw}	955.4^{vw-w}	955.7	1043.7K	205
							968.7^{vw}	968.7^{w-vw}	968.7	1056.7K	
							1004.1^{vvw}				
							1011.3^{vvw}		1011.3	1099.3K	206
								1018.0^{vvw}	1018.0	1033.7L_1	
								1022.6^{vvw}			
							1051.8^{vw-vvw}	1051.8^{vvw}	1051.8	1139.8K	
								1069.8^{vvw}			
								1111.7^{vvw}			
							1116.4^{vw}	1115.4^{vw}	1115.9	1203.9K	
							1123.5^{vw}		1123.5	1211.5K	
								1448.4^{vw}	1448.4	1536.4K	203

Table AII

Bismuth-205 Conversion Lines from Permanent-Magnet Electron Spectrographs

Plate Number 254	245	260	251	Average Energy	Transition Energy	
Spectrograph PM III	PM IV	PM IV	PM II	$\bar{E}$	E_γ	Nuclide
			15.13^{vw}	15.13	L_1 31.12	205 ?
			16.99^{vwb}	16.99	L_1 32.83	205
			18.65^{vwb}			
			22.33^{vw}			
			26.05^{vwb}			
			27.39^{vwb}	27.39	M_1 31.12	205 ?
			28.96^{vwb}	28.96	M_1 37.83	205
			48.56^{vw}			
			56.72^{w-vw}		L_2L_1 Auger	
			57.28^{vvwb}		L_2L_2	
			59.00^{vwb}		L_1L_3	
			59.57^{wb}		L_2L_3	
			60.21^{vw}			
			60.79^{vvw}	60.79	K148.6	205 ?
			61.63^{vw}		L_3L_3	
			62.35^{vw}			
			66.50^{vvw}			
			75.94^{vvw-vw}	75.94	L_1 91.86	205
			76.73^{vvw-vw}	76.73	L_2 91.86	
96.1^{s}		95.7^{s}	95.94^{ms}	95.9	K184.1	206
97.0^{vw}		97.2^{w}		97.1	L_2 112.2	205
98.9^{vw}		99.3^{w}		99.1	L_3 112.2	205
			104.56^{vw}	104.6	K192.6	205
			115.3^{vvw}	115.3	L_2 131.2	
116.0^{vvw}			116.1^{vvw}	116.1	L_2 131.2	205
117.6^{vvw}				117.6	L_3 131.2	

Table AII continued

254 PM III	245 PM IV	260 PM IV	251 PM II	$\bar{E}$	E_γ	Nuclide
133.3^{vw}				133.3	L_1 149.2	205
148.1^{vw}				148.1	K 236.1	206
155.3^{vvw}						
159.2^{vvw}						
161.4^{vvw}						
168.3^{s}			168.5^{w}	168.3	L_1 184.1	206
172.4^{s}		172.5^{s}	172.5^{w}	172.5	K 260.5	205
174.8^{s}		175.0^{w}	174.84^{w-vw}	174.9	K 267.8	206
180.3^{w}				180.3	M_1 184.1	206
183.1^{vw}				183.1	N_1 184.1	206
187.4^{vvw}			192.4^{vvw}	187.4	L_2 202.6	206
$\sim 193.7^{w}$		194.3^{w}	194.5^{vwb}	194.5	K 282.4	205
196.0^{s}		196.1^{s}	196.24^{w}	196.1	K 284.0	205
			216.8			
220.0^{vvw}				220.0	L_1 236.0	206
221.4^{vvw}						
225.0^{vvw}				225.0	K 313.0	206
			226.2^{vvw}			
			236.2^{vvw}			
240.8^{vvw}						
244.3^{w}		244.7^{w-b}		244.6	L_1 260.5	206
246.9^{w}		246.9^{vw-vvw}	247.98^{vw}	246.9	L_1 262.8	206
249.4^{vvw}				249.4	L_3 262.8	206
255.4^{s}	255.3^{s}	255.6^{w-b}	255.5^{w}	255.4	K 343.5	206
261.3^{vw}		261.4^{w-b}		261.4	K 349.3K	205
		266.5^{vwb}		266.5	L_1 282.4	205
268.1^{vw}	267.9^{m}	268.1^{w-b}		268.0	L_1 284.0	205
		273.2^{vvw}				
275.6^{vvw}			275.1^{vw}			
279.9^{vvw}		280.2^{vw}		280.1	M_1 284.0	205
295.1^{vvw}		295.5^{vwb}		295.3	K 383.3	205

Table AII continued

254 PM III	245 PM IV	260 PM IV	251 PM II	$\overline{E}$	E_γ	Nuclide
298.2^{vw}				298.2	L_1 313.5	206
310.1^{m}	310.1^{s}	309.6^{vwb}		310.0	K 398.1	206
327.6^{mw}	327.6^{s}			327.6	L_1 343.5	206
333.7^{vw}	333.6^{vw}	334.0^{vw}		334.0	L_2 349.3	205
339.6^{vwb}	339.6^{vw}			339.6	M_1 342.5	206
370.7^{vw}						
372.8^{vw}						
	382.3^{wm}			382.3	L_1 398.1	206
	387.3^{vw}					
~405.0^{vw}	405.8^{vw}	405.5^{vw}		405.6	K 493.5	205
409.1^{w}	409.1^{s}	409.1^{vw}		409.1	K 497.1	206
		419.4^{vw}				
423.1^{vw}	424.4^{w}	423.7^{w}		423.7	K 511.7	205
428.1^{m}	428.1^{s}	428.2^{vw}		428.1	K 516.1	206
	436.9^{vw}			436.9	K 526.0	205
	443.1^{vw}			443.1	K 531.1	205
	$447.7^{vw?}$					
449.5^{m}	449.5^{s}	449.4^{vwb}		449.5	K 537.4	206
				462.3	K 550.3	205
481.3^{vw}	461.7^{vw}	462.9^{vw}		481.3	L_1 497.1	206
482.3^{w}	483.0^{vs}	482.2^{s}		482.7	K 570.7	205
	485.6^{vw}	485.7^{vw} ?		485.7	K 573.7	205
491.4^{vw}	491.8^{w}	491.6^{w}		491.6	K 579.7	205
	499.1^{w}			499.1	L_1 516	206
500.9^{w}	500.9^{wm}	500.4^{vw}		500.7	L_2 516.1	206
503.1^{vw}	502.7^{vw}			502.9	L_3 516.1	206
	510.3^{vw}			510.3	L_1 526.0	205
512.3^{vw}	512.5^{vw}			512.4	M_2 516.1	206
516.0^{vw}	516.0^{vvwb}			516.0	N 516.1	206
521.7^{vw}	521.7^{vw}			521.7	L_1 537.4	206
532.6^{vw}	533.0^{vw}			532.8	K 620.8 or M_1 537.4	206 206

Table AII continued

254 PM III	245 PM IV	260 PM IV	251 PM II	$\bar{E}$	E_γ	Nuclide
536.8^{vvw}	537.1^{w}			536.9	N_1 537.4	206
		538.2^{vwb}		538.2	K 626.2	205
544.4^{vw}	544.2^{vw}			544.3	K 632.3	206
		$545.6^{vvw?}$				
554.4^{w}	554.7^{vw}	554.6^{vwb}		554.6	L_1 570.7	205
563.7^{vvw}	564.2^{vvw}	563.3^{vwb}		563.7	L_1 579.7	205
		567.0^{vvw}		567.0	M_1 570.7	205
569.6^{vvw}	569.3^{vvw}			569.5	K 657.4	206
	576.2^{vvvw}			576.2	M_1 579.7	205
	594.1^{vvvw}					
615.3^{ms}	615.6^{vs}	615.0^{s}		615.3	K 703.3	205
628.6^{vw}				628.6	M_1 632.3	206
	641.3^{vvwb}			641.3	L_1 657.4	206
		644.4^{vvw}		644.4	L_3 657.4	206
	$657.4^{vvwb?}$	656.4^{vvw}		656.6	K 744.6	205
	671.5^{vvw}	669.7^{vvw}		670.6	758.6K	205
686.3^{vw}				686.3	L_1 702.2	205
	687.9^{w}	688.1^{w}		688.0	L_2 703.3	205
		690.6^{vvw}		690.6	L_3 703.3	205
692.8^{vvw}						
699.5^{vvw}	699.8^{vw}	699.2^{vvw}		699.5	M_2 703.3	205
715.3^{mw}	715.3^{w}			715.3	K 803.4	206
		718.2^{vvw}				
		739.9^{vvw}				
		742.5^{vvw}		742.5	L_1 758.5	205
775.9^{vvw}						
787.5^{vw}	787.4^{vw}			787.5	L_1 803.4	206
792.5^{w}	792.5^{w}			792.5	K 880.8	206
807.3^{vw}	806.5^{w}	806.0^{vvw-vw}		806.6	K 895.2	206
822.4^{vw}	822.5^{vw}	823.2^{vw}		822.7	K 910.7	205
		828.0^{vvw-vw}				
		830.6^{vwb}				
		842.6^{vvwb}				

Table AII continued

254 PM III	245 PM IV	260 PM IV	251 PM II	$\bar{E}$	E_γ	Nuclide
	865.3^{vvw}			865.3	L_1 880.8	206
		879.9^{vvw}		879.9	L_1 895.2	206
	899.4^{w-m}	899.3^{w}		899.4	K 987.5	205
	925.8^{vvw}	926.1^{vw-vvw}		926.0	K1014.0	205
		936.9^{vvw}				
	956.1^{w-m}	955.0^{w}		955.5	K1043.5	205
	971.8^{vvw}			971.8	L_1 987.5	202
	975.8^{vvw}	975.3^{vvw}		975.5	K1063.5	207
	985.3^{vvw}			985.3	K1073.3	205
		1007.7^{vvw}		1007.7	K1095.7	206 ?
	1015.2^{vw}					
		1026.7^{vvw}		1026.7	L_1 1043.5	205
		1047.4^{vvw}				
	1065.6^{vvvw}					
	1102.6^{vw}	1101.7^{vw}		1102.1	K1190.1	205
	1124.8^{vvw}					
	1150.6^{vvw}					
	1170.5^{vvw}					
	1258.2^{vvw}			1258.2	K1346.2	205
	1440.0^{vvw}					
	1529.0^{vvw}			1529.0	K1617.0	205
	1543.0^{vvw}					
	1650.0^{vvw}					

Table AIII

Assignment of Transitions Observed in Permanent-Magnet Electron Spectrographs

	Av E_γ	E_e	Shell	E_γ	Visual intensity	Photo intensity	Probable multipole order	Basis for multipole order assignment and comments
Bi^{203}	First Confidence Group							
	126.4	38.50	K	126.50	vw		E2	L subshell
		111.21	L_2	126.41	s	296		$L_2/L_3/M_2/M_3$=1.3/1.0/.4/.3
		113.39	L_3	126.42	m-s	232		
		122.86	M_2	126.42	w-m	101		E_2 th value L_2/L_3 = 1.5/1.0
		123.27	M_3	126.34	w	62		
		126.13	N'_s	126.54	vvw			
	186.5	98.4	K	186.4	vvs	1040	M1	K/L ratio, L subshell
		170.7	L_1	186.6	ms	200		$K/L_1/M_1$=5.2/1.0/.4
		182.8	M_1	186.6	w	172		th value K/L=5.5
		185.5	N_1	186.4	vw			
	264.0	176.1	K	264.1	vs	770	M1	L subshell, K/L ratio
		248.0	L_1	263.9	m	183		K/L=4.3
		260.1	M_1	264.0	vw			th value K/L=5.6
	819.8	731.6	K	819.6	m-w	102		
		804.1	L_1	820.0	vvw			

Table AIII continued

Av E_γ	E_e	Shell	E_γ	Visual intensity	Photo intensity	Probable multipole order	Basis for multipole order assignment and comments
Bi^{203} continued							
First Confidence Group							
824.9	736.7	K	824.7	vs	1000	M4	Lifetime, K/L ratio
	809.1	L_1	825.0	m	255		$K/L_1/M_1$=3.9/1.0/0.6
	821.1	M_1	825.0	vvw	149		Th value K/L = 3.5
1033.7	945.5	K	1033.5	w-m	35		
	1018.0	L_1	1033.9	vvw			
Second Confidence Group							
60.08	44.23	L_1	60.09	vw		M1	M_1 in Auger Group (56:16)
	59.18	N_1	60.07	w			
117.7	29.61	K	117.61	w		M1	101.84 is also M_1 of 105.5-204
	101.84	L_1	117.69	vw			
	113.82	M_1	117.68	vvw?			
	116.94	N_1	117.83	vvw			
Third Confidence Group							
	293.5	K	381.5	m-s	100		(twice)
	377.4	K	465.4	vvw			(twice)
	518.1	K	606.1	vw	48		(twice)
	537.0	K	625.0	w-vw			(twice)

Table AIII continued

	Av E_γ	E_e	Shell	E_γ	Visual intensity	Photo intensity	Probable multipole order	Basis for multipole order assignment and comments
Bi^{203} continued								
Third Confidence Group								
		620.4	K	708.4	m	75		(twice)
		634.1	K	722.1	w	31		(twice)
		1448.4	K	1536.4	vw	64		(once)
Bi^{204}								
First Confidence Group								
	78.60	63.43	L_2	78.63	s	3081	E2	L subshell
		65.63	L_3	78.66	m-s	2602		$L_2/L_3/M_2/M_3$ = 1.2/1.0/0.35/0.30
		74.69	M_1	78.54	vw			
		75.01	M_2	78.57	m	949		Th value L_2/L_3=1.2/1.0
		75.51	M_3	78.58	w-m	783		
		77.92	N_3	78.56	vw			
	80.22	64.37	L_1	80.23	s	2090	M1	L subshell
		65.03	L_2	80.23	vw			L_1/M_1=1.0/0.27
		76.31	M_1	80.16	s	551		
		79.37	N_1	80.26	w-m			
	100.4	84.6	L_1	100.5	m	269	M1	L subshell
		85.2	L_2	100.4	vvw			
		96.5	M_1	100.4	vw			

Table AIII continued

Av E_γ	E_e	Shell	E_γ	Visual intensity	Photo intensity	Probable multipole order	Basis for multipole order assignment and comments
Bi^{204} continued							
First Confidence Group							
119.8	31.75	K	119.75	w		M1	L subshell
	103.96	L_1	119.81	vvw			
140.9	52.78	K	140.78	s	1234	M1	L subshell
	125.0	L_1	140.9	m	511		$K/L_1/M_1$ = 2.5/1.0/0.45
	137.0	M_1	140.9	vw-w	114		Th value K/L=5.5
144.5	56.50	K	144.5	m		M1	L subshell
	128.6	L_1	144.5	w-m			
	140.6	M_1	144.5	vw			
	143.8	N_1	144.7	vvw			
170.0	81.9	K	169.9	s	374	M1	K/L ratio, L subshell
	154.2	L_1	170.1	w	63		$K/L_1/M_1$=6.0/1.0/1.0
	166.1	M_1	170.0	vw	77		Th value K/L=5.5
176.2	88.05	K	176.1	vvs	1820	M1	L subshell
	160.4	L_1	176.3	m-s	754		$K/L_1/M_1$=2.5/1.0/0.15
	172.4	M_1	176.3	w	112		Th value K/L-5.5
212.7	124.5	K	212.5	m	89		
	197.0	L_1	212.9	vw			
	128.2	K	216.2	vs	1632	M1	L subshell

Table AIII continued

Av E_γ	E_e	Shell	E_γ	Visual intensity	Photo intensity	Probable multipole order	Basis for multipole order assignment and comments
Bi^{204} continued							
First Confidence Group							
216.2	200.4	L_1	216.3	m	532		$K/L_1/M_1$= 3.0/1.0/0.20
	212.3	M_1	216.2	vw	103		Th value K/L=5.5
219.5	131.4	K	219.4	m	502	E2	206.6 is also L_1 of 222.5
	204.3	L_2	219.5	w-m	804		218.6 is also M_1 of 222.5 L subshell, K/L ratio
	206.6	L_3	219.6	m	451		$K/L_2/L_3/M_2/N_2$= 62/1.0/0.56/0.16/0.16
	215.9	M_2	219.5	vvw	131		Th value $K/L_2/L_3$= 1.3/1.0/0.52
	216.3	M_3	219.4	vvw			
	218.6	N_2	219.4	vw	130		
222.5	134.4	K	222.4	s	940	M1	206.6 is L_3 of 219.5, 218.6 is N_1 of 219.5 L subshell
	206.6	L_1	222.5	m	451		$K/L_1/M_1$=2.1/1.0/.30
	218.6	M_1	222.5	vw	130		Th value K/L=5.5
	221.6	N_1	222.5	vvw			

Table AIII continued

	Av E_γ	E_e	Shell	E_γ	Visual intensity	Photo intensity	Probable multipole order	Basis for multipole order assignment and comments
Bi^{204} continued								
First Confidence Group								
	227.1	139.0	K	227.0	w-vw	80		
		211.3	L_1	227.2	vvw			
	240.7	152.7	K	240.7	s	292	M1	L subshell
		224.6	L_1	240.5	w	130		$K/L_1/M_1$=2.2/1.0/.12
		236.8	M_1	240.7	vvw	16		
	249.1	161.3	K	249.3	vvvs	1822	M1	L subshell
		233.1	L_1	249.0	s	541		$K/L_1/M_1$=3.4/1.0/.17
		245.1	M_1	249.0	w-vw	92		Th value K/L=2.5
		248.2	N_1	249.1	vvw			
	289.5	201.5	K	289.5	vvs	1439	M1	L subshell
		273.5	L_1	289.4	m	394		K/L_1=3.7/1.0
								Th value K/L=5.5
	291.0	203.0	K	291.0	s	572	M1	L subshell, K/L ratio
		275.0	L_1	290.9	vvw	75		K/L_1=7.5/1.0
								Th value K/L=5.5
	330.9	242.9	K	330.9	w	170	M1	L subshell, K/L ratio
		314.9	L_1	330.8	vw-vvw	26		K/L_1=6.5/1.0
								Th value K/L=5.5

Table AIII continued

Av E_γ	E_e	Shell	E_γ	Visual intensity	Photo intensity	Probable multipole order	Basis for multipole order assignment and comments
Bi^{204} continued							
First Confidence Group							
375.0	287.0	K	375.0	vvvs	3965	E2	K/L ratio, L subshell
	359.1	L_1	375.0	s	1816		$K/L_1L_2/L_3/M_1/N_1$= 2.2/1.0/.34/.36/.12
	359.7	L_2	374.9	s			
	362.3	L_3	375.3	m	609		Th value $K/L_1L_2/L_3$= 2.5/1.0/.22
	371.1	M_1	375.0	m	649		
	374.2	N_1	375.1	w	215		
	317.5	K	405.5	w	133	M1	L subshell
405.5	389.7	L_1	405.6	vw	41		K/L_1=3.3/1.0 Th value K/L=5.5
412.4	324.4	K	412.4	w	123		
	396.6	L_1	412.5	vw-vvw			
421.8	333.8	K	421.8	vs	318	M1	L subshell, K/L ratio
	405.9	L_1	421.8	w	76		K/L_1=4.2/1.0 Th value K/L=5.5
438.8	350.8	K	438.8	ms	225		
	422.9	L_1	438.8	vw			
501.8	413.9	K	501.9	w	146		
	485.8	L_1	501.7	vvw			

Table AIII continued

Av E_γ	E_e	Shell	E_γ	Visual intensity	Photo intensity	Probable multipole order	Basis for multipole order assignment and comments
Bi^{204} continued							
First Confidence Group							
522.2	434.3	K	522.3	m	119	E2	L subshell, K/L ratio
	506.7	L_{12}	521.9	vw	37		K/L_1L_2=3.1/1.0
	509.2	L_3	522.2	vw			Th value K/L=3.1
532.6	444.6	K	532.6	s	264		
	516.6	L_1	532.5	w			
661.5	573.5	K	661.5	s	214	E1 or M1	L subshell, K/L ratio
	645.6	L_1	661.5	vw	34		K/L_1=6.3
							E1 K/L=6.2
							M1 K/L=5.8
663.4	575.5	K	663.5	w	80	E2	L subshell
	648.1	L_2	663.3	vw	36		K/L_{12}=2.2/1.0
							Th value K/L=4.3
	583.1	K	671.1	vs	810	M1	L subshell, K/L ratio
671.0	655.0	L_1	670.9	w	136		$K/L_1/M_1$=5.9/1.0/.5
	666.9	M_1	670.8	vw	69		Th value K/L_1=5.6
	670.4	N_1	671.3	vw			
710.4	622.4	K	710.4	w	116		
	694.6	L_1	710.5	vvw			

Table AIII continued

Av E_γ	E_e	Shell	E_γ	Visual intensity	Photo intensity	Probable multipole order	Basis for multipole order assignment and comments
Bi^{204} continued							
First Confidence Group							
725.3	637.3	K	725.3	vw	48		
	709.4	L_1	725.3	vvvw			
791.9	704.0	K	792.0	m	91		
	775.9	L_1	791.8	vw			
899.2	811.4	K	899.4	vs	1000	E2	L subshell, K/L ratio
	883.5	L_{12}	899.4	m	201		$K/L_1L_2/L_3$= 5.0/1.0/.18
	885.8	L_3	898.8	vw	37		Th value $K/L_1L_2/L_3$= 4.8/1.0/.13
911.5	823.9	K	911.9	vvs	1330	E5	Lifetime, L subshell K/L ratio
	896.1	L_2	911.3	vs	845		$K/L_2/L_3/M_2/N_2$= 1.6/1.0/.16/.22/.07
	898.4	L_3	911.4	w	132		
	908.0	M_2	911.6	m	184		Th value $K/L_2/L_3$ = 1.7/1.0/.22
	910.4	N_2	911.2	w	62		
918.4	830.3	K	918.3	w-m	110	E2	K/L ratio
	902.7	L_1	918.6	vw	54		K/L_1≈2.0 E2 Th value K/L = 4.9/1.0
	914.3	M_1	918.2	vvw			

Table AIII continued

Av E_γ	E_e	Shell	E_γ	Visual intensity	Photo intensity	Probable multipole order	Basis for multipole order assignment and comments
Bi^{204} continued							
Second Confidence Group							
105.5	89.57	L_1	105.43	vvw			otherwise assign as 177.6K--could be L_1 of 203-117
	101.84	M_1	105.69	vw			
109.1	93.24	L_1	109.10	vw			
	93.90	L_2	109.10	vw			L_3 hidden by 184K-206
	105.75	M_2	109.31	vvw			
164.9	76.9	K	164.9	w			
	149.0	L_1	164.9	w	71		
184.9	169.0	L_1	184.9	vw	88	M1-E2	L subshell
	169.7	L_2	184.9	vw	88		$L_1/L_2=1.0/1.0$
213.5	125.5	K	213.5	w	172	E2	L_3 hidden by $L_1$216
	198.4	L_2	213.6	vw	94		K/L ratio, L subshell $K/L_2=1.8/1.0$ Th value $K/L_2=1.6/1.0$
252.4	164.4	K	252.4	w	82		
	236.8	L_1	252.7	vvw			this is M_1 of 240.7--is braod line
440.2	352.4	K	440.4	vw	54	?	
	424.1	L_1	440.2	vvw	30		$K/L_1=1.8$

Table AIII continued

Av E_γ	E_e	Shell	E_γ	Visual intensity	Photo intensity	Probable multipole order	Basis for multipole order assignment and comments
Bi^{204} continued							
Third Confidence Group							
	80.83	K	168.8	m-w	344		(seen four times)
	121.1	K	209.1	w-vw			(twice)
	244.1	K	332.1	m-w	107		(twice)
	252.6	K	340.6	w-vw	67		(three times)
	288.8	K	376.8	w-m	211		(four times)
	380.3	K	468.3	w	122		(four times)
	454.2	K	542.2	vw	36		(three times)
	457.7	K	545.7	vw	29		(three times
	460.8	K	548.8	w			(three times)
	497.4	K	585.4	w			(four times
	527.2	K	615.2	vw			(twice)
	558.4	K	646.4	vvw			(three times)
	596.3	K	684.3	vvw			(four times)
	630.5	K	718.5	w-m	45		(four times)
	657.2	K	745.2	vw			(twice)
	660.5	K	748.5	vvw	113		(twice)
	677.4	K	765.4	vw			(three times)
	746.3	K	832.3	vw	44		(three times)

Table AIII continued

Av E_γ	E_e	Shell	E_γ	Visual intensity	Photo intensity	Probable multipole order	Basis for multipole order assignment and comments
Bi^{204} continued							
Third Confidence Group							
	744.3	K	834.3	vw	45		(three times)
	759.1	K	844.1	w-m	96		(four times)
	845.6	K	933.6	vvw-vw			(twice)
	968.7	K	1056.7	w-vw	30		(twice)
	1051.8	K	1139.8	vvw			(twice)
	1115.9	K	1203.9	vw			(twice)
	1123.5	K	1211.5	vw			(once)
Bi^{205} Transitions possibly seen in Bi^{203} and Bi^{204} Spectra							
112.5	97.4	L_2	112.6	vvw			
	99.4	L_3	112.4	vvw			
260.5	172.5	K	260.5	m			also 176.2 M_1-204
	245.1P	L_2	260.3	w			also 249.1 M_1-204
	257.1	M_2	260.7	vvw			
281.6	193.6	K	281.6	w			
284.1	196.1	K	284.1	m			
349.6	261.6	K	349.6	vvw			also 262.8 N_1-206
493.9	405.9P	K	493.9	w			also L_1 421.8-204
510.9	422.9P	K	510.9	vw			also 135.8L_1-204

Table AIII continued

	Av E_γ	E_e	Shell	E_γ	Visual intensity	Photo intensity	Probable multipole order	Basis for multipole order assignment and comments
Bi^{205} continued								
	570.3	482.3	K	570.3	w			
	624.9	536.9P	K	624.9	w-vw			also 625.0K-203 intensities off
	703.4	615.3	K	703.3	w			
		688.3	L_1	703.5	vvw			
	1043.7	955.7	K	1043.7	vw			

					Visual intensity	Photo intensity	P and A* Multi-pole order assign.	P and A* K/L_{1+2}	This work K/L_{1+2}	Comments
Bi^{206}										
	184.2	96.0	K	184.0	vvvs	4817	M1	6.0	5.7	
		168.5	L_1	184.4	vs	850				
		180.4	M_1	184.3	w-m					
		183.2	N_1	184.1	vw					
	234.4	146.4	K	234.4	vw		M1			
	262.8	175.1	K	263.1	s	468	M1	6.0	3.2	
		246.7	L_1	262.6	w	145				

* Pryce and Alburger

Table AIII continued

	Av E_γ	E_e	Shell	E_γ	Visual intensity	Photo intensity	P and A* Multi-pole order assign.	P and A* K/L_{1+2}	This work K/L_{1+2}	Comments
Bi^{206} continued										
		258.9	M_1	268.8	vw					
		261.6	N_1	262.5	vvw					
	343.5	255.6	K	343.6	vvs	2061	M1	5.3	4.2	
		327.6	L_1	343.5	m	492				
		339.6	M_1	343.5	w					
		342.6	N_1	343.5	vvw					
	386.2	298.2	K	386.2	vw		M1			
	398.0	310.1	K	398.1	s	977	M1+E2	5.5	5.5	M1-E2 mixing
		382.9	L_2	398.1	w	178				
		385.0	L_3	398.0	vw	114		also 400.6 Pb^{203} L_1		
		394.2	M_2	397.8	vw					
		397.2	N_2	398.0	vvw					
		409.1	K	497.1	s	670	M1+E2	5.7	4.6	
	497.2	481.6	L_1	497.5	w-m	145				
		493.0	M_1	496.9	vvw					
	516.0	428.1	K	516.1	s	946	E3	1.8	1.9	
		500.9	L_2	516.1	m-w	515				

*Pryce and Alburger

Table AIII continued

	Av E_γ	E_e	Shell	E_γ	Visual intensity	Photo intensity	P and A* Multi-pole order assign.	P and A* K/L_{1+2}	This work K/L_{1+2}	Comments
Bi^{206} continued										
		502.9	L_3	515.9	vw	105				
		512.4	M_2	516.0	w-vw					
		515.6	N_2	516.3	vw					
	537.5	449.5	K	537.5	vs	1000	M1 + E2	5.6	6.1	
		521.7	L_1	537.6	m	164				
		524.1	L_3	537.1	vvw					
	620.6	532.6	K	620.6	m	154	M1 + E2	5.3	3.4	
		603.9	L_1	619.8	vw	45				
		617.0	M_1	620.9	w		also L_1 of 632.2-206			
	632.2	544.3	K	632.3	wm	93	M1 + E2		1.1	
		617.0	L_2	632.2	w	86	also M_1 of 620.6-206			
	657.4	569.4	K	657.4	vvw		M1 + E2			
	803.4	715.3	K	803.3	s	331	E2	4.7	6.7	
		787.6	L_1	803.5	w	49				
		800.4	M_1	804.3	vvw					
	880.5	792.5	K	880.5	m	184	E2	4.8	3.9	
		865.3	L_2	880.5	vw	47				
	895.2	807.2	K	895.2	w	118	M1 + E2		3.7	
		879.3	L_1	895.2	vvw	32				

* Pryce and Alburger

Table AIII continued

	Av E_γ	E_e	Shell	E_γ	Visual intensity	Photo intensity	P and A* Multi-pole order assign.	K/L_{1+2}	This work K/L_{1+2}	Comments
Bi^{206} continued										
	1018.8	930.8	K	1018.8	vw		M1 + E2			
	1099.3	1011.3	K	1099.3	vvw		E1			
	123.7	107.8	L_1	123.7	vvw		M1			
	202.4	114.3	K	202.3	vvw		E3			
		187.3	L_2	202.5	vvw					
	313.5	225.5	K	313.5	vw		M1			
	739.3	651.3	K	739.3	vvw		E1			
	754.1	666.1	K	754.1	vw		E2			
	842.1	754.1	K	842.1	vvvw		E1			

	Probable multipole order	Basis for multipole order assignment and comments
Bi^{205}		
First Confidence Group		
112.2 97.1 L_2 112.3 w 113	E2	L subshell
99.3 L_3 112.1 w 81		L_2/L_3=1.4/1.0 Th value L_2/L_3=1.3/1.0

Table AIII continued

Av E_γ	E_e	Shell	E_γ	Visual intensity	Photo intensity	Probable multipole order	Basis for multipole order assignment and comments
Bi^{205} continued							
First Confidence Group							
260.5	172.5	K	260.5	s	833	M1	L subshell
	244.6	L_1	260.5	w			
282.5	194.5	K	282.5	w	333	M1	L subshell
	266.5	L_1	282.4	vw			
284.0	196.1	K	284.1	s	1156	M1	L subshell
	268.0	L_1	283.9	w	244		K/L_1=4.8 Th value K/L=5.5
	280.1	M_1	284.0	vw			
349.3	261.4	K	349.4	w	292	E2	L subshell
	334.0	L_2	349.2	vw			
570.7	482.7	K	570.7	s	765	M1	L subshell
	554.6	L_1	570.5	vw	83		K/L_1=9.2 Th value K/L=5.5
	567.0	M_1	570.9	vvw			
579.7	491.6	K	579.6	w	256		
	563.7	L_1	579.6	vw			
	576.2	M_1	580.1	vvvw			
703.3	615.3	K	703.3	s	1000	E2	L subshell, K/L ratio
	688.0	L_2	703.2	w	183		K/L_2=5.5 Th value K/L_2=4.5
	690.6	L_3	703.6	vvw			
	699.5	M_2	703.1	vvw			

Table AIII continued

Av E_γ	E_e	Shell	E_γ	Visual intensity	Photo intensity	Probable multipole order	Basis for multipole order assignment and comments
Bi^{205} continued							
First Confidence Group							
758.5	670.6	K	758.6	vvw			
	742.5	L_1	758.4	vvw			
987.5	899.4	K	987.4	w-m	205		
	971.8	L_1	987.7	vvw			
1043.5	955.5	K	1043.5	w-m	220		
	1026.7	L_1	1042.6	vvw			
Second Confidence Group							
31.12	15.13	L_1	30.99	vw			
	27.39	M_1	31.24	vvw			
32.83	16.99	L_1	32.85	vw			
	28.96	M_1	32.81	vvw			
91.96	75.94	L_1	91.80	vw-vvw			
	76.73	L_2	91.93	vw-vvw			
131.2	115.3	L_1	131.2	vvw			
	116.1	L_2	131.3	vvw			
	117.6	L_3	130.6	vvvw			
149.0	60.79	K	148.8	vvw			
	133.3	L_1	149.2	vvw-vw			

Table AIII continued

	Av E_γ	E_e	Shell	E_γ	Visual intensity	Photo intensity	Probable multipole order	Basis for multipole order assignment and comments
Bi^{205} continued								
Third Confidence Group								
	192.6	104.56	K	192.6	vw			(seen once)
	383.3	295.3	K	383.3	vw			(seen twice)
	493.5	405.3	K	493.5	vw	110		(three times)
	511.7	423.7	K	511.7	w	160		(three times)
	526.0	436.9	K	525.9	vw			(once)
		510.3	L_1	526.2	vvw			(once)
	531.1	443.1	K	531.1	vvw			(once)
	550.3	462.3	K	550.3	vw			(twice)
	573.7	485.7	K	573.7	vvw			(twice)
	626.2	538.2	K	626.2	vw			(once)
	744.6	656.6	K	744.6	vvw			(twice)
	910.7	822.7	K	910.7	vw			(three times)
	1014.0	926.0	K	1014.0	vvw			(twice)
	1073.3	985.3	K	1073.3	vvw			(once)
	1190.1	1102.1	K	1190.1	vw			(twice)
	1346.0	1258.2	K	1346.0	vvw			(once)
	1617.0	1529.0	K	1617.0	vvw			(once)

Table AIII continued

Bi^{206} and Bi^{207} Transitions seen in Bi^{205} Spectra

	E_e	Shell	E_γ	Visible intensity	Number of times seen
Bi^{207}					
	975.5	K	1063.5	vw	2

Bi^{206}

Visual Intensity of K-line

E_γ	Shells Seen	Plate Number 245 Spectrograph PM II	254 PM III	260 PM IV
184.1	$KL_1M_1N_1$	T.B.	s	s
236.0	KL_1	T.B.	vw	-
262.8	KL_1L_3	T.B.	s	w
343.6	KL_1M_1	s	s	w
398.1	KL_1L_3 ?	s	m	vw
497.1	KL_1	s	w	vvw
516.1	$KL_2L_3M_2N_2$	s	m	vw
537.4	$KL_1M_1N_1$	s	m	vw
620.8	K	vw	vw	-
632.3	K M_1 ?	vw	vw	-
657.4	KL_1	vvw	vvw	

Table AIII Continued

Bi^{206} continued

E_γ	Shells Seen	Plate Number 245 Spectrograph PM II	254 PM III	260 PM IV
803.4	KL_1	w	m-w	vvw
880.8	KL_1	w	w	-
895.2	KL_1	w	vw	vvw
1095.7	K ?	-	-	vvw
202.6	K	vvw		
313.5	KL_1	vvw		

Assignment of Electron Lines

Pb^{203}

Av E_γ	E_e	Shell	E_γ	Visual intensity	Photo intensity	Probable mult. order	Comments
279.1	193.7	K	279.2	vvs	1000	M1-E2	
	263.7	L_1	279.1	s	246	α=29	$K/L_1/L_2/L_3$= 13/3.3/1.9/1.0
	264.3	L_2	279.0	m	145		
	266.3	L_3	279.0	w	78		$K/L_1 L_2$=2.6
	275.3	M_1	279.0	w			
	278.3	N_1	279.1	vw			
400.6	315.3	K	400.8	m	100	M1	
	385.0	L_1	400.4	vw			

Table AIV

Conversion-line intensities in photographic plates

E_{e^-}	$^2\rho$	I_p	η	Intensity I	Transition energy E_γ	Relative intensity I_s	Nuclide
Plate No. 180, PM I, Bi^{203} and Bi^{204}							
52.72	30.14	1.6	0.56	86	140.9K	1293	204
63.37	33.20	4.7	0.64	244	$78.62L_2$	3670	204
64.38	33.48	3.7	0.65	191	$80.21L_1$	2873	204
65.55	33.79	3.7	0.65	192	$78.62L_3$	2888	204
74.97	36.5	1.2	0.73	60	$78.62M_2$	902	204
75.15	36.36	1.0	0.73	50	$78.62M_3$	752	204
76.30	36.65	0.6	0.74	30	$80.21M_1$	451	204
81.91	38.07	0.5	0.78	24	170.0K	361	204
84.64	38.75	0.4	0.80	19	$100.4L_1$	286	204
					x15.04		204
88.08	39.59	2.5	0.82	121	176.2K	1820	Sec. Std.
Plate No. 215 $Bi^{203,204}$ PM I							
44.19	27.48	1.5	0.49	84	$60.07L_1$	--	203
52.67	30.12	2.5	0.56	134	140.9K	1074	204
59.18	32.03	1.2	0.62	62	$60.07N_1$	--	203
63.31	33.19	7.8	0.64	405	$78.62L_2$	3247	204
64.24	33.44	4.8	0.65	247	$80.21L_1$	1980	204
65.59	33.79	6.4	0.65	333	$78.62L_3$	2670	204
74.96	36.3	2.5	0.73	124	$78.62M_2$	994	204
75.40	36.4	1.2	0.73	60	$78.62M_3$	481	204
76.27	36.6	1.4	0.74	69	$80.21M_1$	553	204
77.81	37.0	1.2	0.75	59	$78.62N_2$	473	204
84.34	38.7	0.8	0.80	39	$100.4L_1$	312	204
					8.018		204
88.00	39.6	4.7	0.82	227	176.2K	1820	Sec. Std.

Table AIV continued

E_e^-	2_p	I_p	η	Intensity I	Transition energy E_γ	Relative intensity I_s	
Plate No. 148 Bi^{204} PM II							
52.90	16.08	3.9	0.56	112	140.9K	1607	
63.58	17.71	7.7	0.64	213	78.62L_2	3057	
64.47	17.84	5.3	0.65	145	80.21L_1	2081	
65.78	18.03	6.6	0.65	183	78.62L_3	2626	
75.12	19.35	3.0	0.73	80	78.62M_2	1148	
75.59	19.42	3.1	0.73	82	78.62M_3	1177	
76.35	19.52	1.8	0.74	47	80.21M_1	674	
76.92	19.60	0.8	0.74	21	80.21$M_{2,3}$	301	
78.05	19.75	0.8	0.75	21	78.62N_1	301	
80.87	20.13	0.9	0.77	24	168.8K	344	
82.07	20.29	1.1	0.78	29	170.0K	416	
84.64	20.63	0.9	0.80	23	100.4L_1	330	
88.00	21.08	5.4	0.82	139	176.2K	1995	
125.02	25.50	1.5	0.94	41	140.9L_1	588	
128.18	25.85	4.0	0.94	110	216.2K	1579	
131.62	26.23	1.3	0.94	36	219.5K	517	
134.49	26.55	2.1	0.93	60	222.5K	861	
160.44	29.30	1.9	0.83	67	176.2L_1 x4.35	961	
161.3	29.39	3.6	0.83	127	249.3K	1822	Sec. Std.
201.59	33.39	2.0	0.70	95	289.5K	1363	
Plate No. 148 Bi^{206} PM II							
96.1	22.09	8.8	0.88	221	184.2K	3070	
168.47	30.13	1.9	0.80	72	184.2L_1	1000	
Plate No. 162 Bi^{204} PM II							
52.82	16.07	7.1	0.56	204	140.9K	963	
63.44	17.69	18.0	0.64	498	78.62L_2	2351	
64.40	17.83	11.0	0.65	302	80.21L_1	1425	
65.64	18.01	17.0	0.65	471	78.62L_3	2223	

Table AIV continued

E_e^-	2ρ	I_p	η	Intensity I	Transition energy E_γ	Relative intensity I_s	
Plate 162 Bi^{204} PM II							
75.01	19.34	6.0	0.73	159	$78.62M_2$	750	
75.54	19.41	5.6	0.73	149	$78.62M_3$	703	
76.31	19.52	4.6	0.74	121	$80.21M_1$	524	
78.00	19.75	2.8	0.75	74	$78.62N_1$	349	
81.83	20.26	2.8	0.78	73	170.0K	345	
84.58	20.62	1.2	0.80	31	$100.4L_1$	146	
88.00	21.07	13.0	0.82	334	176.2K	1576	
124.97	25.49	3.8	0.94	103	$140.9L_1$	486	
128.19	25.86	13.2	0.94	363	216.2K	1713	
131.70	26.24	4.7	0.94	131	219.5K	618	
134.48	26.54	7.4	0.93	211	222.5K	996	
152.63	28.50	2.3	0.87	75	240.7K	354	
					x4.720		
161.28	29.39	10.1	0.83	386	249.3K	1822	Sec. Std.
201.57	33.39	6.5	0.70	310	289.5K	1463	
Plate 162 Bi^{206} PM II							
95.94	22.07	25.0	0.88	627	184.1K	5169	
168.52	30.13	3.2	0.80	121	$184.1L_1$	998	
175.09	30.79	4.0	0.78	157	262.5K	1294	
255.5	38.39	3.9	0.60	250	343.4K	2061	Sec. Std.
Plate No. 179 Bi^{203} PM II							
98.47	22.38	90.5	0.89	2275	186.5K	1040	
111.21	23.91	25.5	0.94	649	$126.4L_2$	296	
113.39	24.17	19.8	0.94	509	$126.4L_3$	232	
122.86	25.25	8.3	0.94	223	$126.4M_2$	101	
123.37	25.31	5.0	0.94	135	$126.4M_3$	62	
170.81	30.36	11.6	0.80	441	$186.5L_1$	200	
176.19	30.90	42.6	0.77	1709	264.0K	2701	
182.81	31.56	4.0	0.75	168	$186.5M_1$	772	
248.04	37.72	6.5	0.61	402	$264.0L_1$	183	Sec. Std.

Table AIV continued

E_{e^-}	2ρ	I_p	η	Intensity I	Transition energy E_γ	Relative intensity I_s	
Plate No. 179 Bi^{204} PM II							
88.00	21.07	89	0.82	2290	176.2K	1890	
124.63	25.46	4.00	0.94	108	212.7K	89	
124.97	25.49	20.50	0.94	556	140.9L_1	458	
125.58	25.56	7.70	0.94	209	213.0K	172	
128.10	25.85	70.8	0.94	1947	216.2K	1603	
128.60	25.90	13.50	0.94	372	144.5L_1	306	
131.41	26.21	16.2	0.94	452	219.5K	372	
134.48	26.54	41.0	0.93	1170	222.5K	963	
136.95	26.82	4.8	0.93	138	140.9M_1	114	
139.06	27.05	3.3	0.92	97	227.1K	80	
149.12	28.12	2.7	0.88	86	164.9L_1	71	
152.63	28.50	11.7	0.87	383	240.7K	315	
154.21	28.66	2.3	0.86	77	170.1L_1	63	
160.33	29.29	19.0	0.84	663	176.2L_1	546	
161.28	29.39	62.50	0.83	2213	249.3K	1822	Sec. Std.
164.48	29.72	3.0	0.81	110	252.4K	91	
165.88	29.90	2.5	0.81	92	170.0M_1	76	
169.04	30.18	2.8	0.79	107	184.9L_1	88	
169.70	30.24	2.8	0.79	107	184.9L_2	88	
172.54	30.53	4.0	0.78	157	176.2M_1	129	
198.52	33.09	2.4	0.70	114	213.6L_2	94	
200.40	33.27	9.5	0.70	452	216.2L_1	372	
201.45	33.37	43.2	0.70	2059	289.5K	1695	
203.09	33.31	10.5	0.69	507	216.7L_3 291.0K	417	
204.40	33.45	16.1	0.69	781	219.5L_2	643	
206.56	33.65	11.6	0.69	566	219.5L_3 227.5L_1	466	
215.50	34.37	2.5	0.68	126	219.5M_2	104	
218.56	35.00	2.8	0.66	148	222.5M_1	122	
224.63	35.57	2.3	0.66	124	240.7L_1	102	
233.13	36.35	11.5	0.64	653	249.1L_1	538	

Table AIV continued

E_{e^-}	2ρ	I_p	η	Intensity I	Transition energy E_γ	Relative intensity I_s	
Plate No. 179 Bi^{204} PM II continued							
242.89	37.24	4.0	0.62	240	330.9K	198	
244.16	37.36	2.1	0.62	127	332.1K	105	
245.08	37.45	2.5	0.62	151	249.1M_1	124	
252.51	38.11	1.3	0.61	81	340.6K	67	
273.13	39.95	6.8	0.57	477	289.5L_1	393	
Plate No. 179 Bi^{206} PM II							
95.94	22.07	~192	0.88	4185	184.1K	4464	
168.52	30.13	20.6	0.80	776	184.1L_1	828	
175.09	30.79	10.5	0.78	414	262.5K	442	
180.42	31.32	8.3	0.76	342	184.1M_1	365	
183.26	31.61	3.7	0.75	156	184.1N_1	166	
246.73	37.60	2.2	0.62	133	262.5L_1	142	
255.55	38.39	30.2	0.60	1932	343.4K	2061	Sec. Std.
Pb^{203}							
193.84	32.64	94.0	0.72	4261	279.1K	1000	
263.69	39.11	15.8	0.59	1047	279.1L_1	246	
264.30	39.17	9.3	0.59	617	279.1L_2	145	
266.35	39.30	5.0	0.59	333	279.1L_3	78	
Bi^{205}							
196.24	32.86	2.4	0.71	111	284.1K		
Plate No. 194 Bi^{204} PM III							
152.7	13.06	19.0	0.86	289	240.7	206	
161.2	13.43	158.0	0.83	2556	249.3K	1822	
164.3	13.61	6.2	0.82	103	252.4K	73	
166.3	13.71	6.5U	0.82	109	170.0M_1	78	
172.4	14.00	7.5	0.79	133	176.2M_1	95	
193.6	14.96	4.6	0.73	94	281.6K	67	
200.2	15.26	44.5U	0.70	970	216.2L_1	691	
201.4	15.31	79.2U	0.70	1732	289.5K	1234	
202.8	15.37	33.5U	0.70	736	291.0K	525	

Table AIV continued

E_e-	2ρ	I_p	η	Intensity I	Transition energy E_γ	Relative intensity I_s
Plate No. 194 Bi^{204} continued						
204.1	15.43	35.7U	0.70	787	219.5L_2	561
206.4	15.53	22.7	0.69	511	219.5L_3 or 227.5L_1	364
212.2	15.79	6.0	0.68	139	216.2M_1	99
215.9	15.95	5.0	0.68	117	219.5M_2	84
218.6	16.06	4.7	0.67	113	219.5N_1 or 222.5M_1	81
224.4	16.32	5.2	0.66	129	240.7L_1	92
233.1	16.68	22.0	0.65	565	249.1L_1	403
236.8	16.84	0.9	0.65	23	240.7M_1	16
242.9	17.10	6.0	0.63	163	330.9K	116
244.0	17.16	5.5U	0.62	152	332.1K	108
245.2	17.20	3.0U	0.62	83	249.1M_1	59
273.6	18.36	14.3	0.58	453	289.5L_1	323
275.0	18.42	3.3U	0.58	105	291.0L_1	75
287.0	18.91	106.4	0.56	3592	375.0K	2560
288.8	18.98	8.3	0.56	281	376.8K	200
314.9	20.04	1.0	0.55	36	330.9L_1	26
317.3	20.13	3.7	0.53	141	405.5K	100
324.4	20.39	3.3	0.53	127	412.4K	91
333.7	20.75	9.3	0.52	371	421.8K	264
350.9	21.41	6.0	0.51	252	438.8K	180
352.6	21.48	1.8	0.51	76	440.2K	54
359.0	21.72	49.0	0.50	2129	375.0L_1 L_2	1517
362.1	21.82	15.3	0.50	668	375.0L_3	476
371.1	22.18	16.8	0.49	760	375.0M_1	542
374.5	22.29	5.7	0.49	259	375.0N_1	185
380.5	22.54	2.8U	0.49	129	468.3K	92
389.7	22.88	1.2	0.48	57	405.5L_1	41

Table AIV continued

E_{e^-}	2ρ	I_p	η	Intensity I	Transition energy E_γ	Relative intensity I_s	
Plate No. 194 Bi^{204} PM III continued							
406.1	23.50	1.0U	0.47	50	421.8L_1	37	
413.9	23.78	3.0	0.47	152	501.9K	108	
424.1	24.16	0.8U	0.46	42	440.2L_1	30	
434.4	24.54	2.2	0.45	120	522.4K	86	
444.6	24.91	4.8	0.45	266	532.6K	190	
454.2	25.30	0.9	0.45	51	542.2K	36	
458.0	25.40	0.7	0.44	40	545.7K	29	
507.0	27.15	0.8	0.42	52	522.2L_1 L_2	37	
573.7	29.51	4.7	0.41	338	661.5K	241	
575.4	29.59	1.5U	0.41	108	663.4K	77	
583.0	29.83	15.0	0.40	1119	671.0K	798	
622.4	31.20	2.3	0.40	179	710.4K	128	
630.6	31.48	1.0	0.39	81	718.5K	58	
637.4	31.71	1.0	0.39	81	725.3K	58	
647.8	31.71	0.6	0.39	49	663.4L_2	35	
655.0	32.41	2.2	0.39	183	671.0L_1	131	
657.7	32.43	0.6	0.39	50	671.0L_3 ?	37	
666.2	32.70	0.8	0.39	67	754.5K	48	
703.5	33.97	1.2	0.39	105	791.9K	75	
811.5	37.61	13.8	0.37	1403	899.2K	1000	primary std.
823.9	38.02	18.3	0.37	1880	911.5K	1340	
830.7	38.25	1.5	0.37	155	918.4K	110	
883.8	40.01	2.5	0.37	270	899.2L_1	192	
Plate No. 194 Bi^{206} PM III (only stronger lines read)							
168.3	13.80	50.5	0.80	871	184.1L_1	809	
174.8	14.10	29.5	0.78	533	262.5K	495	
255.4	17.63	75.5	0.60	2218	343.5K	2061	
310.1	19.81	34.5	0.54	1266	398.1K	1176	
409.1	23.60	14.5	0.468	731	497.2K	679	

Table AIV continued

E_e^-	2ρ	I_p	η	Intensity I	Transition energy E_γ	Relative intensity I_s	
Plate No. 194 Bi^{206} PM III continued							
428.1	24.31	19.9	0.46	1052	516.1K	978	
449.5	25.08	19.3	0.45	1076	537.4K	1000	primary std.
481.6	26.23	2.6	0.44	155	497.2L_1	144	
715.3	34.36	4.3	0.383	386	803.4K	359	
Plate No. 178 $Bi^{203, 204}$ PM III							
Bi^{203}							
248.0	17.31	16.0	0.61	454	264.0L_1	183	
293.4	19.16	7.3	0.56	250	381.5K	100	
518.1	27.55	1.8	0.42	118	606.1K	48	
620.4	31.13	2.5	0.40	195	708.4K	79	
731.7	34.93	3.0	0.38	276	819.7K	111	
736.5	35.09	16.9	0.38	1561	824.9K	1000	primary std.
808.8	37.52	4.5	0.37	456	824.9L_1	184	
Bi^{204}							
202.8	15.37	34.U	0.70	747	291.0K	773	
204.1	15.43	53	0.70	1168	219.5L_2	1209	
206.4	15.53	22.5	0.69	506	219.5L_3 227.5L_1	524	
212.2	15.79	4.5	0.68	104	216.2M_1	108	
215.9	15.95	8.5	0.68	199	219.5M_2	206	
218.6	16.06	7.5	0.67	180	219.0N's 222.5M_1	186	
224.6	16.30	7.7	0.66	190	240.7L_1	197	
233.1	16.68	25.7	0.65	660	249.1L_1	683	
242.9	17.10	7.0	0.63	190	330.9K	197	
245.2	17.20	7.0	0.62	194	+332.1K 249.1M_1	201	
273.6	18.36	14.2	0.58	450	289.5L_1	466	
287.0	18.91	153.6	0.56	5187	375.0K	5370	
288.8	18.98	6.3	0.56	214	376.8K	222	

Table AIV continued

E_{e^-}	2ρ	I_p	η	Intensity I	Transition energy E_γ	Relative intensity I_s	
Plate No. 178 Bi^{204} PM III continued							
317.3	20.13	4.2	0.53	160	405.5K	166	
324.3	20.38	3.9	0.53	150	412.4K	155	
333.7	20.75	9.0	0.52	359	421.8K	372	
350.9	21.41	6.2	0.51	260	438.8K	269	
359.0	21.72	47.0	0.50	2042	$375.0L_1L_2$	2114	
362.1	21.82	16.4	0.50	716	$375.0L_3$	741	
371.1	22.18	16.1	0.49	729	$375.0M_1$	755	
374.0	22.29	5.2	0.49	237	$375.0N_1$	245	
380.0	22.54	3.20	0.49	147	468.3K	152	
406.1	23.50	2.20	0.47	110	$421.8L_1$	114	
413.9	23.78	3.5	0.47	177	501.9K	183	
434.4	24.54	2.7	0.45	147	522.4K	152	
444.6	24.91	6.4	0.45	354	532.6K	366	
573.7	29.51	3.4	0.41	248	661.5K	257	
575.4	29.59	0.9	0.41	65	663.4K	67	
583.0	29.83	12.8	0.40	955	671.0K	989	
622.4	31.20	1.9	0.40	148	710.4K	153	
630.6	31.48	0.7	0.39	57	718.5K	59	
655.0	32.41	1.7	0.39	141	$671.0L_1$	146	
666.2	32.57	1.3	0.39	109	748.5K	113	
713.5	33.97	1.0	0.39	87	791.9K	90	
758.9	35.85	1.6	0.38	151	844.1K	156	
811.5	37.61	9.5	0.37	966	899.2K	1000	primary std.
823.8	38.02	10.8	0.37	1110	911.5K	1149	
829.7	38.25	1.0	0.37	103	918.4K	107	
883.8	40.01	4.5	0.37	487	$899.2L_1$	504	

Table AIV continued

E_{e^-}	2ρ	I_p	η	Intensity I	Transition energy E_γ	Relative intensity I_s	
Plate No. 178 Bi^{206}, Bi^{205}, Pb^{203} PM III							
225.5	16.35	4.4	0.66	109	313.5K	58	
246.9	17.26	10.0	0.62	278	262.8L_1	149	
255.4	17.63	131	0.60	3849	343.5K	2062	
298.2	19.36	2.3	0.56	80	386.2K	42	
310.1	19.81	39.6	0.54	1453	398.1K	778	
327.6	20.52	23.8	0.53	921	343.5L_1	492	
339.6	20.98	5.5	0.51	226	343.5M_1	121	
382.9	22.60	7.0	0.48	330	398.1L_2	178	
385.0	22.71	4.5	0.48	213	398.1L_3	114	
409.1	23.60	24.5	0.468	1236	497.2K	662	
428.1	24.31	32.3	0.46	1707	516.1K	914	
449.5	25.08	33.5	0.45	1867	537.4K	1000	primary std.
481.3	26.23	5.5	0.44	328	497.2L_1	176	
500.9	26.94	14.6	0.43	915	516.1L_2	490	
503.1	27.02	3.3	0.43	207	516.1L_3	111	
512.3	27.35	4.0	0.42	260	516.1M_2	139	
521.7	27.67	4.9	0.42	328	537.4K_1	176	
532.6	28.08	4.5	0.42	301	620.4K	161	
Bi^{206}							
544.4	28.48	2.1	0.41	146	632.2K	78	
715.3	34.36	6.0	0.383	538	803.3K	288	
787.6	36.81	0.6	0.38	58	803.3L_1	31	
792.5	36.99	2.1	0.378	206	880.5K	110	
807.3	37.47	2.5	0.377	248	895.2K	133	
Pb^{203}							
315.6	20.04	23.2	0.54	861	400.8K	230	
193.7	14.96	~175	0.72	3636	279.1K	971	
263.8							
264.8	17.97	123	0.59	3746	279.1L_1L_2	1000	

Table AIV continued

E_{e^-}	2ρ	I_p	η	Intensity I	Transition energy E_γ	Relative intensity I_s	
Plate No. 178 Pb^{203} continued							
266.4	18.07	31.5	0.59	965	279.1L_3	258	
275.6	18.44	41.7	0.575	1337	279.1M_1	357	
278.3	18.55	12.8	0.57	417	279.1N_1	111	
Bi^{205}							
196.0	15.07	16.5	0.71	349	284.1K	2029	
482.3	26.27	3.3	0.435	199	570.3K	1157	
615.3	30.95	2.2	0.395	172	703.3K	1000	primary std.
Plate No. 147 Bi^{204} PM IV							
444.6	15.42	23.U	0.45	788	532.6K	236	
573.3	18.25	14.8	0.41	659	661.5K	197	
575.6	18.30	6.5 U	0.41	290	663.4K	87	
583.2	18.46	52.5	0.40	2423	671.0K	725	
630.3	19.47	4.4	0.39	220	718.5K	66	
637.5	19.62	3.0U	0.39	151	725.3K	45	
648.4	19.85	2.2	0.39	112	663.4L_2	33	
655.0	20.00	8.0	0.39	410	671.0L_1	123	
657.2	20.04	3.5	0.39	180	671.0L_3 ?	54	
666.9	20.25	5.8 U	0.39	301	671.0M_1	90	
704.4	21.03	6.0	0.39	324	791.9K	97	
744.4	21.87	3.0	0.38	178	832.3K	52	
746.4	21.91	2.7	0.38	156	834.3K	47	
759.5	22.19	2.7	0.38	158	844.1K	47	
811.3	23.26	53.2	0.37	3344	899.2K	1000	primary std.
824.0	23.52	80.7	0.37	5130	911.5K	1534	
830.5	23.66	5.8U	0.37	371	918.4K	111	
883.5	24.75	11.0	0.37	736	899.2L_1	220	
885.8	24.79	2.1U	0.37	141	899.2L_3	42	
896.1	25.00	45.0	0.37	3041	911.5L_2	909	
898.4	25.05	7.7U	0.37	521	911.5L_3	156	
902.7	25.14	3.2U	0.37	217	918.4L_1	65	

Table AIV continued

E_{e^-}	2ρ	I_p	η	Intensity I	Transition energy E_γ	Relative intensity I_s	
Plate No. 147 Bi^{204} continued							
908.0	25.25	10.0	0.37	682	911.5M_2	204	
910.4	25.30	3.2	0.37	219	911.5N_2	65	
968.7	26.48	1.5	0.36	110	1056.7K	33	
Plate No. 147 Bi^{206} PM IV							
428.1	15.05	~97	0.46	~3174	516.1K	754	
449.5	15.52	122	0.45	4208	537.4K	1000	primary std.
480.3	16.22	14.0	0.44	516	497.2L_1	123	
500.9	16.67	58.3	0.43	2260	516.1L_2	537	
502.7	16.71	11.0U	0.43	427	516.1L_3	101	
512.5	16.93	14.8	0.42	597	516.1M_2	142	
515.8	17.00	6.5U	0.42	263	516.1N	63	
521.7	17.12	15.6	0.42	636	537.4L_1	151	
532.6	17.37	15.0	0.42	620	620.4K	147	
544.2	17.62	10.5	0.41	451	632.2K	107	
569.3	18.16	3.0 U	0.41	133	657.4K	32	
603.9	18.90	4.0	0.40	189	620.4L_1	45	
617.6	19.16	7.5 U	0.397	362	620.0M_1 632.0L_1	86	
715.3	21.26	17.8	0.383	988	803.4K	235	
788.1	22.77	4.6	0.38	276	803.4L_1	66	
792.5	22.89	12.8	0.378	775	880.5K	184	
807.1	23.17	7.0U	0.377	430	895.2K	102	
865.3	24.38	3.0	0.37	198	880.5L_2	47	
879.9	24.65	2.0	0.37	133	895.2L_1	32	
930.8	25.71	4.5	0.362	320	1018.8K	76	
Plate No. 177 Bi^{203}							
620.0	19.22	8.2	0.40	394	708.4K	70	
634.0	19.51	3.5	0.39	175	722.1K	31	
731.5	21.57	9.3	0.38	528	819.7K	94	
736.9	21.69	98.2	0.38	5605	824.9K	1000	primary std.

Table AIV continued

E_e^-	2ρ	I_p	η	Intensity I	Transition energy E_γ	Relative intensity I_s	
Plate No. 177 Bi^{203} continued							
809.0	23.19	29.1 U	0.37	1824	824.9L_1	325	
821.1	23.43	13.2	0.37	836	824.9M_1	149	
945.5	25.97	2.7	0.36	195	1033.5K	35	
1449.0	36.02	3.0	0.30	360	1536.4K	64	
Bi^{204}							
573.0	18.25	12.8	0.41	570	661.5K	161	
576.0	18.30	7.0	0.41	312	663.4K	88	
583.2	18.46	56.0	0.40	2584	671.0K	728	
622.0	19.24	4.8 U	0.39	237	710.4K	67	
630.0	19.47	5.6	0.39	280	718.5K	79	
637.0	19.62	2.8	0.39	141	725.3K	40	
646.0	19.82	2.4	0.39	122	661.5L_1	34	
648.0	19.85	2.8	0.39	143	663.4L_2	40	
655.0	20.0	10	0.39	513	671.0L_1	144	
657.0	20.04	3.0	0.39	154	671.0L_3 ?	43	
666.0	20.25	3.2	0.39	166	671.0M_1	47	
704.4	21.03	6.8	0.39	367	791.9K	103	
744.4	21.87	2.2 U	0.38	127	832.3K	36	
746.2	21.91	2.6	0.38	150	834.3K	42	
759.5	22.19	5.2	0.38	304	844.1K	86	
811.5	23.26	56.5	0.37	3551	899.2K	1000	primary std.
824.0	23.52	72.5	0.37	4608	911.5K	1298	
830.5	23.66	6.2 U	0.37	396	918.4K	112	
883.0	24.75	10.1	0.37	676	899.2L_2	190	
885.0	24.79	~1.7 U	0.37	114	899.2L_3	32	
896.0	25.00	41.0	0.37	2770	911.5L_2	780	
899.0	25.05	5.6 U	0.37	379	911.5L_3	107	
903.0	25.14	2.2 U	0.37	149	918.4L_1	42	
908.0	25.75	8.5	0.37	580	911.5M_2	163	
911.0	25.30	3.0	0.37	205	911.5N_1	58	
966.0	26.48	1.3	0.36	96	1056.7K	27	

Table AIV continued

E_e-	2ρ	I_p	η	Intensity I	Transition energy E_γ	Relative intensity I_s	
Plate No. 177 Bi^{206}							
449.5	15.52	27.3	0.45	942	537.5K	1000	primary std.
602.5	18.90	3.5	0.40	165	620.4L_2	175	
715.3	21.26	7.5	0.383	416	803.4K	441	
792.5	22.89	4.0	0.378	242	880.5K	257	
Plate No. 254 Bi^{205} PM III							
97.0	10.16	4.7	0.88	54	112.2L_2	113	
98.9	10.27	3.3	0.88	39	112.2L_3	81	
172.4	14.00	22.3	0.78	400	260.5K	833	
193.7	14.96	7.7	0.72	160	282.5K	333	
196.0	15.07	26.5	0.72	555	284.0K	1156	
261.3	17.86	4.7	0.60	140	349.3K	292	
268.1	18.14	3.8	0.59	117	284.0L	244	
405.3	23.45	0.7	0.47	35	493.5K	73	
423.1	24.11	1.4	0.46	73	511.7K	152	
482.3	26.27	6.2	0.44	370	570.7K	771	
491.4	26.59	2.0	0.43	124	579.7K	258	
615.3	30.95	6.2	0.40	480	703.3K	1000	primary std.
Plate No. 260 Bi^{205} PM IV							
405.6	14.49	5.5	0.47	170	493.5K	147	
423.7	14.91	6.0	0.46	194	511.7K	168	
482.2	16.22	23.8	0.44	877	570.7K	759	
491.6	16.43	7.7	0.43	294	579.7K	254	
554.6	17.81	2.2	0.41	96	570.7L_1	83	
615.3	19.11	24.2	0.40	1156	703.3K	1000	primary std.
688.1	20.66	4.0	0.39	212	703.3L_2	183	
899.3	25.03	3.5	0.37	237	987.5K	205	
955.0	26.17	3.5	0.36	254	1043.5K	220	

Table AV

Conversion-line intensities
Lead-203, Lead-204, Lead-205, Lead-206, Thallium-203

	Spectrograph									
	PM I	PM I	PM II	PM II	PM II	PM III	PM III	PM IV	PM IV	
	Plate No.									
E_γ	180	215	148	162	179	194	178	147	177	Average
Bi^{203}										
186.5K					1040					1040
$126.4L_2$					296					296
$126.4L_3$					232					232
$126.4M_2$					101					101
$126.4M_3$					62					62
$186.5L_1$					200					200
264.0K					770					770
$186.5M_1$					77					77
$264.0L_1$					183		183			183
381.5K							100			100
606.1K							48			48
708.4K							79		70	75
722.1K									31	31
819.7K							111		94	102
824.9K							1000		1000	1000

Table AVcontinued

E_γ	Spectrograph PM I Plate No. 180	PM I 215	PM II 148	PM II 162	PM II 179	PM III 194	PM III 178	PM IV 147	PM IV 177	Average
Bi^{203} continued										
$824.9L_1$							184		325	255
$824.9M_1$									149	149
1033.5K									35	35
1536.4K									64	64
Pb^{204}										
140.9K	1293	1074	1607	963						1234
$78.62L_2$	3670	3247	3057	2351						3081
$80.21L_1$	2873	1980	2081	1425						2090
$78.62L_3$	2888	2670	2626	2223						2602
$78.62M_2$	902	994	1148	750						949
$78.62M_3$	752	481	1177	703						783
$80.21M_1$	451	553	674	524						551
$80.21M_2$			301							301
$78.62N_2$		473	301	349						374
168.8K			344							344
170.0K	361		416	345						374
$100.4L_1$	286	312	330	146						269
176.2K	1820	1820	1995	1576	1890					1820

Table AV continued

E_γ	Spectrograph PM I Plate No. 180	PM I 215	PM II 148	PM II 162	PM II 179	PM III 194	PM III 178	PM IV 147	PM IV 177	Average
Pb^{204} continued										
212.7K					89					89
140.9L_1			588	486	458					511
213.5K					172					172
216.2K			1579	1713	1603					1632
144.5L_1					306					306
219.5K			517	618	372					502
222.5K			861	996	963					940
140.9M_1					114					114
227.1K					80					80
164.9L_1					71					71
240.7K				354	315	206				292
170.1L_1					63					63
176.2L_1			961		546					754
249.3K			1822	1822	1822	1822				1822
252.4K					91	73				82
170.1M_1					76	78				77
184.9L_1					88					88
184.9L_2					88					88
176.2M_1					129	95				112

Table AV continued

E_γ	Spectrograph PM I Plate No. 180	PM I 215	PM II 148	PM II 162	PM II 179	PM III 194	PM III 178	PM IV 147	PM IV 177	Average
Pb^{204} continued										
213.6 L_2					94					94
216.2 L_1					372	691				532
289.5 K			1363	1463	1690	1234				1439
291.0 K					417	525	773			572
219.5 L_2					643	561	1209			804
219.5 L_3 222.5 L_1					466	364	524			451
216.2 M_1						99	108			103
219.5 M_2					104	84	206			131
219.5 N_2 222.5 M_1					122	81	186			130
240.7 L_1					102	92	197			130
249.1 L_1					538	403	683			541
240.7 M_1						16				16
330.9 K					198	116	197			170
332.1 K					105	108	201			107
249.1 M_1					124	59				92
340.6 K					67					67

Table AV continued

E_γ	Spectrograph PM I Plate No. 180	PM I 215	PM II 148	PM II 162	PM II 179	PM III 194	PM III 178	PM IV 147	PM IV 177	Average
Pb^{204} continued										
289.5 L_1					393	323	466			394
291.0 L_1						75				75
375.0K						2560	5370			3965
376.8K						200	222			211
330.9 L_1						26				26
405.5K						100	166			133
412.4K						91	155			123
421.8K						264	372			318
438.8K						180	269			225
440.2K						54				54
375.0 $L_1 L_2$						1517	2114			1816
375.0 L_3						476	741			609
375.0 M_1						542	755			649
375.0 N_1						185	245			215
468.3K						92	152			122
405.5 L_1						41				41
421.8 L_1						37	114			76
501.9K						108	183			146

Table AV continued

E_γ	Spectrograph PM I Plate No. 180	PM I 215	PM II 148	PM II 162	PM II 179	PM III 194	PM III 178	PM IV 147	PM IV 177	Average
Pb^{204} continued										
$440.2L_1$						30				30
522.4K						86	152			119
532.6K						190	366	236		264
542.2K						36				36
545.7K						29				29
$522.2L_1L_2$						37				37
661.5K						241	257	197	161	214
663.4K						77	67	87	88	80
671.0K						798	989	725	728	810
710.4K						128	153		67	116
718.5K						58	59	66	79	66
725.3K						58		45	40	48
$661.5L_1$									34	34
$663.4L_2$						35		33	40	36
$671.0L_1$						131	146	123	144	136
745.2K						37		54	43	45
$671.0M_1$								90	47	69
748.5K							113			113

Table AV continued

Spectrograph	PM I	PM I	PM II	PM II	PM II	PM III	PM III	PM IV	PM IV	
Plate No.										
E_γ	180	215	148	162	179	194	178	147	177	Average
Pb^{204} continued										
791.9K						75	90	97	103	91
832.3K								52	36	44
834.3K								47	42	45
844.1K							156	47	86	96
899.2K						1000	1000	1000	1000	1000
911.5K						1340	1149	1534	1298	1330
918.4K						110	107	111	112	110
899.2L_2						192	504?	220	190	201
899.2L_3								42	32	37
911.5L_2								909	780	845
911.5L_3								156	107	132
918.4L_1								65	42	54
911.5M_2								204	163	184
911.5N_2								65	58	62
1056.7K								33	27	30
Pb^{203}-Tl^{203} Transitions Intensities										
279.K					1000		971			
279.1L					246		1000			
279.1L_2					145					

Table AV continued

Spectrograph	PM I	PM I	PM II	PM II	PM II	PM III	PM III	PM IV	PM IV	
Plate No.										
E_γ	180	215	148	162	179	194	178	147	177	Average
Pb^{203}-Tl^{203} continued										
279.1L_3					78		258			
279.1M_1							357			
279.1N_1							111			
400.6K							230			

	PM III	PM IV	Intensities Bergstrom etal
	254	260	
Pb^{205} Transition intensities			
112.0L_2	113		
112.0L_3	81		
260.5K	833		1100
282.0K	333		400
284.0K	1156		1500
349.0K	292		280
284.0L	244		
493.5K	73	147	110
511.7K	152	168	220
570.7K	771	759	740

Table AV continued

E_γ	Spectrograph PM III Plate No. 254	PM IV 260	Intensities Bergstrom etal
Pb^{205} continued			
579.7K	258	254	240
570.7L_1		83	
713.3K	1000	1000	1000
703.3L_2		183	
987.5K		205	275
1043.5K		220	325

E_γ	Spectrograph PM II Plate No. 179	PM II 162	PM III 178	PM III 194	PM IV 177	PM IV 147	Pryce and Alburger Intensities	This work average intensities
Pb^{206} Transition intensities								
184.1K	4464	5169					13,460	4817
184.1L_1	828	998		809				
262.5K	442	1294		495			1010	468
184.1M_1	365							
184.1N_1	166							
313.0K			58					

Table AV continued

E_γ	Spectrograph PM II Plate No. 179	PM II 162	PM III 178	PM III 194	PM IV 177	PM IV 147	Pryce and Alburger Intensities	This work average intensities
Pb^{206} continued								
$262.5L_1$	142		149					
343.3K	2061	2061	2062	2061			3173	2061
386.2K			42				63	42
398.1K			778	1176			846	977
$343.5L_1$			492					
$343.5M_1$			121					
$398.1L_2$			178					
$398.1L_3$			114					
497.2K			662	679			659	670
516.4K			914	978			938	946
537.4K			1000	1000	1000	1000	1000	1000
$497.2L_1$			176	144		123		
$516.0L_2$			490			537		
$516.1L_3$			111			101		
$516.1M_2$			139			142		
$516.1N's$						63		
$537.4L_1$			176			151		

Table AV continued

E_γ	Spectrograph PM II Plate No. 179	PM II 162	PM III 178	PM III 194	PM IV 177	PM IV 147	Pryce and Alburger Intensities	This work average intensities
Pb^{206} continued								
620.4K			161			147	130	154
632.2K			78			107	101	93
657.4K						32		
$620.4L_2$					175	45		
$632.0L_1$						86		
803.4K			288	359	441	235	408	331
$803.0L_1$			31			66		
880.5K			110		257	184	231	184
895.2K			133			102	154	118
$880.5L_2$						47		
$895.2L_1$						32		
1018.8K						76	53	76

LIST OF TABLES

Number	Title
1	Transitions obtained on magnetic-lens spectrometer
2	Lead and thallium binding energies
3	List of transitions found in Bi^{203}, Bi^{204}, and Bi^{205} decay
4	Comparison of Bi^{203} and Bi^{204} transitions with reported results
5	Comparison of Pb^{203}, Bi^{205}, and Bi^{207} transition energies with reported results
6	Auger lines
7	Energy standards involving Bi^{206} and I^{131}
8	Numerical correlations of Pb^{203}, Pb^{204}, and Pb^{205}
9	Total chance expectations in numberical correlations
10	Electron-Electron coincidence results
11	Pb^{203m} half-life measurements
12	Conversion lines observed in Pb^{204m} in experimental search for Pb^{205m}
13	Multipole order of 1766.4- and 1777.4- kev transitions in Pb^{205}

LIST OF ILLUSTRATIONS

Figure No.	Title
1.	Bi^{205} gamma-ray spectrum (+ Bi^{207} spectrum)
2.	Bi^{204} and Pb^{204m} gamma-ray spectrum
3.	Bi^{203} gamma-ray spectrum
4 a, b, c	Photographic-plates obtained in Bi^{203} and Bi^{204} work
5.	Densitometer curve for Bi^{204}-Bi^{206}, 800-830 kev
6.	Probability distribution of transitions
7.	Pb^{203m} gamma-ray spectrum
8.	Pb^{204m} decay scheme
9.	Half-life measurements in search for Pb^{205m} isomeric state
10.	Pb and Tl closed cycles
11.	Pb - Tl odd-neutron binding energies
12.	Statistical distribution of transitions in Pb^{204} and Pb^{205}
13.	Proposed energy-level diagram - Pb^{205}
14.	Proposed energy-level diagram - Pb^{204}
15.	Proposed energy-level diagram - Pb^{203}

BIBLIOGRAPHY

1. Haxel, Jensen, and Suess, Phys. Rev. 75, 1766 (1949).
2. M. Goeppert-Mayer, Phys. Rev. 75, 1969 (1949).
3. M. Goeppert-Mayer and J. H. D. Jensen, "Elementary Theory of Nuclear Shell Structure," New York, John Wiley and Sons, Inc., 1955.
4. M. H. L. Pryce, Proc. Phys. Soc. (London) A65, 773 (1952).
5. D. E. Alburger and M. H. L. Pryce, Phys. Rev. 92, 514 (1953).
6. D. E. Alburger and M. H. L. Pryce, Phys. Rev. 95, 1482 (1954).
7. W. W. True, Phys. Rev. 101, 1342 (1956).
8. D. E. Alburger and A. W. Sunyar, Phys. Rev. 99, 695 (1955).
9. Sunyar, Alburger, Friedlander, Goldhaber, and Scharff-Goldhaber, Phys. Rev. 78, 326 (1950)(A).
10. D. Maeder and A. H. Wapstra, Phys. Rev. 93, 1433 (1954).
11. N. J. Hopkins, Phys. Rev. 88, 680 (1952).
12. V. K. Fischer, Phys. Rev. 99, 764 (1955).
13. V. E. Krohn and S. Raboy, Phys. Rev. 95, 1354 (1954).
14. V. E. Krohn and S. Raboy, Phys. Rev. 97, 1017 (1955).
15. Bergkvist, Bergström, Herrlander, Hultberg, Slätis, Sokolowski, Wapstra, and Wielding, Phil. Mag. 46, 65 (1955).
16. G. J. Nijgh, "Nuclear Spectroscopic Investigations of Some Isotopes of Cesium, Lead, and Mercury" (thesis), University of Amsterdam, 1955.
17. Sunyar, Alburger, Friedlander, Goldhaber, and Scharff-Goldhaber, Phys. Rev. 79, 181 (1950).
18. G. Backström, Arkiv Fysik 10, 29 (1955).
19. E. L. Kelly, "Bi(α, 2n)At^{211} Apparent Cross Section for the Electrostatistically Deflected Alpha Beam of the 184-Inch Cyclotron," UCRL-277, Jan. 1949.
20. Hollander, Perlman, and Seaborg, Revs. Modern Phys. 25, 469 (1953).
21. Cheng, Ridolfo, Pool, Kundu, Phys. Rev. 98, 231A (1955).
22. W. W. Meinke, "Chemical Procedures Used in Bombardment Work at Berkeley," UCRL-432, Aug. 1949.

23. F. Nelson and K. A. Kraus, J. Am. Chem. Soc. 76, 5916 (1954).
24. D. G. Karraker and D. H. Templeton, Phys. Rev. 81, 646 (1950).
25. Templeton, Howland, and Perlman, Phys. Rev. 72, 755 (1947).
26. Bergström, Stockendal, McDonell, and Schmorak, to be published in Arkiv för Fysik.
27. G. K. Wertheim and R. V. Pound, Phys. Rev. 102, 185 (1956).
28. H. M. Neumann and I. Perlman, Phys. Rev. 78, 191 (1950).
29. G. D. O'Kelley, "Spectrometric Electron Energies" (thesis), UCRL-1243, May 1951.
30. M. Kalkstein and J. M. Hollander, "A Survey of Counting Efficiencies for a One and One-Half Inch Diameter by One Inch High Sodium Iodide Crystal," UCRL-2764, Oct. 1954.
31. T. O. Passell, "Internal Conversion of Gamma Radiation in the L Subshells" (thesis), UCRL-2528, March 1954.
32. W. G. Smith, "I. Neutron-Deficient Isotopes in the Noble Metal Region. II. Conversion Electron Spectra of Some Heavy Elements" (thesis), UCRL-2974, June 1955.
33. I. Bergström and A. Wapstra, Phil. Mag. 46, 61 (1955).
34. M. Rose, "Beta and Gamma Ray Spectroscopy," edited by K. Siegbahn, Amsterdam, North Holland Publishing Company, 1955.
35. Hill, Church, and Mihelich, Rev. Sci. Instr. 23, 523 (1952).
36. J. P. Prescott, Proc. Phys. Soc. (London) 67A, 254 (1954).
37. Wapstra, Maeder, Nijgh, and Ornstein, Physica 20, 169 (1954).
38. S. Thulin and K. Nybö, Arkiv. Fysik 7, 289 (1954).
39. A. H. Wapstra, quoted in G. J. Nijgh, thesis, University of Amsterdam, 1955, p. 62.
40. A. Yanin and F. Schmidt, Phys. Rev. 100, 171 (1955).
41. H. Slätis, Arkiv Fysik 8, 441 (1954).
42. R. A. Dudley, Nucleonics 12, 24 (1954).
43. L. Cranberg and J. Halpern, Rev. Sci. Instr. 20, 641 (1949).
44. W. A. Wooster, Proc. Roy. Soc. (London), A769, 729 (1927).
45. H. C. Hoyt and J. W. M. DuMond, Phys. Rev. 91, 1027 (1953).
46. F. S. Stephens, Jr., "Decay Schemes and Nuclear Spectroscopic States in the Heavy-Element Region" (thesis), UCRL-2970, June 1955.

47. D. Strominger "Experimental Study of Nuclear Isomers in the Millimicrosecond Lifetime Range" (thesis), UCRL-3374, June 1956.

48. Bendel, Toms, and Tobin, Phys. Rev. 99, 672A (1955).

49. I. Bergström and R. D. Hill, Arkiv Fysik 8, 21 (1954).

50. W. F. Biller, "Characteristics of Bismuth Fission Induced by 340-Mev Protons" (thesis), UCRL-2067, Jan. 1953.

51. R. H. Goeckermann, "Characteristics of Bismuth Fission with High-Energy Particles" (thesis), UCRL-251, Dec. 1948.

52. Glass, Thompson, and Seaborg, J. Inorg. Nucl. Chem. 1, 3 (1955).

53. J. R. Huizenga and C. M. Stevens, Phys. Rev. 96, 548 (1954).

54. J. R. Huizenga and J. Wing, Phys. Rev. 102, 926 (1956).

55. J. A. Harvey, Phys. Rev. 81, 353 (1951).

56. Kinsey, Bartholomew, and Walker, Phys. Rev. 82, 380 (1951).

57. Hanson, Duffield, Diven, and Palevsky, Phys. Rev. 82, 380 (1951).

58. H. Brysk and M. E. Rose, "Theoretical Results on Orbital Capture," ORNL-1830, Jan. 1955.

59. R. W. Hoff and J. O. Rasmussen, Jr., "Concerning ft Values and L/K Ratios for Orbital Electron Capture," UCRL-4511, May 1955.

60. M. H. L. Pryce, Proc. Phys. Soc. (London) A65, 773 (1952).

61. J. A. Harvey, Can. J. Phys. 31, 278 (1953).

62. Sliv, privately circulated tables.

63. T. R. Gerholm, Rev. Sci. Instr. 26, 1069, (1955).

64. J. Swan and R. Hill, Phys. Rev. 91, 424 (1953).

65. R. Montalbetti, Can. J. Phys 30, 660 (1952).

66. F. Asaro, private communication.